



UNIVERSITY OF CAPE TOWN
IYUNIVESITHI YASEKAPA • UNIVERSITEIT VAN KAAPSTAD

Department of Civil Engineering

Track-Bridge Interaction Effects in Heavy Haul Railway Viaducts

Prepared by:

Mixo Ngwenya

Prepared for:

Prof. Pilate Moyo

Date:

13 February 2022

*Submitted in partial fulfilment of the requirements for the degree of Master of Science in
Structural Engineering*

The copyright of this thesis vests in the author. No quotation from it or information derived from it is to be published without full acknowledgement of the source. The thesis is to be used for private study or non-commercial research purposes only.

Published by the University of Cape Town (UCT) in terms of the non-exclusive license granted to UCT by the author.

Plagiarism Declaration

I know the meaning of plagiarism and declare that all the work in the document, save for that which is properly acknowledged, is my own. This thesis/dissertation has been submitted to the Turnitin module (or equivalent similarity and originality checking software) and I confirm that my supervisor has seen my report and any concerns revealed by such have been resolved with my supervisor."

Mixo Ngwenya
MPHMIX001

Date



Acknowledgements

Firstly, to **God**, indeed your grace is sufficient. Thank you for seeing me through this journey. There were so many times when I wanted to give up and walk away and at each point you renewed my strength and kept me going. I will praise all the days of my life!

Mr Nchongi Ngwenya (Snr), Daddisto, in your eyes there is nothing I cannot do. You never had any doubt that I would one day be at the end of this journey. You believe in me more than I believe in myself and this is the greatest gift any father can give their daughter. Thank you, Daddy!

Mrs Rhulani Ngwenya, Dimamzo, my prayer warrior. Thank you for carrying me in prayer. Throughout this journey you constantly reminded me that no challenge is too big for God. On my worst days your words of encouragement, gifts, acts of service and love made me feel better. Thank you for setting a good example of a woman who can do it all, have a great career and continue learning whilst making a house a home.

Dr Mabowa and Dr Wisani Makhomisane, Uncle Mabs and Mama Wisi, I will forever be grateful for your love and support. You were never too busy to lend a listening ear. The laughter and great dinners made this journey even more bearable.

Mrs Grace Mahungo, Granny, No amount of gratitude could ever be sufficient. Thank you for praying for me and always reminding me to lean on God during this study.

To my siblings, **Mr Nchongi Ngwenya (Jnr)** and **Mr Ntlaweni Ngwenya (Jnr)**, setting a good example for you has always been my greatest desire. May this study always be a reminder that your dreams are valid!

Mr Mkhuleko Dlamini, Nkosi, your friendship has carried me throughout this study. I am grateful for the words of encouragement and the meals that you had delivered to me when you knew that I would be too busy to cook.

Lastly, I owe an enormous amount of gratitude to my supervisor, **Prof Pilate Moyo**, for his supervision. Thank you for your guidance and for believing in me.



Abstract

When continuously welded rails are placed over a bridge, the track and the bridge interact via the ballast in the case of ballasted track or track slab in the case of non-ballasted track. This interaction, commonly referred to as track-bridge interaction results in force transfer between the track and the bridge. With the demand to increase freight haulage on heavy haul railway lines intensifying to meet mineral export demands, there is a need to understand the manifestation of rail bridge interactions in heavy haul railway bridges. Understanding the manifestation of these forces is critical for the management of the infrastructure during operation.

Whilst track-bridge interactions effects design limits in high-speed rail have been documented, to the author's knowledge there has been no documented report that addresses track bridge interactions in the design of new heavy haul railway bridges and the management old heavy haul railway bridges.

Resultantly, this study explored the observed patterns of rail forces, longitudinal deck displacements, ambient temperature, concrete temperature and rail temperature on the Olifants River Railway Bridge.

Thereafter, the observed patterns were used investigate the effect of rail temperature variation on rail forces and the longitudinal displacement of the deck. Examine the effect of variation in concrete temperature on the longitudinal deck displacement, rail forces and variation in rail temperature as well as the effect of longitudinal deck displacement on rail forces. The effects of the presence of a train on the longitudinal displacement of the deck, rail forces and concrete temperature will also be investigated. Finally, this study developed a predictive multiple linear regression model that will assist in the management and maintenance heavy haul railway bridges.

This study demonstrated that rail temperature variation is inversely proportion to the rail forces in the rail, longitudinal deck displacement is directly proportional to concrete temperature variation and that longitudinal deck displacement of the bridge deck and rail forces in the rail are inversely proportional.

However, the correlation between the longitudinal deck displacement and the rail temperature, rail temperature in the track and concrete temperature in the deck, concrete temperature in the deck and the rail forces in the track could not be established conclusively. The effect of the presence of the train on the longitudinal displacement of the deck, rail forces and concrete temperature could also not be established conclusively.



Table of Contents

Plagiarism Declaration	i
Acknowledgements	ii
Abstract	iii
Table of Contents	iv
List of Figures	vi
List of Tables	viii
Glossary	ix
1. Introduction	1
1.1 Background and Context	1
1.2 Justification of Study	2
1.3 Objectives of Study	3
1.4 Scope and Limitations	3
2. Literature Review	5
2.1 Introduction	5
2.2 Geometric and Material Properties of Railway bridge	6
2.2.1 Introduction	6
2.2.2 Bridge Deck	6
2.2.3 Ballasted Track Geometry	9
2.2.4 Railway Track Connections	13
2.3 Rail–Bridge Interaction	16
2.3.1 Temperature Variation in the Rails	17
2.3.2 Acceleration and Braking Stresses on the Rail	17
2.3.3 Bridge Deck-end Rotation	18
2.3.4 Temperature Variation in the Bridge Deck	18
2.3.5 Problems Associated with Additional Stresses	19
2.4 Summary of Chapter	19
3. Olifants River Railway Bridge: A Case Study	21
3.1 Viaduct Description	21
3.2 Loads on the Railway Viaduct	24



3.2.1 Temperature	24
3.2.2 Vertical Train Loads	24
3.2.3 Braking and Acceleration Loads	24
3.2.4 Load Summary	25
3.3 Monitoring Systems	26
3.3.1 WIM – WIM System	26
3.3.2 Saldanha System	27
4. Methodology	32
4.1 Data Cleaning/Preparation	33
4.1.1 Data Cleaning/Preparation – Saldanha System	33
4.1.2 Data Cleaning/Preparation – WIM -WIM System	36
4.2 Data Mining	39
4.2.1 Data Mining SS Data	39
4.2.2 Data Mining WIM – WIM Data	40
4.3 Linear Regression Analysis Theory	40
4.4 Linear Regression Analysis in Python	42
4.4.1 Track - Bridge Interaction Investigation Using Single Variate Regression	42
4.4.2 Multiple Linear Regression Predictive Maintenance Model	43
5. Data Analysis	45
5.1 Data Descriptions	45
5.1.1 Longitudinal Deck Displacement Statistical Summaries	45
5.1.2 Rail Forces Statistical Summaries	47
5.1.3 Ambient Temperature Statistical Summaries	55
5.1.4 Concrete Temperature Statistical Summaries	56
5.1.5 Rail Temperature Statistical Summaries	57
5.1.6 Train Categories	58
5.2 Observed Patterns	61
5.2.1 Longitudinal Deck Displacement	61
5.2.2 Rail Forces Left Rail Saldanha Deck	62
5.2.3 Rail Forces Right Rail Saldanha Deck	63
5.2.4 Rail Forces Left Rail Sishen Deck	64
5.2.5 Rail Forces Right Sishen Deck	65
5.2.6 Ambient Temperature	66



5.2.7 Concrete Temperature	67
5.2.8 Rail Temperature	68
5.2.9 Summary of the Section	69
5.3 Track Bridge Interactions/Associations	70
5.3.1 Introduction	70
5.3.2 Effect of Rail Temperature Variation	70
5.3.3 Effect of Concrete Temperature Variation	72
5.3.4 Effect of the Longitudinal Deck Displacement	75
5.3.5 Effect of the Presence of Train	76
5.3.6 Effect of Ambient Temperature Variation	78
5.3.7 Summary of the Section	80
5.4 Predictive Multiple Linear Regression Model Discussion	82
6. Conclusions	6-87
7. Recommendations	89
8. Bibliography	90

List of Figures

Figure 2-1: Depiction of the two sub-systems of a railway bridge.....	6
Figure 2-2: Open Deck (Comstock, 2011).....	7
Figure 2-3: Embedded deck (National Academies of Sciences, 2012).	7
Figure 2-4: Ballasted deck (Riley, 2018).....	8
Figure 2-5: Direct Fixation Deck (Kim <i>et al.</i> , 2019).	9
Figure 2-6: Typical Cross Section of a Typical Ballasted Railway Track(Elkhoury et al., 2018).	10
Figure 2-7: Rail gauge	11
Figure 2-8: Fishplate rail joint (Kadam, 2021).	14
Figure 2-9: Behaviour of CWR under the effect of temperature changes (Pauwels, 2015).	16
Figure 2-10: Depiction of Deck - end Rotation.	18
Figure 3-1:Olifants River Viaduct Geometry Busatta(2018).	22
Figure 3-2: Pier 11 and 12 Bearing Configuration.	23
Figure 3-3: Olifants River Viaduct Cross Section(Bester et al., 1973).	23
Figure 3-4: Depiction of Deck End Rotations Due to Vertical Loads.....	24
Figure 3-5: The SS and TTC System Layouts (Freyer, 2004)......	29



Figure 4-1: Methodology Process.....	32
Figure 4-2: Depiction of Saldanha System Raw Data Format.....	33
Figure 4-3: Saldanha System Channel Legend.....	33
Figure 4-4: Depiction of Removing Rows with Errors.....	35
Figure 4-5: Type Zero Error.	36
Figure 4-6: WIM-WIM Data.	37
Figure 4-7: Train Naming Convention in this Study.	38
Figure 4-8: R Script used to plot time series graphs.....	39
Figure 4-9: Linear Regression Python Script.	43
Figure 5-1:: Longitudinal Deck Displacement Probability Density Functions.	46
Figure 5-2: Saldanha Left Rail Force Probability Density Functions.	48
Figure 5-3: Saldanha Right Rail Force Probability Density Function.....	50
Figure 5-4: Sishen Right Rail Force Probability Density Function.....	52
Figure 5-5: Sishen Right Rail Force Probability Density Function.....	54
Figure 5-6: Ambient Temperature Statistical Summary.....	55
Figure 5-7: Concrete Temperature Probability Density Function.	56
Figure 5-8: Rail Temperature Probability Density Function.	57
Figure 5-9: Seasonal comparison of categorized loaded trains for the 2016 period.....	60
Figure 5-10: Seasonal comparison of categorized unloaded trains for the 2016 period.....	60
Figure 5-11: Longitudinal deck displacement time series.	61
Figure 5-12: Saldanha Deck Left Rail Force time series.....	62
Figure 5-13: Saldanha Deck Right Rail Force time series.....	63
Figure 5-14: Sishen Deck Left Rail Force time series.....	64
Figure 5-15: Sishen Deck Right Rail Force time series.....	65
Figure 5-16: Ambient temperature time series.	66
Figure 5-17: Concrete temperature time series.....	67
Figure 5-18: Rail temperature time series.....	68
Figure 5-19: (a) Training results of RFSiR3 vs RTR. (b) Training results of RFSiR3 vs RTR.	70
Figure 5-20: (a) Training results of DDSiR vs RTR. (b) Testing results of DDSiR vs RTR....	71
Figure 5-21: (a) Training results of DDSiR vs CTS. (b) Testing results of DDSiR vs CTS.....	72
Figure 5-22: (a) Training results of RFSiR3 vs CTS. (b) Testing results of RFSiR3 vs CTS...	73
Figure 5-23: (a) Training results of RTR vs CTS. (b) Testing results of RTR vs CTS.....	74
Figure 5-24: (a) Training results of RFSiR3 vs DDSiR. (b) Training results of RFSiR3 vs DDSiR.....	75
Figure 5-25: (a) Δ RFSiR3 vs Loaded Train Categories (b) Δ RFSiR3 vs Unloaded Train Categories.	76
Figure 5-26: (a) Δ DDSiR vs Loaded Train Categories (b) DDSiR vs Unloaded Train Categories.	76
Figure 5-27: Δ CTS vs Loaded Train Categories (b) Δ CTS vs Unloaded Train Categories.....	77



Figure 5-28: (a) Training results of RFSiR3 vs ATS. (b) Testing results of RFSiR3 vs ATS. .	78
Figure 5-29: (a) Training results of DDSiR vs ATS. (b) Testing results of DDSiR vs ATS. ...	79
Figure 5-30: Predictive Multiple Linear Regression Model Interface.	86
Figure 5-31: Predictive Multiple Linear Regression Model Interface Results.	86

List of Tables

Table 2-1: Types of rails and shape (Kaewunruen and Remennikov, 2008).	11
Table 3-1: ORV Bearing Configuration.	21
Table 3-2: Train Categorization (Bussatta, 2018)	25
Table 3-3: SS Warning and Alarm Levels (Freyer, 2004).	30
Table 4-1: Channel number and related channel names.	34
Table 4-2: Train Categories for this Study.	38
Table 4-3: Dependent and Independent Variables for Linear Regression.	42
Table 5-1: Longitudinal Deck Displacement Statistical Summary.	45
Table 5-2: Saldanha Left Rail Force Statistical Summary.	47
Table 5-3: Saldanha Right Rail Force Statistical Summary.	49
Table 5-4: Sishen Left Rail Force Statistical Summary.	51
Table 5-5: Sishen Right Rail Force Statistical Summary.	53
Table 5-6: Ambient Temperature Statistical Summary.	55
Table 5-7: Concrete Temperature Statistical Summary.	56
Table 5-8: Rail Temperature Statistical Summary.	57
Table 5-9: Categorization of loaded trains that travelled across the ORV in 2016.	58
Table 5-10: Categorization of unloaded trains that travelled across the ORV in 2016.	59
Table 5-11: Training and Testing Results of RFSiR3 vs RTR.	70
Table 5-12: Training and Testing Results of DDSiR vs RTR.	71
Table 5-13: Training and Testing Results of DDSiR vs CTS.	72
Table 5-14: Training and Testing Results of RFSiR3 vs CTS.	73
Table 5-15: Training and Testing Results of RTR vs CTS.	74
Table 5-16: Training and Testing Results of RFSiR3 vs DDSiR.	75
Table 5-17: Training and Testing Results of RFSiR3 vs ATS.	78
Table 5-18: Training and Testing Results of DDSiR vs ATS.	79
Table 5-19: Model Step 1 - Predicting fail force from forecast temperature.	82
Table 5-20: Model Step 2 - Predicting rail temperature from variables in step 1.	83
Table 5-21: Model Step 3 - Predicting longitudinal deck displacement from variables in step 2.	84
Table 5-22: Model Step 4 - Predicting concrete temperature from variables in step 3.	85



Glossary

CWR	Continuously Welded Rail
ERRI	European Rail Research Institute
FPR	Fish Plated Rail
HH	Heavy Haul
ITCMS	Integrated Train Condition Monitoring System
LVDTs	Linear Variable Differential Transformers
PSC	Prestressed Concrete
RC	Reinforced Concrete
RMSE	Root Mean Squared Error
RNB	Reinforced Neoprene Bearing
SB	Sliding Bearing
SS	Saldanha System
TFR	Transnet Freight Rail
TTC	Track Testing Centre
WIM	Weigh In Motion
WIM-WIM	Wheel Impact Monitor And Weigh In Motion System



1. Introduction

1.1 Background and Context

The continual growth of the trade industry has driven the need to transport larger quantities of goods than ever before and therefore requires longer trains to meet the demands of the industry. This need was met in part by the introduction of the Heavy Haul railway systems. Heavy Haul railway lines are described by the International Heavy Haul Association as railway lines that meet at least two of the following; supports a train that is at least 5000 metric tons in weight, hauls 20 million metric tons of annually and supports at least 25 metric tons per axle.

Today there are several Heavy Haul railway lines which span over valleys and rivers and makes use of bridges in order to do so successfully(Wei and Wang, 2011). This then introduced what is widely referred to as heavy haul railway bridges. In recent years, the use of continuously welded rail (CWR) has been dominant as opposed to fish plated rail(FPR). Significantly reduced maintenance costs are associated with CWR in comparison to FPR(Ali AsifK *et al.*, 2016). CWRs are formed by welding rails together from end to end to form one continuous rail that extends more than 1 km. CWRs comprise of three zones; two 150m breather zones at each end within which expansion and contraction is permitted and one central zone where free expansion and contraction is constrained. (De Backer, et al., 2017).

Schanack et al. (2014), in a study investigating the relative displacement method for track – structure, argued that by placing a continuously welded rail on a bridge; irrespective of whether the track and deck are joined by ballast or by direct elastic fastening, the two systems will be interconnected. Resultantly, the consequences of the behaviour of the track has an effect on the behaviour of the bridge and vice versa.

In a railway bridge, the track and bridge experience longitudinal stresses and strains due to the actions applied on them, respectively. The track experiences tensile and compressive stresses due to rail temperature variation, braking and acceleration forces that act on the track. As the track and bridge are interconnected these longitudinal rail stresses are then transmitted to the bridge deck as additional stresses.

On the other hand, the bridge experiences tensile and compressive stresses due to concrete temperature variation and vertical train loads that result in deck-end rotation and as the track and bridge are interconnected these longitudinal deck stresses are then transmitted to the rail as additional stresses. This phenomenon is referred to as track-bridge interaction effects.(Popović *et al.*, 2018)

When the additional stresses become too large the design limits of track will be exceeded and this leads to track anomalies (UIC, 2001). For railway bridges track anomalies may take the form of track buckling or track breaking.



Although rail-bridge interaction in heavy haul railway bridges have not been documented according to the author's knowledge. Multiple studies on rail bridge interaction effects design limits in high-speed railway bridges have been carried out.

These studies have informed the design limits for track bridge interaction effects that have been put forth by the European Rail Research Institute (ERRI) subcommittee D213. The ERRI has established that the maximum permissible additional compressive stress in the rail is 72 N/mm^2 and maximum permissible additional tensile stress in the rail is 90 N/mm^2 . According to the ERRI this definition applies to concrete bridges with a maximum expansion length of 90 m (Dutoit, 2009). Expansion length is the distance between the thermal center point and the opposite end of the deck. The recommendations by the ERRI will influence the design of railway bridges in the future, however to the author's knowledge there exists no reported recommendations to assist in the management and maintenance of old heavy haul railway bridges with expansion lengths that are greater than 90m that could potentially experience additional stresses that exceed design limits of the railway bridge.

The intention of this study is to understand track-bridge interactions in heavy haul railway viaducts that have an expansion length greater than 90 m and subsequently design a predictive model to ensure the efficient management of such structures.

This study will achieve this by exploring the observed patterns of rail forces, longitudinal deck displacements, ambient temperature, concrete temperature and rail temperature over time. Investigating the effect of rail temperature variation on rail forces and the longitudinal displacement of the deck. Examine the effect of variation in concrete temperature on the longitudinal deck displacement, rail forces and variation in rail temperature as well as the effect of longitudinal deck displacement on rail forces. The effects of the presence of a train (vertical train loads) on the longitudinal displacement of the deck, rail forces and concrete temperature will also be investigated. Finally, this study will go on to develop a predictive multiple linear regression model that will assist in the management and maintenance heavy haul railway bridges with an expansion length that is greater than 90m.

1.2 Justification of Study

As the demand to increase freight haulage on heavy haul routes intensifies, there is an even greater need to understand the manifestation of rail bridge interactions in heavy haul railway bridges. This is because the growth of existing mining areas in conjunction with the increasing demand of iron ore and coal have led mine owners and railway line operators to gradually increase the capacity of the export lines in South Africa (Kuys, 2009).

This has resulted in a significant increase in train speeds, axle loads and the number of train wagons (Kuys, 2011). The increase in rail traffic on existing railway bridge structures might lead



to significant increase in rail-bridge interaction effects, which could lead to track buckling and track breaking, should the effects increase beyond the design limits of the track.

Whilst there are design restrictions to limit effects of rail-bridge interaction to the author's knowledge there exists no reported recommendations to assist in the management and maintenance of old railway bridges with expansion lengths of more than 90 m. There is therefore a necessity to (i) explore the observed patterns of rail forces, longitudinal deck displacements, ambient temperature, concrete temperature and rail temperature over time, (ii) investigate the effect of rail temperature variation on rail forces and the longitudinal displacement of the deck, (iii) examine the effect of variation in concrete temperature on the longitudinal deck displacement, rail forces and variation in rail temperature as well as the effect of longitudinal deck displacement on rail forces, (iv) investigate the effects of the presence of the train (vertical train loads) on the longitudinal displacement of the deck, rail forces and concrete temperature and (v) develop predictive multiple linear regression model that will assist in the management and maintenance heavy haul railway bridges with an expansion length greater than 90m.

1.3 Objectives of Study

The intention of this study is to understand track-bridge interactions in railway viaducts that have an expansion length greater than 90 m and subsequently design a predictive model to ensure the efficient management of such structures through the following objectives:

1. Explore the observed patterns of rail forces, longitudinal deck displacements, ambient temperature, concrete temperature and rail temperature over time.
2. Investigate the effect of rail temperature variation on rail forces and the longitudinal displacement of the deck.
3. Examine the effect of variation in concrete temperature on the longitudinal deck displacement, rail forces and variation in rail temperature as well as the effect of longitudinal deck displacement on rail forces.
4. Investigate the effects of the presence of the train (vertical train loads) on the longitudinal displacement of the deck, rail forces and concrete temperature.
5. Develop a predictive model which makes use of ambient temperature forecasts to predict rail forces, longitudinal deck displacement, rail temperature and concrete temperature estimates that can assist in planned infrastructure management.

1.4 Scope and Limitations

This study will be limited to heavy haul railway bridges with an expansion length greater than 90m. Long term actions that introduce the influence of creep and shrinkage on rail bridge interactions will not be considered. The bridge was constructed more than 40 years ago and therefore these effects are negligible.



The investigation of the actions on the bridge will be limited to longitudinal deck displacement, damage to piers and bearing pads will not be included in this study.

The analysis in this study will be limited to data obtained from the Weigh in Motion (WIM) system and the Saldanha system for the period August 2015 to December 2018. The two systems and the datasets are managed by the railway operator.

Using the available data WIM system and Saldanha system it is not possible to accurately quantify longitudinal forces due to acceleration and braking. Resultantly the effect of braking and acceleration will not be investigated in this study. This study will investigate the effects of the presence of the train on the track instead.



2. Literature Review

2.1 Introduction

The structural integrity of heavy haul railway bridges is among the most essential mandates of railway developments around the world. Particularly in recent years, with the general trend of increasing axle loads and operating speeds of trains, the condition of railway bridges is of great concern, particularly for old bridges, which are often subject to higher loads than originally envisaged. (Hajjalizadeh and Žnidarič, 2020)

Heavy Haul (HH) railway lines are described by the International Heavy Haul Association as railway lines that meet at least two of the following; supports a train that is at least 5000 metric tons in weight, hauls 20 million metric tons of revenue annually and supports at least 25 metric tons per axle.

In SA, HH railway transport was introduced in the 1970s to export iron ore and coal. The South African 861 km long Iron Ore Export Line connects the mining areas in Sishen in the Northern Cape Province to the Saldanha Bay Harbour in the Western Cape Province (Lombard, 1982). South Africa also boasts of a Coal Export Line which is 748 km long. This coal line links the coal mines in Black Hill outside Ermelo in the Mpumalanga Province, to the Richards Bay Coal Terminal located in Kwazulu-Natal (Von Gericke, 1986).

In last decades, the growth of existing mining areas, the increasing demand of iron ore and coal and the strong competition of foreign iron ore- and coal exporting countries have led mine owners and railway line operators to gradually increase the capacity of the export lines in SA (Busatta and Moyo, 2015). This has resulted in a significant increase in rail traffic as train speeds, axle loads and the number of train wagons have been increased (Kuys, 2011). However, the increase in rail traffic on existing railway bridge structures might lead to significant increase in rail-bridge interaction effects. The increase in rail bridge interaction effects could result in track buckling and track breaking, should the effects increase beyond the design limits of the track.

Thus, this literature review will describe the geometric and material properties of railway bridges. It will explore the use of CWRs in railway bridges and its influence on track bridge interaction effects. The review will define rail bridge interaction effects and discuss in detail the actions through which these effects are manifested. Furthermore, it will highlight instances where rail-bridge interaction effects in HH railway bridges could result in track anomalies and thus indicate the need to understand rail-bridge interaction effects in HH railway bridges and the need for guidelines to maintain existing HH railway bridges.

In closing, this study will highlight that, although rail bridge interaction effects design limits have been studied extensively in high-speed rail, rail-bridge interaction effects in HH railway



bridges have not been documented and that there exists no documented guidelines on the maintenance of HH railway bridges.

2.2 Geometric and Material Properties of Railway bridge

2.2.1 Introduction

Railway bridges are made up of two sub-systems, the railway track and the bridge deck as represented in Figure 2-1. Railway Bridges must be safe and efficient in order to support train wheels that run at various speeds with different axle loads. For this objective to be accomplished, both the sub-systems of the structure must be able to fulfil the desired requirements under various loads and speeds amongst other requirements. (Indraratna, et al., 2011). This chapter will discuss in detail the structure of the railway track and mention the four types of bridge decks specific to railway bridges.

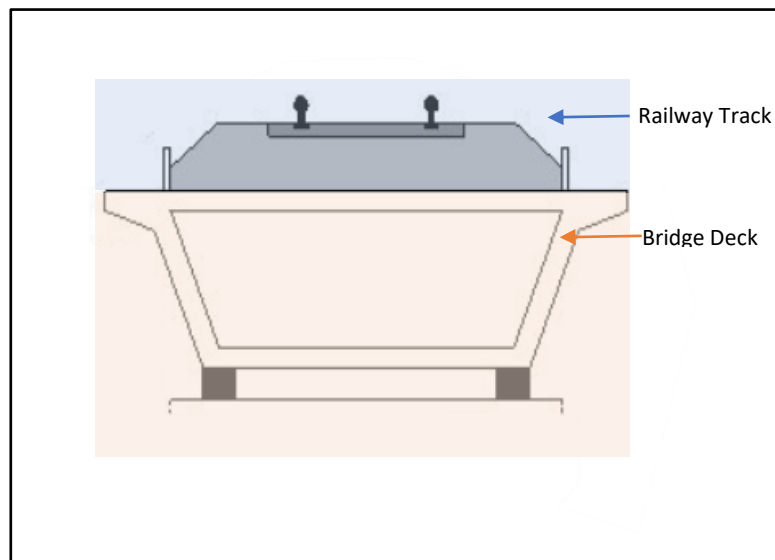


Figure 2-1: Depiction of the two sub-systems of a railway bridge.

2.2.2 Bridge Deck

The bridge deck acts as a supporting structure for the rail. There are four types of bridge decks that railway bridges are typically supported on; open deck, embedded deck, ballasted deck and direct fixation deck. The earliest railway bridge featured open deck construction (McCammon & Richards, 2006). In open deck, the track and its ties (commonly referred to as sleepers) are laid directly on timber bridge ties (AREMA, 2003).

The use of timber makes the structure quite light in comparison to, ballasted decks, embedded decks and direct fixation decks. An open deck is shown in Figure 2-2.





Figure 2-2: Open Deck (Comstock, 2011).

The embedded deck construction was introduced to accommodate vehicles that cross railway bridges. In an embedded railway deck the only portion of the track that is visible is the running surface of the track structure. The remainder of the track structure is concealed by the roadway pavement such that the body of the track structure is concealed. (National Academies of Sciences, 2012) . An embedded deck is shown in Figure 2-3.



Figure 2-3: Embedded deck (National Academies of Sciences, 2012).



In the 20th century ballasted deck was introduced for urban rail in response to the public's complaints about the noise and vibration from open deck railway bridges (National Academies of Sciences, 2012). For a ballasted deck, crushed stone(ballast) is placed between the bridge deck and track ties in order to provide better track stability. The ballast holds the track in place as the train travels over it (Jamal, 2017). A ballasted railway bridge is shown in Figure 2-4



Figure 2-4: Ballasted deck (Riley, 2018).

In the 1960s, direct fixation tracks were developed as lighter alternative to ballasted deck. Although more expensive than ballasted decks, direct fixation decks have significantly lower dead load than ballasted decks and all the benefits of ballasted deck. Direct fixation decks consisted of timber ties and half-length ties embedded into a poured concrete deck. Contemporary direct fixation decks have eliminated the embedded ties and instead rail fasteners are anchored into a concrete substrate that incorporates rail restraint, acoustic attenuation and electrical isolation features. (National Academies of Sciences, 2012). A contemporary direct fixation deck is shown in Figure 2-5 overleaf.





Figure 2-5: Direct Fixation Deck (Kim *et al.*, 2019).

This study will focus on heavy haul railway bridges with a ballasted deck.

2.2.3 Ballasted Track Geometry

Ballasted railway tracks represent one of the largest worldwide networks catering to freight and passenger transportation (Stansfield, 2019). The stability of heavy-haul trains at high speeds strongly relies on the track conditions (Stansfield, 2019). The ballasted railway tracks provides trains with a surface for wheels to roll on. Ballasted railway track typically consists of two parallel lines steel rails supported on sleepers made of timber or prestressed concrete (Elkhoury *et al.*, 2018). The track is typically laid on a bed ballast which is supported by track formation (Faris *et al.*, 2018). Fastenings are used to secure the rail on the ties such that movements between the rail and the ties are prohibited (Hagaman, 1991). All friction and longitudinal displacements must be between the ties and the ballast.



For railway bridges track formation is replaced by the bridge decks. Typical ballasted track geometry is shown in Figure 2-6 . The sections below will discuss the main components that make up the ballasted track structure; rails, sleepers and ballast as well as their functions.

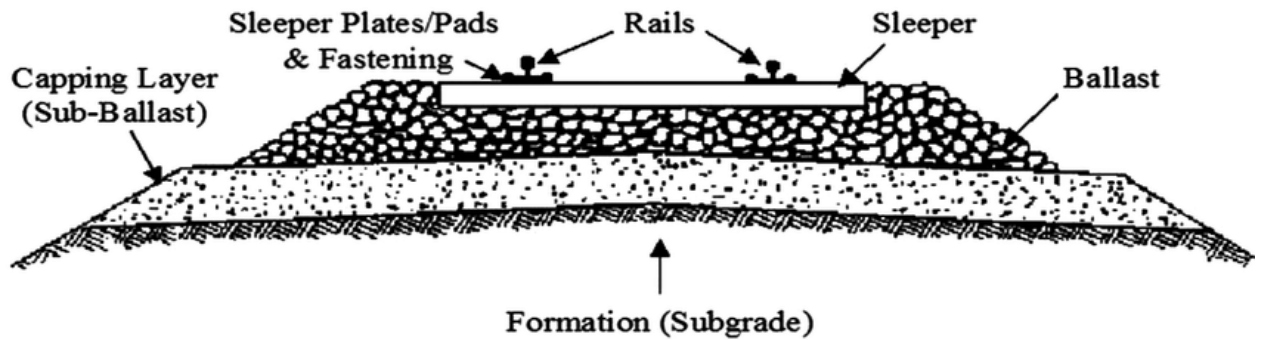


Figure 2-6: Typical Cross Section of a Typical Ballasted Railway Track(Elkhoury et al., 2018).

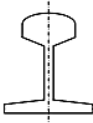
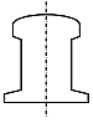
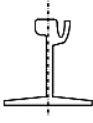
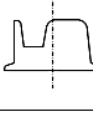
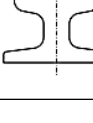
2.2.4.1 Rails

Rails are the longitudinal steel members that guide the train wheels evenly and continuously by offering the rigid tyre that rolls on it a rigid surface. A railway track consists of two rails. In order to fulfil their main function rails must have sufficient stiffness to serve as beams that transfer concentrated wheel loads to the sleeper supports without deflection between supports (Tzanakakis, 2013). Rails also act with train tyres to steer the vehicles in the desired direction (Mundrey, 2010). Furthermore, rail sections are designed to have an optimal weight of steel, maximum possible stiffness and adequate strength and durability in order to maintain a steady shape and smooth track configuration ((Waters & Selig, 1994).

Table 2-1 overleaf, describes rail profiles and their applications. Flat-bottomed rail is most used for ballasted rail, it is also referred to as Vignole rail (Kaewunruen and Remennikov, 2008). The Flat-bottomed rail is divided into three parts, the rail head, rail web and rail foot. The rail head which is the top surface that contacts the wheel tyre, the middle part referred to as the web supports the rail head and the rail foot which is the bottom of the rail that is responsible for distributing the load from the web to the underlying sleepers (Mundrey, 2010).



Table 2-1: Types of rails and shape (Kaewunruen and Remennikov, 2008).

Shape	Profile type:	Applications:
	Flat-bottom rail	Standard rail track
	Construction rail	Manufacturing of automobiles and switch parts
	Grooved rail	Railway track embedded in pavements, roads, yards
	Block rail	Railway track used in concrete slab as part of Nikex-structure
	Crane rail	Heavy load hoisting cranes with high wheel loads

2.2.4.2 Rail Gauge

The gauge of track is the distance between the inner edges of the heads of rails in a track, measured at 16 mm below the top surface of the rail. The rail gauge is shown in Figure 2-7. The most widely used gauge in the world is the standard gauge, which is equal to 1435 mm. The standard gauge is commonly used in South Africa and in some countries in Europe and North America. However, the gauge on the Olifants River Iron Ore line, is a 1067 mm narrow gauge. The narrow gauge is commonly used in East Africa and North Africa use narrow gauge, whilst the broad gauge is commonly used in Finland and Mangolia. It is important to note that some countries use more than one type of rail gauge.



Figure 2-7: Rail gauge



2.2.4.3 Sleepers

Made from a range of material such as timber, concrete or steel; sleepers are beams that span across the two rails; keeping the fastening system in place such that the gauge is maintained. Loads are received from the rail and distributed by the sleepers to the supporting ballast over a wider area (Esveld, 2001). Furthermore vertical, lateral and longitudinal movements are anchored in the ballast.

Sleepers can be typically made of timber, concrete or even steel. Timber sleepers are still present world-wide in older tracks. The challenge with timber is its tendency to rot around fastenings that are meant to preserve the geometry of the track. Although steel would not present such a challenge, steel sleepers are expensive and are predominantly used in special circumstances (Esveld, 2001). Concrete sleepers are said to be more economical in various countries due to its mass production in pre-cast yards. While concrete sleepers are much heavier than timber and thus is able to resist movement more efficiently, they have a disadvantage in that they cannot be cut to size for turnouts or special track work (Mundrey, 2010). Although, concrete sleepers work well under most conditions, its performance under high cyclic loading and impact loads from heavy haul freight trains is of great concern (Indraratna, et al., 2011).

2.2.4.4 Ballast

Ballast is coarse aggregate that acts as a loadbearing platform which supports sleepers and rails, it also drains moisture that is introduced into the system through the ballast and takes it away from the rails and sleepers. As represented in Figure 2-6 in section 2.2.3. The ballast is placed above the formation which is also referred to as the subgrade(Elkhoury *et al.*, 2018).

Composed of rock aggregates originating from quality igneous or metamorphic rock quarries, ballast layers are usually 250-350 mm thick. The ballast uniformly transmits the stress that is imposed at the sleeper-ballast interface to the subgrade layer at a reduced stress level. Additionally, S. S. *et al.*, (2018) advances that ballast not only provides acceptable stability to the sleepers against vertical, longitudinal and lateral forces, it assists in absorbing shock from dynamic loads. The ballast's ability to absorb shock may be attributed to the rough interlocking particles which have limited spring-like action (Tzanakakis, 2013).

Although well-cemented sedimentary rocks may be used for lighter trains, it is common practice to use crushed angular hard stones and rock aggregates with a uniform gradation. It is however to be noted that the source of ballast varies from country to country based on availability, quality, economic consideration and the surrounding environment (Indraratna, et al., 2011).



2.2.4.5 Sub-Ballast

Sub-ballast is a transition material layer between the upper layer of large-particle and the lower layer of fine-graded subgrade which acts as a filter. The sub-ballast is usually composed of well-graded crushed rock or sandy mixture with thickness of 15 cm. This transition layer reduces the migration of fine material into the ballast and thus ensures that drainage is not interrupted by facilitating the transportation of water away from the subgrade (Tzanakakis, 2013). (Indraratna, et al., 2011) explains that in recent years the function of the sub-ballast has been modified such that the sub-ballast prevents excessive loading on soft grade soils by distributing the stress from the ballast layer into the subgrade over a wider area.

2.2.4.6 Subgrade

The ground on which the track structure is built is referred to as subgrade. The subgrade is either naturally deposited soil or artificially placed fill material. Its main function is to resist traffic induced stresses at the sub-ballast-subgrade interface. Instability or failure of subgrade will inevitably result in unacceptable distortion of track geometry and alignment and thus it is imperative that the subgrade has sufficient stiffness and bearing capacity to resist traffic induced loads (Tzanakakis, 2013). If a track is to be constructed on soft soil, the subgrade may be stabilised by some ground improvement techniques (Indraratna, et al., 2011).

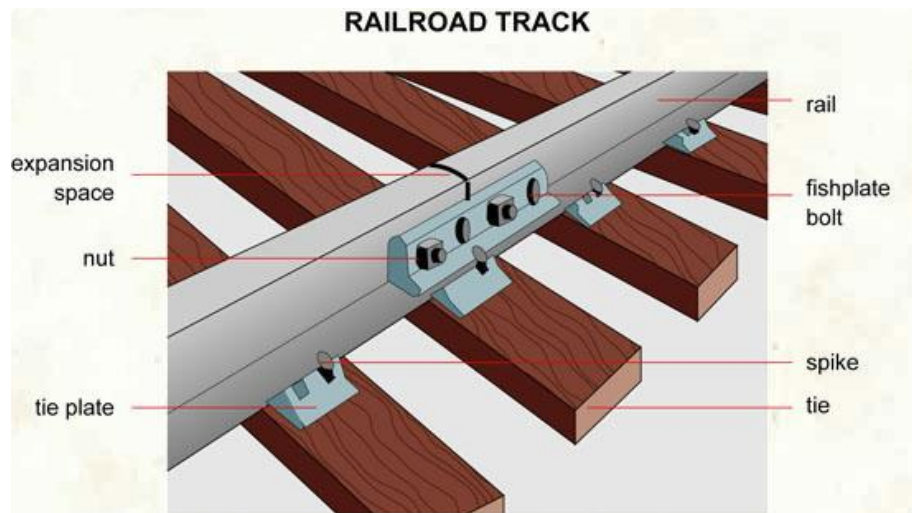
2.2.4 Railway Track Connections

The rails in railway track are manufactured in fixed lengths and are joined end to end to ensure a continuous surface on which the train runs. There are two main types of methods that are used to join rails, bolting and welding. This section will explain how the rails are joined together using bolting and welding as well as table the advantages and disadvantages of both of these methods.



2.2.4.1 Jointed Railway Tracks

Fishplates are used to form a connection between separate lengths of rail to provide continuity. This is achieved by employing two solid steel bars to join rails together using fishbolts and nuts. The point at which the two rails are joined together using a fishplate is referred to as a rail joint. A fishplate rail joint shown in Figure 2-8.



These fishplate rail joints hold the rail ends in position both in the horizontal and vertical plane (Kadam, 2021). Additionally, the joint allows for simple replacement of any rail from

Figure 2-8: Fishplate rail joint (Kadam, 2021).

the track. Fishplates are usually 600mm long and are used in pairs; they are placed on either side of the rail (Esveld, 2001).

One of the finest properties of the joint is its ability to allow contraction and expansion of the rails through the small gap between the rails (Esveld, 2001). However, a major problem of jointed tracks, which is responsible for more than 60 % of all rail failures, is due to bolt holes acting as stress raisers and acting as a focal point of fatigue failure. This problem is attributed to the passage of each wheel causing severe knocking on the rail joints (Mundrey, 2010).

Overtime jointed tracks have become less desirable with the introduction of modern trains as they require excessive maintenance and weaken the track structurally (Esveld, 2001). For many years the fish-plated joint had been the only method to join the pieces together until the introduction of Continuously welded rails (CWR) (Bruestle and Manager, 1996). CWR allow for a more rapid and smooth movement in comparison to rail joints and results in reduced maintenance costs. (Sung & Han, 2018).

2.2.4.2 Continuously Welded Rail

CWR refers to the way in which rails are joined together in order to form a single track and are defined by Ali AsifK *et al.* (2016) as rails that are at least 1 km in length. Although, CWR



is normally one continuous rail, it may at times contain joints to allow for insulated linkages that electrically separate track segments for signalling purposes.

Continuously welded rails are subject to longitudinal stresses due to thermal forces in the rail as well as braking and acceleration forces on the rail.

Whilst, jointed railway tracks typically contract when the temperature decreases and expand when the temperature increases (Lim, Park and Kang, 2003). CWR tracks are typically split up into three zones; the central zone and two breather zones at either the end of the central zone and approximately 150 m from the expansion devices at either end of the CWR (De Backer *et al.*, 2019). The three zones are represented in Figure 2-9 overleaf.

In the central zone no displacements of the rails occur due to the stiffness that the ballast offers. However, in the breather zones the expansion devices at the ends of the CWR have a variation of opening of 50 mm and permit displacement at the ends of the CWR (Pauwels, 2015). In essence, unlike jointed railway tracks, CWR only expand and contract in the breather zones.

In the central zone as the ballast opposes the free movement of the rails under temperature changes, longitudinal forces develop in the rail in addition to the longitudinal forces on the rail due to braking and acceleration forces. The displacement of the rails relative to the sleepers, due to longitudinal forces, is prevented by the fasteners that exert a clamping force onto the rail.

For the case of a continuous welded rail on an embankment this clamping force is such that all the longitudinal forces on the rail are transmitted to the sleepers and consequently to the ballast which is placed on the ground. (Kumar and Upadhyay, 2013). It is important to note that the modern railway track design is such that the stiffness of rail/sleeper connection is greater than the stiffness of the sleeper/ballast connection. Consequently, in CWR over embankments buckling occurs at the sleeper/ballast connection level.



In contrast, for the case of the CWR over a bridge the clamping force is such that the longitudinal forces on the rail are transmitted to the sleepers and then to the ballast that is placed on the bridge to the bridge deck. These longitudinal forces that are transferred to the bridge deck are additional to the longitudinal forces that already exist in the bridge deck (Popović *et al.*, 2018). These longitudinal forces in the bridge deck will induce longitudinal displacement in the bridge deck. In-turn the longitudinal displacement of the of the bridge deck will induce longitudinal forces in the rail which will be additional to the forces that already exist in the rails (Ramondence, et al., 2009).

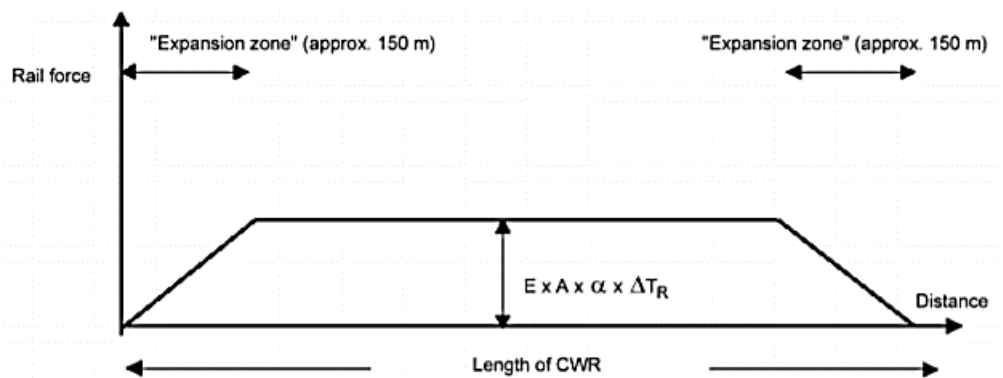


Figure 2-9: Behaviour of CWR under the effect of temperature changes (Pauwels, 2015).

Schanack *et al.*, (2014) in a study investigating the relative displacement method for track – structure, explained that by placing a continuously welded rail on a bridge; irrespective of whether the track and deck are joined by ballast or by direct elastic fastening, the two systems are interconnected. Resultantly, the consequences of the behaviour of the track has an effect on the behaviour of the bridge and vice versa. This phenomenon is referred to as track-bridge interaction effects.

2.3 Rail–Bridge Interaction

When CWR are placed on a bridge deck the track and bridge are interconnected irrespective of whether the track and bridge are joined either through ballast or directly by elastic fastening. As a consequence of the two sub-systems being interconnected, interaction between the sub-systems arises characterized by the behaviour of the bridge having an effect on the behaviour railway track and inversely the behaviour of the railway track having an effect on the behaviour of the bridge (Kostet, 2018).

According to Goicolea-ruigómez, (2020), Track- Bridge Interaction in high speed railway tracks can be visualized by considering the effects of the following actions: (i) temperature variation in the rails, (ii) braking and acceleration forces on the rails, (iii) deck end rotation of the bridge deck, (iv) temperature variation in the bridge deck which leads to the



longitudinal displacement of the bridge deck and (v) movement of the substructure and foundation.

Movement of the substructure and the foundation of a railway-bridge also results in rail bridge interaction effects; however, it will not be a part of this study.

2.3.1 Temperature Variation in the Rails

As temperature varies in CWR, the breather zones in the rail as defined in section 2.2.4.2 have a tendency to contract when the rail cools down and expand when the rail heats up. According to Illsley, (2020) in the central zone displacement is prohibited and resultantly as the rail cools down tensile stresses develop in the rail and as the rail heats up compressive stresses develop in the rail.

Since the railway track is connected to the bridge deck as compressive stresses develop in the rail, the rail will attempt to displace the bridge deck in the same direction as the compressive stresses in the rail(Illsley, 2020). The bridge deck will resist this attempt due to the stability that is provided to the bridge deck by its substructure. As the bridge deck resists this displacement, tensile stresses will develop in the rail (Narenda, 2011). The same is true for tensile stresses in the rails they induce compressive stresses in the bridge deck and its supporting structures.

These induced stresses that occur due to the interaction of the track and the bridge are referred to as additional longitudinal stresses(Illsley, 2020). These additional stresses are the largest in the region above the bridge supports(Lee *et al.*, 2015). Rail stresses due to temperature variation are proportional to additional longitudinal deck stresses. Additional longitudinal stresses in the deck induce longitudinal deck displacement, consequently rail stresses are proportional to the longitudinal deck displacement.

2.3.2 Acceleration and Braking Stresses on the Rail

Acceleration and braking stresses produce longitudinal stresses on the rail(Lee *et al.*, 2015). As the train accelerates it will exert tensile stresses at the front of the train and compressive stresses at the back of the train. The opposite is true for braking forces, as the train applies braking stresses it will exert compressive stresses at the front of the train and tensile stresses at the back of the train (Narenda, 2011).

Because the track and the bridge are interconnected the compressive stresses in the rail will try to drag the rails and the bridge in the compressive direction(Illsley, 2020). Due to the stability afforded to the bridge deck by its substructure it will resist this movement and tensile stresses will be induced in the bridge deck. These induced tensile stresses are referred to as additional longitudinal tensile forces. Similar behaviour is expected of the tensile stresses in the rails they will induce compressive stresses in the bridge deck. These induced stresses are



referred to as additional longitudinal compressive forces (Illsley, 2020). These additional stresses are the largest in the region above the bridge supports (Lee *et al.*, 2015).

The additional longitudinal stresses in the bridge deck bring about longitudinal deck displacement. It can thus be said that Acceleration and braking stresses are proportional to longitudinal deck displacement.

2.3.3 Bridge Deck-end Rotation

Trains on the track apply a vertical load on the railway bridge and the deck bends as shown in Figure 2-10. The bending of the deck causes rotation at the ends of the deck. If the deck is simply supported, the rotation at the ends causes compressive stresses on the top face and tensile stresses on the bottom face (Popović *et al.*, 2018). The stiffness and depth of the bridge deck has an effect on the extent to which the deck bends.

However, because the track is laid on top face of the bridge deck it will resist the compressive stresses being applied by the deck and thus inducing additional tensile stresses on the rail (Narenda, 2011). The normal load exerted by the train is proportional to the additional longitudinal stresses in the rail. Greater train axles will result in greater additional stresses (Yun *et al.*, 2019). These additional stresses are the largest in the region above the bridge supports (Lee *et al.*, 2015).

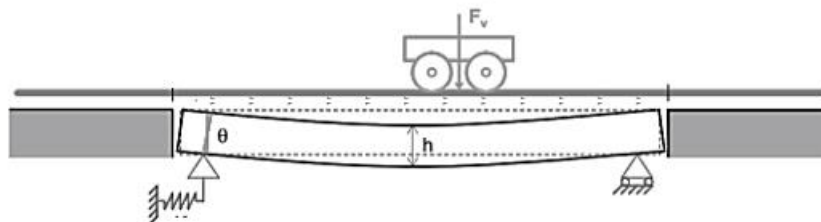


Figure 2-10: Depiction of Deck - end Rotation.

2.3.4 Temperature Variation in the Bridge Deck

Temperature variation in the bridge deck induces contraction and expansion of the deck such that the deck displaces longitudinally. Since the railway track is connected to the bridge deck as the deck contracts and thermal compressive stresses develop in the deck, the deck will attempt to displace the rail in the same direction as the compressive stresses in the deck (Yun *et al.*, 2019). The rail will resist this attempt and additional tensile stresses will develop in the rail. The same is true for tensile stresses in the deck they induce compressive stresses in the rail.



The bridge deck tends to expand in proportion to its expansion length, therefore the longer the bridge the greater the displacement on the bridge and thus the larger additional stresses occur(Lee *et al.*, 2015).

2.3.5 Problems Associated with Additional Stresses

The development of high-speed rail bridges particularly in European countries prompted the need for stricter design requirements for high-speed railway bridges. In order to meet geometric requirements such as maximum gradient and minimum radii in high -speed railway, longer railway bridges are necessary(Goicolea-ruigómez, 2020).

In considering the rail bridge interaction effects, with reference to the introduction of additional stresses in the rail, the need for longer viaducts highlighted additional requirements that should be met by railway bridges. As highlighted in the sections above this is because the bridge deck tends to expand in proportion to its expansion length, therefore the longer the bridge the greater the displacement on the bridge and thus larger additional stresses occur which could potentially lead to track anomalies(Lee *et al.*, 2015).

Track anomalies occur when the design limits of the rail are exceeded (UIC, 2001). For railway bridges track anomalies may take the form of track buckling or track breaking. If additional compressive stresses become too large the design limits of the rail will be exceeded and the rail will buckle. On the other hand, if additional tensile stresses become too large the design limits of the rail will be exceeded and the rail will break.

In light of the need to restrict the additional stresses in the track, the European Rail Research Institute(ERRI) subcommittee D213 spent numerous years researching track-bridge interactions in high speed railway bridges and put forward that if the additional compressive and tensile stresses in the rails and the relative displacement of the bridge are not kept under control, two main types of anomalies will ensue, rail fracture and the disruption of the link between the track and bridge such that track stability is no longer guaranteed (Dutoit, 2009). The ERRI defined under control as additional compressive stresses of not more than 72N/mm^2 , additional tensile stresses of not more than 90N/mm^2 and 5mm deck displacement. It should be appreciated that these recommendations are limited to standard gauges and bridge decks with a span of 90m or less (UIC, 2001).

2.4 Summary of Chapter

From this chapter it can be deduced that by placing CWRs on a bridge irrespective of whether the track and bridge are joined by ballast or by elastic fastening; the two structures are interconnected. This introduces what is referred to as track bridge interactions. As a result, rail temperature variation and braking and acceleration stresses transmits longitudinal additional stresses to the bridge deck and its supporting structure. Deck temperature variation and deck end rotation due vertical train loads transmit additional longitudinal stresses to the



rail track. However, it is important to note that stresses on the supporting structure of the bridge deck will not be studied in this dissertation.

This chapter also highlighted that in high-speed railway bridges rail stresses due to temperature variation are proportional to additional longitudinal deck stresses, acceleration and braking stresses are proportional to longitudinal deck displacement, the normal load exerted by the train is proportional to the additional longitudinal stresses in the rail and that longitudinal deck displacement due to temperature variation are proportional to additional longitudinal rail stresses.

Furthermore, that the introduction of high-speed rail prompted the development of rail bridge interaction effects design restrictions to prevent track anomalies.

Based on the literature reviewed, it is inferred that rail-bridge interaction effects in heavy haul railway bridges have not been documented. Especially, the effects of rail temperature variation and braking and acceleration on longitudinal resultant deck displacement as well as the effect of a deck temperature variation and deck end rotation due vertical train loads on resultant rail stresses.

Additionally, whilst recommendations by the ERRI will influence the design of railway bridges in the future, to the author's knowledge there exists no documented recommendations to assist in the management and maintenance of old heavy haul railway bridges with expansion lengths that are greater than 90m and that could potentially experience additional stresses that exceed design limits that have been put forward by the ERRI.

Therefore, this study seeks to understand how rail forces, longitudinal deck displacements, rail temperatures and concrete temperatures behave over time. It seeks to examine the effects of the variation of rail temperature, concrete temperature and ambient temperature respectively on longitudinal deck displacement as well as to investigate the effects of longitudinal deck displacements, ambient temperature, concrete temperature and rail temperature respectively on the resultant rail. Additionally, it will investigate the effect of the presence of a train on rail forces, concrete temperature and longitudinal deck displacement. To conclude, this study will use a multiple linear regression predictive model to predict the forces in the rail at a given ambient temperature. It is essential to note that this study will not investigate the effects of acceleration and braking stresses on the bridge deck.

This study will use the Olifants River Bridge as a case study to achieve the above-mentioned objects.



3. Olifants River Railway Bridge: A Case Study

The Olifants River Viaduct is located in the Western Cape Province of South Africa, between two small towns; Lutzville and Vredendal. According to the South African Weather Service the ambient temperature range in and around the Lutzville and Vredendal towns is between 0 °C and 50 °C. The Olifants River viaduct hauls more than 20 million metric tons of revenue annually and supports 30 metric tons per axle (Kuys, 2011).

This viaduct has been in operation since 1976 when the Iron Ore Export Line was introduced. The following sections will provide a description of the viaduct as presented in the drawings that were obtained from Transnet Freight Rail, a description of the loads that are exerted on the viaduct as well as the systems that monitor the effects of these loads.

3.1 Viaduct Description

The viaduct consists of a single box prestressed concrete (PSC) girder. As represented in Figure 3-1 below, it is 1035m long and consists of 23 equally spaced spans which are supported by 22 reinforced concrete (RC) piers and abutments at either end. Two expansion joints are located at piers 11 and 12 such that the viaduct is divided into 3 structurally independent girders. The two 495 m major girders are located on piers 1 – 11 and 12 – 23 and a 45m short girder is supported on pier 11 – 12. Piers 11 and 12 support the both the short and long span as indicated in Figure 3-1.

The three PCS girders are longitudinally post - tensioned members which are vertically prestressed by a set of 26mm diameter bars. These bars are introduced inside. The girders do not have transverse beams or diaphragms and transversal prestressing was not applied. The cross section is uniform along the entire viaduct.

The RC tapered piers have a H-type cross section with flanges that are oriented transversally along the direction of the viaduct. Piers 1 – 4 and 20 – 24 were constructed on spread footing and piers 5 – 19, which lie on the bed of the Olifants River valley, were constructed on piled foundations. The piers have different heights ranging from 17.85 m to 51.50 m due to variable topography.

Two different types of bearings, reinforced neoprene bearing (RNB) and sliding bearing(SB) have been placed between the girders and the piers. RNB are also positioned on the Sishen and Saldanha abutments respectively. The configuration of the bearings at each pier have been indicated in Table 3-1 below.

Table 3-1:ORV Bearing Configuration.

Piers	Bearings
1 - 4	RNB
5 - 10	SB
11 - 12	RNB & SB
13 - 17	SB
18 - 22	RNB



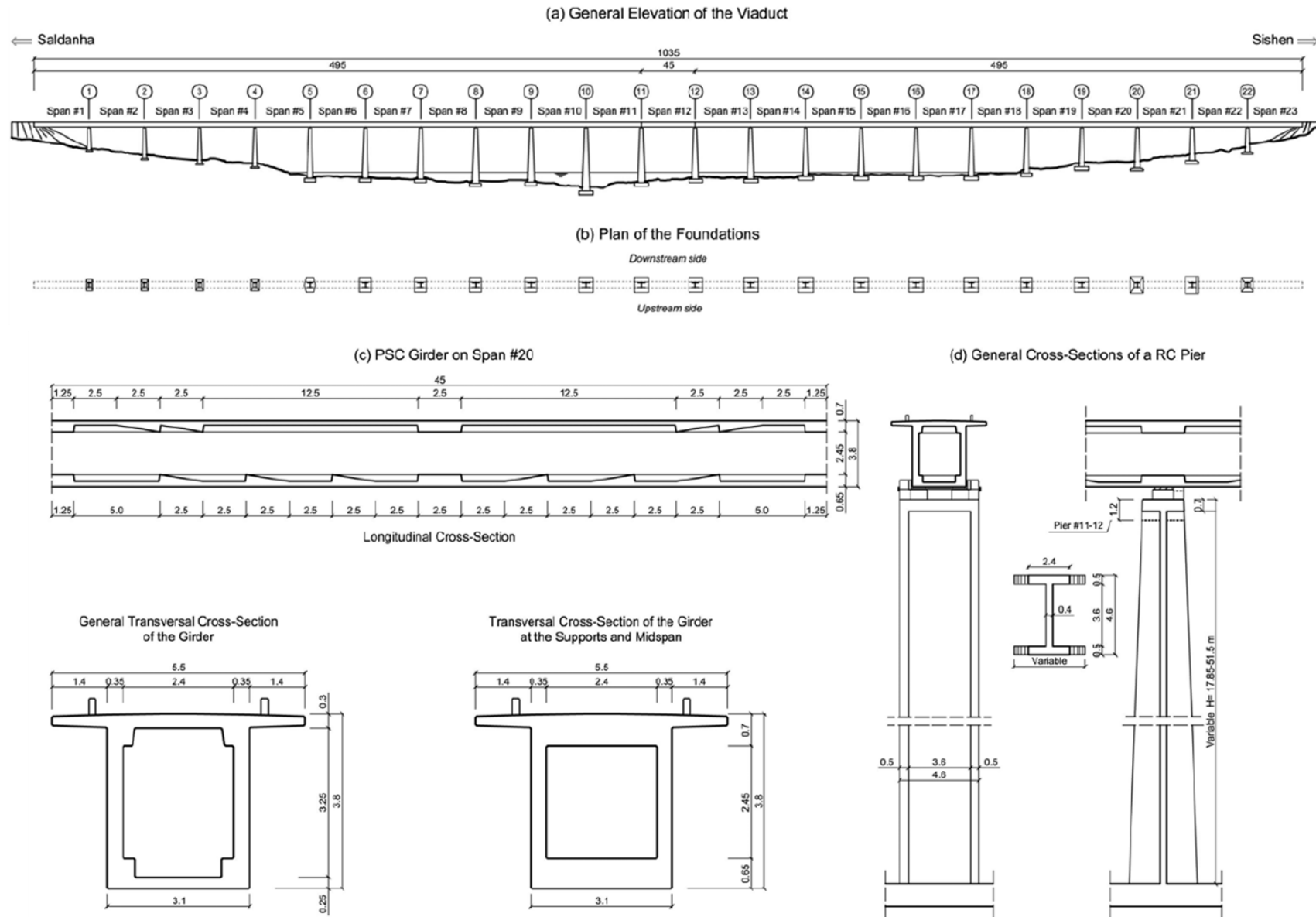


Figure 3-1: Olifants River Viaduct Geometry Busatta(2018).



Piers 11 and 12 have two types of bearings RNB under the simply supported drop span girder and the SB under the Saldanha and Sishen major girders as represented in Figure 3-2. RNB behaves as a hinge whereas SB behave a slider permitting longitudinal displacements due to the thermal effects occurring in the long span girders. Additionally, bearings have been mounted against the webs of the girders to resist lateral forces.

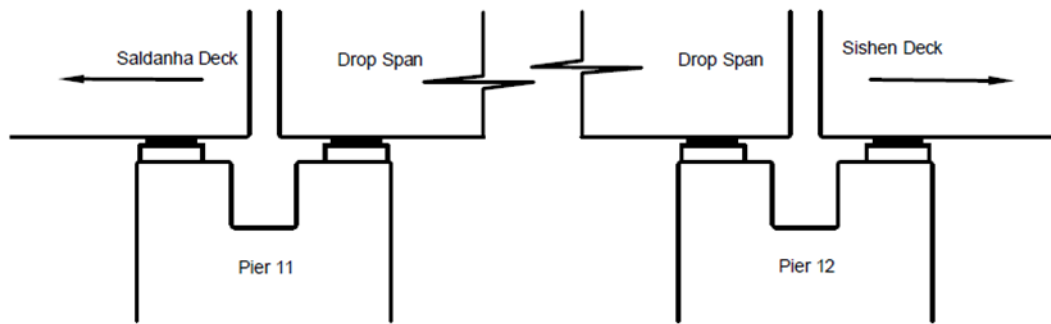


Figure 3-2: Pier 11 and 12 Bearing Configuration.

The Olifants River Viaduct carries a single railway line which facilitates the transportation of iron ore from Sishen to Saldanha Bay, where the ore is exported from. The 861 km continuously welded rails (CWR) travels over the entire length of the bridge. PY wing concrete sleepers span across the two rails such that the fastening system is held in place and that the 1067 mm gauge is maintained. Figure 3-3 shows the CWR and PY wing sleepers laying on the ballast which on top of the girder(Bester *et al.*, 1973).

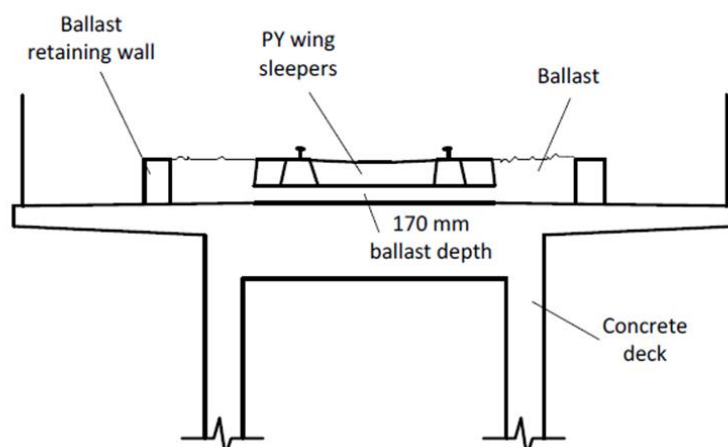


Figure 3-3: Olifants River Viaduct Cross Section(Bester *et al.*, 1973).



3.2 Loads on the Railway Viaduct

As mentioned previously the railway line and girder form a single system. Thus, for the Olifants River Viaduct to support trains this single system is meant to resist various loads such as temperature, vertical train loads, braking and acceleration forces.

3.2.1 Temperature

Change in ambient temperature is directly proportional to a change in concrete temperature and rail temperature. Essentially as ambient temperature increases concrete temperature will increase and because the 495 m long ends concrete girder segments of the viaduct are unrestrained towards the 45 m long concrete girder drop span, the 495 m segments will begin to expand in the direction of the drop span (Maree, 1987). The CWR on the concrete deck will resist this movement resulting in axial stresses in the opposing direction to that of the concrete deck expansion (Maree, 1987).

Similarly, the ambient temperature increases the rail temperature will increase and because the CWR on the bridge forms part of the central zone in the rail where expansion and contraction are not permitted, axial stresses will develop in the rail which will be transmitted to the concrete deck, bearings and the piers. However, for the purpose of this study rail stresses transmitted to the bearings and pier will not be investigated.

3.2.2 Vertical Train Loads

Empty and loaded trains of various lengths travel on the Sishen – Saldanha line (Bester, 2015). Considering the on the research that has been carried out on track-bridge interactions in high-speed rail, it is suggested that whilst the trains are on the bridge, they exert vertical loads on the track and consequently on the bridge deck resulting in deck end rotations as is shown in Figure 3-4. As the deck end rotates the rail will resist this displacement resulting in axial stresses in the rail.

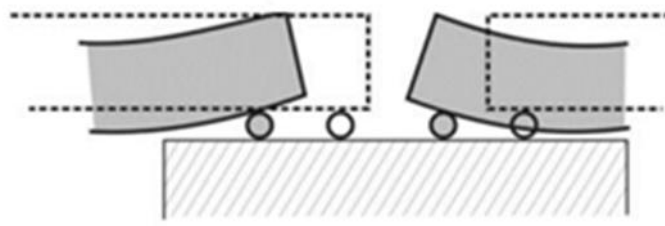


Figure 3-4: Depiction of Deck End Rotations Due to Vertical Loads.

3.2.3 Braking and Acceleration Loads

During the 2015 – 2017 period Transnet Freight Rail(TFR) operated various lengths of unloaded and loaded trains on the Sishen – Saldanha Iron Ore Route, the longest train that was operated during that period was a 342-wagon train. In October 2019, TFR launched a 4 km long train with 375 wagons (Liedtke, 2019). The use of powerful locomotives to pull these heavier and longer trains increases the longitudinal forces applied to a rail in service. Section 2.3 suggests that these



longitudinal forces due to acceleration and braking on the rail are then transmitted to the concrete deck, bearing pads and piers.

Simply, section 2.3 suggests that when trains accelerate, they exert compressive stresses on the rail and because the rail and deck form a single system, tensile stresses build up in the concrete deck in response to the compressive stresses in the rail. Conversely, trains that brake on the rail viaduct exert tensile stresses in the rail which results in compressive stresses in the concrete deck.

Furthermore, it is implied in section 2.3 that the magnitude of these stresses is influenced by the mass and the length of the trains. Consequently, loaded trains will exert greater braking and acceleration stresses than unloaded trains and longer trains will exert greater stresses than shorter trains.

The train categorization developed by Busatta(2018) is shown in Table 3-2. This train categorization with the addition of two new categories, which will be discussed in the Methodology, will be used in this study. It is important to note that using the available data it is not possible to accurately quantify longitudinal forces due to acceleration and braking. Resultantly the effect of braking and acceleration will not be investigated in this study. This study will investigate the effects of the presence of the train on the track instead. This study will investigate the effect of the presence of a train on rail forces, rail temperature, concrete temperature and longitudinal deck displacement.

Table 3-2: Train Categorization(Bussatta,2018)

Category	No. of Locomotives	No. of Wagons
A	1-2	12-60
B	2-3	84-124
C	2-4	184-228
D	4-6	312-342

3.2.4 Load Summary

The following loads act on the rail:

- Rail temperature stresses
- Braking and accelerating stress
- Stresses due to contraction and expansion of the deck
- Stresses transmitted from deck end rotations (train loads)

The following loads act on the bridge deck:

- Concrete temperature stresses
- Deck end rotation stresses



- Stresses transmitted from rail temperature
- Stresses due the trains braking and accelerating on the rail.

The description of the loads above further demonstrates how the track and the bridge deck interact to form one system. Any load that acts on the track will act on the bridge deck and vice versa. However, should any of these forces increase beyond the resistance limits of the track, the track will buckle or break, the concrete deck will expand and contract, the bridge piers and bearing pads will be catastrophically damaged and thus compromising the structural integrity of the heavy haul railway viaduct.

To prevent this from happening Transnet Freight Rail has installed 2 monitoring systems; the Wheel Impact Monitor and Weigh in Motion system (WIM-WIM) and the Saldanha System. The Weigh-in-Motion system monitors amongst other parameters changes in velocities and loads per axle ensuring that the prescribed loads and changes in velocity are not exceeded and the Saldanha System which monitors the temperature forces, rail forces and longitudinal deck displacement.

3.3 Monitoring Systems

3.3.1 WIM – WIM System

WIM-WIM is a strain gauge-based measuring system that is intended to identify wheel irregularities that introduce high dynamic forces into the track, weigh the train and identify bogies that are skew relative to the rail track. A bogie is described by (Bruton, 2011) as a chassis or framework carrying wheels that are attached to a vehicle such as a railway carriage.

The Sishen – Saldanha heavy haul line has two WIM–WIM systems namely SLK.SLK2.WIM.01 and SLK.K804.804.WIM.01 located at 175 km and 804 km from Sishen, respectively. SLK.SLK2.L04.WIM.01 is located on the 4th span of the Olifants viaduct. On the 4th span there are multiple strain measuring stations covering the full wheel rotation in order to allow for the maximum dynamic load that is exerted on the rail to be measured.

With the use of 32 strain gauges and a 32 channels data acquisition system, WIM-WIM uses a trigger to detect train passage and thereafter determines locomotives and wagon vehicle types, the speed of each vehicle as it passes over the sensor installation, skew bogies, maximum dynamic wheel mass and static bogie mass. It is to be noted that the detection of train passage is independent of the direction of the train. WIM-WIM samples data at a rate of 2.5 kHz per channel which is sufficient to capture speeds up to 150km/h. This is ideal because the speed limit on the bridge is 50 km/h. The system works by measuring the strains in the rail that are caused by the wheel contact force. Measured strains provide the dynamic mass while the filtered signal provides the static mass of the axle. This system weighs cars to an accuracy within 2% when calibrated and weighs total mass to an accuracy of within 0.5%.

A substantial amount of data processing is carried out by the system allowing for only the relevant information to be transmitted to the Integrated Train Condition Monitoring System (ITCMS) from where it can be viewed and downloaded using Transnet intranet. All Transnet Freight Rail WIM-



WIM systems transmit information to ITCMS. Relevant information is defined by Transnet as the following:

- **Date and Time** – Date and Time of the first vehicle on the 4th span is assigned to all the vehicles of a particular train.
- **Train Direction** - Up Towards Sishen and Down towards Saldanha Bay.
- **Train number** - Each train as a unique number.
- **Vehicle Orientation** - Forward or reverse which is only valid if the vehicle number has been logged.
- Vehicle Position in train
- **Component Name** - “SLK.SLK2.L04.WIM.01” in this case
- **Vehicle Type** - Each vehicle is either a locomotive or a wagon.
- **Vehicle Number** - All the vehicles that make up a train are numbered from 1 in the order which they have been arranged.
- **Component Number** - May refer to the wheel, axle bogie or vehicle side which is only valid if the vehicle number has been logged.
- **Wheel Dynamic Load** - The maximum instantaneous load for each wheel, in tonnes, recorded by the system.
- **Bogie Mass** - Quasi-Static load, in tonnes, exerted by the wheels of one bogie on the rails.
- **Vehicle Side Mass** – Quasi-Static load exerted by the wheels of one bogie on the rails.
- **Lateral Force** – Force exerted on the rails by the wheels
- **Gauge Spreading Force** -
- **Skewness of Each Bogie** -
- **Wheel Diameter** - characterizes wheels based on size
- **Speed of Vehicle** – Speed of each train as each vehicle passes over span 4

It is also important to note that data from WIM-WIM can also be accessed on site. To investigate the effect of the presence of a train on rail forces, rail temperature, concrete temperature and longitudinal deck displacement; the following information will be extracted:

- **Date and Time**
- **Train Direction**
- **Train number**
- **Component Name**
- **Vehicle Type**
- **Vehicle Number**
- **Speed**

3.3.2 Saldanha System

As mentioned in section 0, the geometry and boundary conditions of the Olifants River Viaduct can facilitate the increase of interaction forces beyond the design limits of the rail. Concern over the magnitude of these forces motivated the development of a system for their measurement; the Saldanha System (Freyer, 2004). To date there are currently two systems that have been installed



on the Olifants River Viaduct namely the Saldanha System (SS) and the Track Testing Centre (TTC) System. The layout of the two systems is displayed in Figure 3-5 overleaf. TTC acts as a backup system should the SS malfunction.

The measured data is summarized as follows:

- **Deck Deflection Saldanha Deck Left**
- **Deck Deflection Saldana Deck Right**
- **Deck Deflection Sishen Deck Left**
- **Deck Deflection Sishen Deck Right**
- **Rail Force Saldanha Deck Right Leg 1**
- **Rail Force Saldanha Deck Right Leg 2**
- **Rail Force Saldanha Deck Right Leg 3**
- **Rail Force Saldanha Deck Right Leg 4**
- **Rail Force Saldanha Deck Left Leg 1**
- **Rail Force Saldanha Deck Left Leg 2**
- **Rail Force Saldanha Deck Left Leg 3**
- **Rail Force Saldanha Deck Left Leg 4**
- **Rail Force Sishen Deck Right Leg 1**
- **Rail Force Sishen Deck Right Leg 2**
- **Rail Force Sishen Deck Right Leg 3**
- **Rail Force Sishen Deck Right Leg 4**
- **Rail Force Sishen Deck Left Leg 1**
- **Rail Force Sishen Deck Left Leg 2**
- **Rail Force Sishen Deck Left Leg 3**
- **Rail Force Sishen Deck Left Leg 4**
- **Rail Temperature Left**
- **Rail Temperature Right**
- **Ambient Temperature North**
- **Ambient Temperature South**
- **Concrete Temperature North**
- **Concrete Temperature South**

The SS transmits the measured parameters to the bridge data processor situated at the traffic control office in Saldanha Bay. The transmitted data is displayed in graphical format and monitored by traffic control personnel for warning and alarm conditions. This data is monitored in real time by Transnet Freight Rail (Pty) Ltd personal.



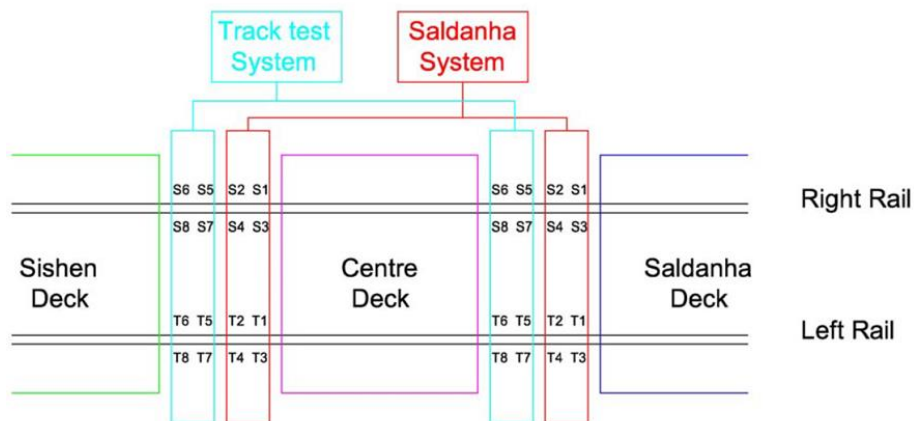


Figure 3-5: The SS and TTC System Layouts (Freyer, 2004).

Four W100 Linear Variable Differential Transformers (LVDTs) are attached to the inner side of the concrete decks over the expansion joints. The LVDTs have the capacity to measure from -100 mm to 100 mm. In the neutral position of the bridge, the LVDTs are fixed to 0 mm. A negative reading represents contraction and a positive reading expansion.

120 Ω XY Strain gauges are fixed to the neutral axis of the rail directly above the deck expansion joints. As per Figure 3-5, there are four locations represented by S and T, on which measurements are taken and at each of these locations four readings for rail force readings are captured. Negative readings refer to compressive forces and positive readings refer to tensile forces.

While the rail force and longitudinal deck displacement are measured using the same instruments for the SS and TTC System, different temperature sensors are utilized for the two systems. The SS employs the PT100 thermo resistors for ambient, concrete and rail temperature. Strain gauge technology is used for the for ambient, concrete and rail temperature.

Instruments are fitted on the left and right rail on the drop span. Ambient temperature is measured using a Stevenson screen which is mounted on the bridge railing directly above the drop span and concrete temperature is measured using instruments that are fixed on the inside of the right and left web of the concrete girder at span 9.

Data from the SS and TTC System is captured at a frequency of 0.006 Hz, and it is monitored by a computer software which converts the measured strains from the rail and bridge into longitudinal deck displacement, rail force and temperature. Warning and alarm levels are programmed into the system and are triggered at critical rail force values. The trigger levels and the actions that need to be carried out at each level have been presented in Table 3-3 overleaf.



Table 3-3: SS Warning and Alarm Levels (Freyer, 2004).

Type of Trigger	Rail Force Category	Action to be Taken
Warning Level	Between -800 kN and -900 kN	<ul style="list-style-type: none"> • Trains may proceed across the bridge at a speed restriction of 15 km/h. • The speed restriction shall remain until the force has dropped below 800 kN and a Track Inspector has inspected the track condition and declared the track safe for the passage of trains at speed greater than 15 km/h.
Warning Level	Between 1300 kN and 1400 kN	<ul style="list-style-type: none"> • Trains may proceed across the bridge at a speed restriction of 15 km/h. • The speed restriction shall remain until the force has dropped below 1300 kN and a Track Inspector has inspected the track condition and declared the track safe for the passage of trains at a speed greater than 15 km/h.
Alarm Level	Greater than -900 kN	<ul style="list-style-type: none"> • All trains shall be instructed to stop at the approach to the bridge • A Track Inspector shall immediately inspect the track condition • No train may cross the bridge until the force has dropped below 900 kN and the track is declared safe for the passage of trains by a Track Inspector. • As soon as the force has dropped below 900 kN and the track is declared safe for the passage of trains, actions shall be taken as per the rail force category that applies.
Alarm Level	Between 1400 kN and 1500 kN	<ul style="list-style-type: none"> • All trains shall be instructed to stop at the approach to the bridge. • Trains may only proceed across the bridge at a speed restriction of 15 km/h and piloted by a Track Inspector after the track has been declared safe for the passage of trains. • The speed restriction and piloting by a Track Inspector shall remain until the force has dropped below 1400 kN. As soon as the force has dropped below 1400 kN, actions shall be taken as per the rail force category that applies.
Alarm Level	Greater than 1500 kN	<ul style="list-style-type: none"> • All trains shall be instructed to stop at the approach to the bridge. • A Track Inspector shall immediately inspect the track condition.



		<ul style="list-style-type: none"> • No train may cross the bridge until the force has dropped below 1500 kN and declared safe for the passage of trains by a Track Inspector. • As soon as the force has dropped below 1500 kN and the track is declared safe for the passage of trains, actions shall be taken as per the rail force category that applies.
--	--	---

Data from the SS will be used to:

- Explore the observed patterns of rail forces, longitudinal deck displacements, ambient temperature, concrete temperature and rail temperature over time.
- Investigate the effect of rail temperature variation on rail forces and the longitudinal displacement of the deck.
- Examine the effect of variation in concrete temperature on the longitudinal deck displacement, rail forces and variation in rail temperature as well as the effect of longitudinal deck displacement on rail forces.
- Investigate the effects of the presence of the train(vertical train loads) on the longitudinal displacement of the deck, rail forces and concrete temperature.
- Develop a predictive model which makes use of ambient temperature forecasts to predict rail forces, longitudinal deck displacement, rail temperature and concrete temperature estimates that can assist in planned infrastructure management.



4. Methodology

This chapter describes the procedure that was implemented to (i) explore the observed patterns of rail forces, longitudinal deck displacements, ambient temperature, concrete temperature and rail temperature over time, (ii) investigate the effect of rail temperature variation on rail forces and the longitudinal displacement of the deck, (iii) examine the effect of variation in concrete temperature on the longitudinal deck displacement, rail forces and variation in rail temperature as well as the effect of longitudinal deck displacement on rail forces, (iv) investigate the effects of the presence of the train (vertical train loads) on the longitudinal displacement of the deck, rail forces and concrete temperature and (v) develop predictive multiple linear regression model that will assist in the management and maintenance heavy haul railway bridges with an expansion length greater than 90m.

The methodology in this chapter proposes a 4-step process as shown in Figure 4-1.

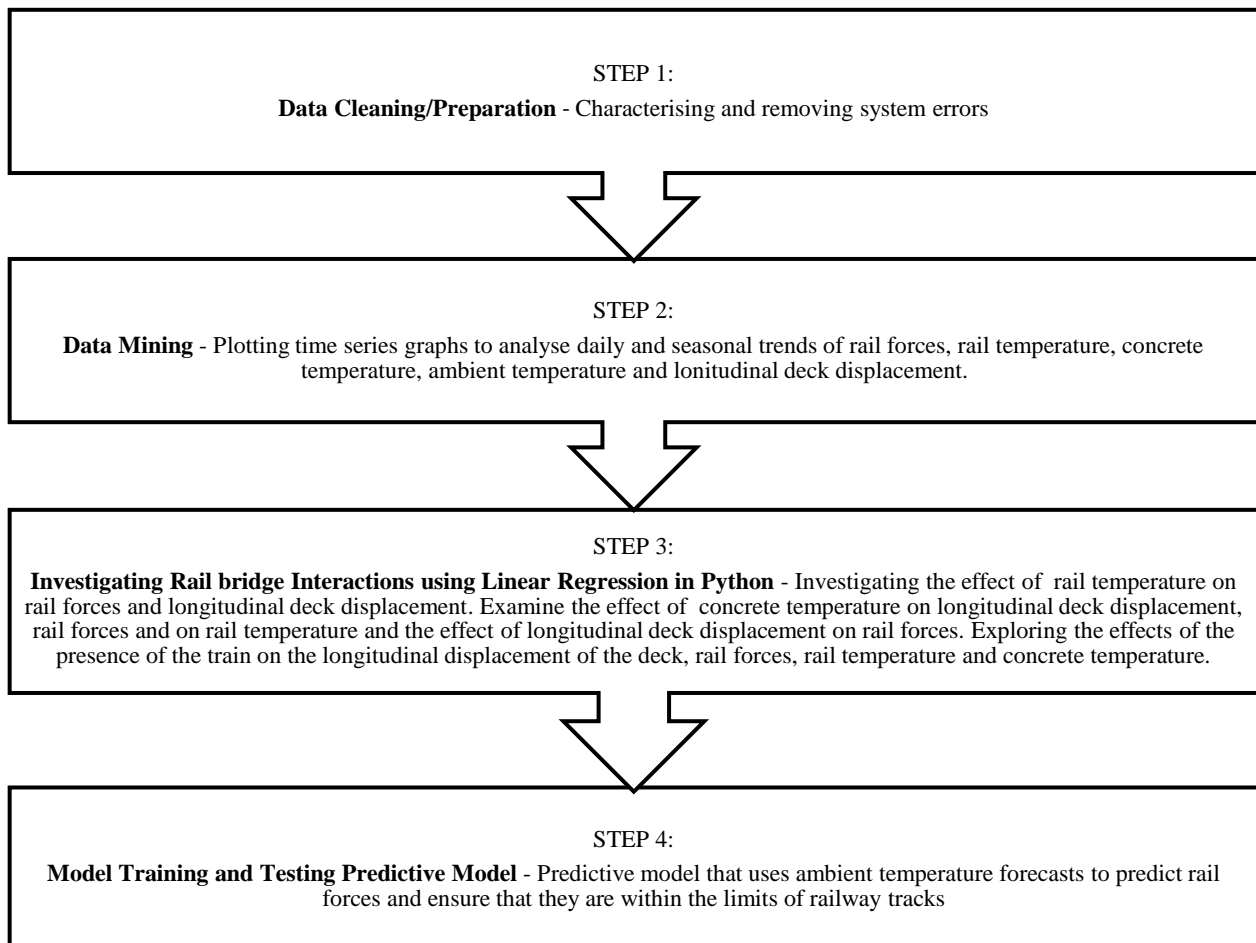


Figure 4-1: Methodology Process



4.1 Data Cleaning/Preparation

Two sets of data were used for this study, the data from WIM – WIM System and that from SS. This section details the various methods that were used to clean and prepare both sets of data.

4.1.1 Data Cleaning/Preparation – Saldanha System

The Saldanha System data was obtained in Microsoft Access file types as shown in Figure 4-2. The data received was logged from August 2015 – January 2019. It can be seen on Figure 4-2 that each column represents data acquisition channels for the respective measurements as detailed in section 3.3.2.

Row_ID	Reading_Date	Ch1	Ch2	Ch3	Ch4	Ch5	Ch6	Ch7	Ch8	Ch9	Ch10	Ch11
3	2016/01/01 00:00:41	24,59	10,98	-8,09	-8,11	583	297	277	269	155	149	177
4	2016/01/01 00:03:41	24,54	10,94	-8,18	-8,18	579	300	280	272	158	153	180
5	2016/01/01 00:06:41	24,49	10,91	-8,25	-8,26	578	305	283	274	160	156	183
6	2016/01/01 00:09:41	24,43	10,83	-8,33	-8,34	575	306	287	277	163	158	185
7	2016/01/01 00:12:41	24,35	10,76	-8,42	-8,42	570	312	287	279	166	159	188
8	2016/01/01 00:15:41	24,29	10,7	-8,48	-8,49	569	312	292	282	169	163	190
9	2016/01/01 00:18:41	24,23	10,64	-8,55	-8,56	567	313	295	286	170	166	193

Figure 4-2: Depiction of Saldanha System Raw Data Format.

The raw data from Transnet Freight Rail (Pty) Ltd was accompanied by a table indicating the measurement that each channel represents. The legend is shown in Figure 4-3.

No.	Channel	Units	Value
0	Deck Deflection Sald Deck Left	mm	
1	Deck Deflection Sald Deck Right	mm	
2	Deck Deflection Sish Deck Left	mm	
3	Deck Deflection Sish Deck Right	mm	
4	Rail Force Sald Deck Right Leg 1	kN	
5	Rail Force Sald Deck Right Leg 2	kN	
6	Rail Force Sald Deck Right Leg 3	kN	
7	Rail Force Sald Deck Right Leg 4	kN	
8	Rail Force Sald Deck Left Leg 1	kN	
9	Rail Force Sald Deck Left Leg 2	kN	
10	Rail Force Sald Deck Left Leg 3	kN	
11	Rail Force Sald Deck Left Leg 4	kN	
12	Rail Force Sishen Deck Right Leg 1	kN	
13	Rail Force Sishen Deck Right Leg 2	kN	
14	Rail Force Sishen Deck Right Leg 3	kN	
15	Rail Force Sishen Deck Right Leg 4	kN	
16	Rail Force Sishen Deck Left Leg 1	kN	
17	Rail Force Sishen Deck Left Leg 2	kN	
18	Rail Force Sishen Deck Left Leg 3	kN	
19	Rail Force Sishen Deck Left Leg 4	kN	
20	Left Rail Temperature	°C	
21	Right Rail Temperature	°C	
22	Air Temperature	°C	
23	Air Temperature	°C	
24	Concrete Temperature North	°C	
25	Concrete Temperature South	°C	
26	Not used		
27	Not used		

Figure 4-3: Saldanha System Channel Legend



The raw data was converted to Microsoft excel file types and each column was renamed as indicated in the table below. Thereafter the data was cleaned. The respective measurements from each channel will be referred to as variables for this study.

Table 4-1: Channel number and related channel names.

Channel No.	Channel Name According Transnet Channel List	New Column Name
1	Deck Deflection Saldanha Deck Left	DDSaL
2	Deck Deflection Saldana Deck Right	DDSaR
3	Deck Deflection Sishen Deck Left	DDSiL
4	Deck Deflection Sishen Deck Right	DDSiR
5	Rail Force Saldanha Deck Right Leg 1	RFSaR1
6	Rail Force Saldanha Deck Right Leg 2	RFSaR2
7	Rail Force Saldanha Deck Right Leg 3	RFSaR3
8	Rail Force Saldanha Deck Right Leg 4	RFSaR4
9	Rail Force Saldanha Deck Left Leg 1	RFSaL1
10	Rail Force Saldanha Deck Left Leg 2	RFSaL2
11	Rail Force Saldanha Deck Left Leg 3	RFSaL3
12	Rail Force Saldanha Deck Left Leg 4	RFSaL4
13	Rail Force Sishen Deck Right Leg 1	RFSiR1
14	Rail Force Sishen Deck Right Leg 2	RFSiR2
15	Rail Force Sishen Deck Right Leg 3	RFSiR3
16	Rail Force Sishen Deck Right Leg 4	RFSiR4
17	Rail Force Sishen Deck Left Leg 1	RFSiL1
18	Rail Force Sishen Deck Left Leg 2	RFSiL2
19	Rail Force Sishen Deck Left Leg 3	RFSiL3
20	Rail Force Sishen Deck Left Leg 4	RFSiL4
21	Rail Temperature Left	RTL
22	Rail Temperature Right	RTR
23	Ambient Temperature North	ATN
24	Ambient Temperature South	ATS
25	Concrete Temperature North	CTN
26	Concrete Temperature South	CTS



Data cleaning is the process of detecting and removing corrupt or inaccurate data. It is essential to ensure that the analysis process does not generate unreliable results.

According to the South African Weather Service the ambient temperature range in and around the Lutzville and Vredendal towns was between 0 °C and 50 °C. Additionally, according to alarm information received from Transnet Freight Rail (Pty) Ltd, for the data that was logged from August 2015 to January 2019, the tensile rail forces recorded had not been greater than 2000 kN and the compressive forces have not been greater than -1500 kN.

Therefore, ambient temperature greater than 50 °C and less than 0 °C was identified as an error. Similarly, rail forces above 2000 kN and -1500 kN were identified as errors. These errors were treated by using a filter function in R software to delete the entire row on which the errors occur as shown in Figure 4-4 below. The red circles represent the error identified and the black line represents the row to be deleted.

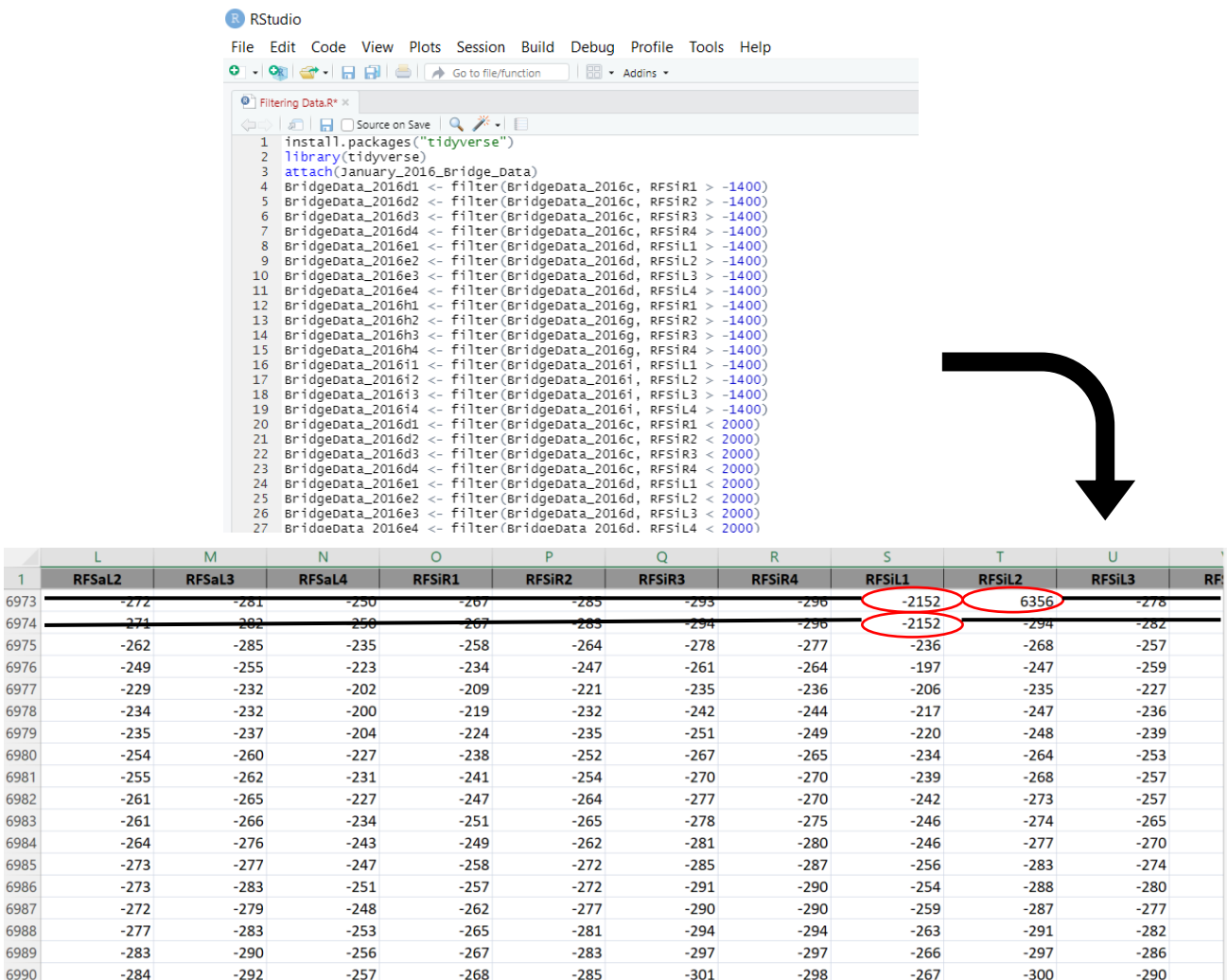


Figure 4-4: Depiction of Removing Rows with Errors.



Empty cells as well as more than 3 consecutive 0's in a column as depicted in below in Figure 4-5 were classified as errors. These errors were treated by deleting the entire row on which the error occurred just as it was illustrated in Figure 4-4.

1	RFSaL3	RFSaL4	RFSiR1	RFSiR2	RFSiR3	RFSiR4	RFSiL1	RFSiL2	RFSiL3
2	266	294	293	283	270	278	0	0	283
3	269	292	294	283	273	278	0	0	282
4	270	297	300	287	277	283	0	0	288
5	276	302	303	291	281	288	0	0	293
6	280	307	308	297	285	293	0	0	296
7	286	311	313	300	291	297	0	0	302
8	289	315	316	306	294	301	0	0	306
9	293	320	320	308	298	306	0	0	309
10	296	323	324	313	301	310	0	0	315
11	301	327	329	317	306	314	0	0	316
12	305	331	331	320	310	317	0	0	321
13	309	333	336	324	313	321	0	0	324
14	312	335	337	329	316	323	0	0	328
15	315	340	341	330	319	328	0	0	331
16	318	344	344	333	321	326	0	0	334
17	321	347	347	334	324	331	0	0	335
18	322	348	350	340	327	332	0	0	338

Figure 4-5: Type Zero Error.

After filtering out the errors, time series graphs were plotted using R software to check for other outliers. Additionally, the ambient temperature range as captured by the SS was compared to the ambient temperature range that was supplied by SAWS for the 2015 – 2018 period. These comparisons revealed the following:

- In July 2017 the system was off.
- The ambient temperature data recorded by SS was significantly higher than that recorded by SAWS.

Given the result of the comparisons as listed above and that the 2015 Data received from Transnet Freight Rail(Pty) Ltd, was only last five months of the year, it was decided that this study will be based on 2016 data to capture seasonal changes and decrease uncertainties. Approximately 0.1% of the data was erroneous and therefore removing the erroneous data will have negligible effects on this study.

4.1.2 Data Cleaning/Preparation – WIM -WIM System

WIM-WIM System makes use of 32 strain gauges and a 32-channel data acquisition system to detect train passage and thereafter records various information as detailed in section 3.3.1. For this study the information as represented in Figure 4-6 below was extracted from the WIM-WIM system database.



Column1	H	C	D	E	F	G	H	I	J	K	L	M	N	
	D	SLK.SLK2.L04.WIM.01	2016/01/27 12:22	Down	20160127-122156D	L	?		1	Speed [V]	NA	NA	21.2	km/h
	D	SLK.SLK2.L04.WIM.01	2016/01/27 12:22	Down	20160127-122156D	L	?		2	Speed [V]	NA	NA	21.8	km/h
	D	SLK.SLK2.L04.WIM.01	2016/01/27 12:22	Down	20160127-122156D	W	?		3	Speed [V]	NA	NA	22.3	km/h
	D	SLK.SLK2.L04.WIM.01	2016/01/27 12:22	Down	20160127-122156D	W	?		4	Speed [V]	NA	NA	22.7	km/h
	D	SLK.SLK2.L04.WIM.01	2016/01/27 12:22	Down	20160127-122156D	W	?		5	Speed [V]	NA	NA	23.1	km/h
	D	SLK.SLK2.L04.WIM.01	2016/01/27 12:22	Down	20160127-122156D	W	?		6	Speed [V]	NA	NA	23.5	km/h
	D	SLK.SLK2.L04.WIM.01	2016/01/27 12:22	Down	20160127-122156D	W	?		7	Speed [V]	NA	NA	23.9	km/h
	D	SLK.SLK2.L04.WIM.01	2016/01/27 12:22	Down	20160127-122156D	W	?		8	Speed [V]	NA	NA	24.2	km/h
	D	SLK.SLK2.L04.WIM.01	2016/01/27 12:22	Down	20160127-122156D	W	?		9	Speed [V]	NA	NA	24.6	km/h
	D	SLK.SLK2.L04.WIM.01	2016/01/27 12:22	Down	20160127-122156D	W	?		10	Speed [V]	NA	NA	24.9	km/h
	D	SLK.SLK2.L04.WIM.01	2016/01/27 12:22	Down	20160127-122156D	W	?		11	Speed [V]	NA	NA	25.3	km/h
	D	SLK.SLK2.L04.WIM.01	2016/01/27 12:22	Down	20160127-122156D	W	?		12	Speed [V]	NA	NA	25.6	km/h
	D	SLK.SLK2.L04.WIM.01	2016/01/27 12:22	Down	20160127-122156D	W	?		13	Speed [V]	NA	NA	25.9	km/h
	D	SLK.SLK2.L04.WIM.01	2016/01/27 12:22	Down	20160127-122156D	W	?		14	Speed [V]	NA	NA	26.3	km/h
	D	SLK.SLK2.L04.WIM.01	2016/01/27 12:22	Down	20160127-122156D	W	?		15	Speed [V]	NA	NA	26.6	km/h
	D	SLK.SLK2.L04.WIM.01	2016/01/27 12:22	Down	20160127-122156D	W	?		16	Speed [V]	NA	NA	26.9	km/h
	D	SLK.SLK2.L04.WIM.01	2016/01/27 12:22	Down	20160127-122156D	W	?		17	Speed [V]	NA	NA	27.2	km/h
	D	SLK.SLK2.L04.WIM.01	2016/01/27 12:22	Down	20160127-122156D	W	?		18	Speed [V]	NA	NA	27.5	km/h

Figure 4-6: WIM-WIM Data.

The raw WIM-WIM data represents the following below:

- **Component Name** - “SLK.SLK2.L04.WIM.01” in this case
- **Time** – Date and Time of the first vehicle on the 4Th span is assigned to all the vehicles of a particular train.
- **Direction** – This indicates the direction of the train. Up is towards Sishen during which the trains are unloaded and down is towards Saldanha Bay during which the trains are loaded.
- **Train number** - Each train has a unique number.
- **Vehicle Number** - Represented by L or W. L is for locomotives and W is for wagons.
- **Vehicle Orientation** - Forward or reverse which is only valid if the vehicle number has been logged.
- **Vehicle Position in train** – Numbers represent the position of the vehicle on the train.

The data was cleaned using a Matlab script from a study that investigated reliability based live loads for structural assessment of bridges on heavy-haul railway lines authored by Matongo(2018). The study made use of the same data.

. The data was grouped into loaded trains which travel from Sishen to Saldanha Bay with iron ore in the wagons and unloaded trains which travel from Saldanha Bay to Sishen with empty wagons. Duplicate time stamps for the same trains were defined as errors and these errors were deleted from the data set, using the above-mentioned Matlab script. To ensure that the train data is comparable to the data measured in the SS, this study will use WIM- WIM data that was recorded for the 2016 period.

In preparation to investigate the effect the presence of a train has on rail forces, rail temperature, concrete temperature and longitudinal deck displacement; the trains were allocated unique names



and categorized based on the number of locomotives and wagons as explained in section 3.2.3. The name of each train will signify the order in which wagons and locomotives are arranged. The naming convention is shown in Figure 4-7. The letter ‘L’ as annotated in Figure 4-7 represents the locomotives in the train and the letter ‘W’ represents the number of wagons in the train.

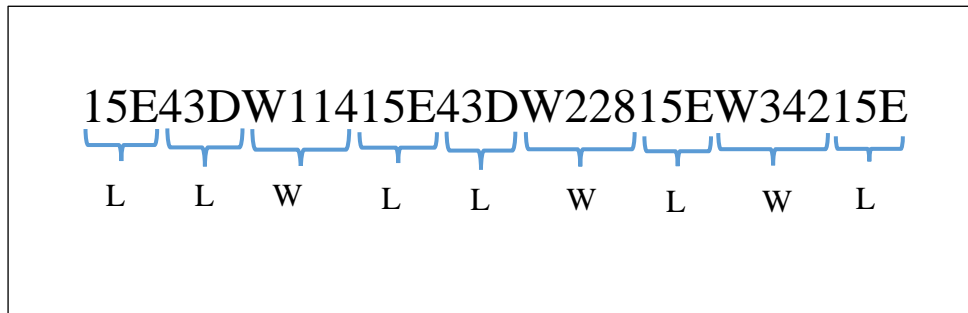


Figure 4-7: Train Naming Convention in this Study.

Using a Python script, the data was categorized into the 6 different groups as shown in Table 4-2. category A – D as shown in Table 4-2 was obtained from Busatta(2018) and category E to F was added. Category E represents trains that comprised of just locomotives and no wagons. Group F represents just wagons, which is logged as an error because a train cannot function without a locomotive. The process of categorizing trains into groups assisted in investigating the effect that the presence of a train has on rail forces, rail temperature, concrete temperature and longitudinal deck displacement.

Table 4-2: Train Categories for this Study.

Category	No. of Locomotives	No. of Wagons
A	1-2	12-60
B	2-3	84-124
C	2-4	184-228
D	4-6	312-342
E	1-2	0
F	0	1-342



4.2 Data Mining

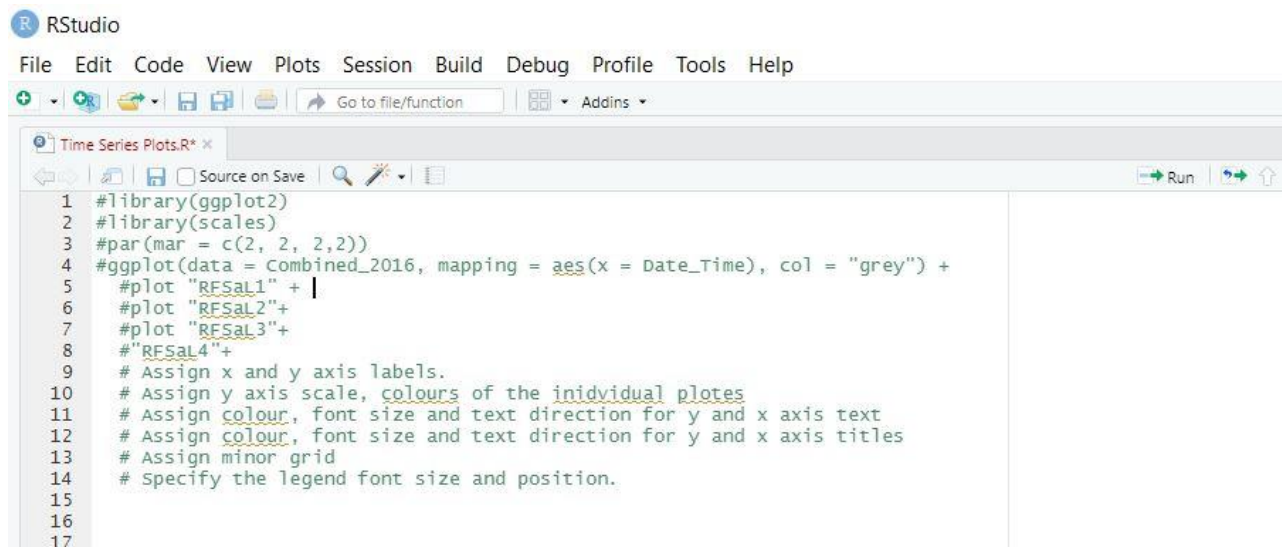
4.2.1 Data Mining SS Data

As mentioned in section 4.1.1, this study will use the SS data that was recorded for the 2016 period. Rail forces are measured at four locations on the ORV as shown in Figure 3-5 in section 3.3.2. At each of these locations four measurements of rail forces are taken. The measures of central tendency; mean and median, were computed for the rail force variables at all these locations. The dispersion of these variables was described using standard deviation and range. Additionally, the 25th percentile, 75th percentile, minimum and maximum were also computed. To conclude the section on descriptive statistics for rail forces the probability density function was defined.

On the other hand, one measurement of longitudinal deck displacement is taken at four locations as described in section 3.3.2. These measured variables were described using measures of central tendency; mean and median. The dispersion of the data was represented using standard deviation and range. Additionally, the 25th percentile, 75th percentile, minimum and maximum were also computed. The probability density function of longitudinal deck displacements was also defined.

Two measurements on either side of the ORV are taken of the ambient temperature, concrete temperature and rail temperature. These temperatures were described using measures of central tendency, mean and median. This data's dispersion was specified using the standard deviation and range. The measures of position, 25th percentile, 75th percentile, minimum and maximum values were also computed. To conclude the section on descriptive statistics for temperatures the probability density function was defined.

After statistical summaries had been computed for all the variables measured by the SS as listed above, time series graphs were plotted to investigate the observed pattern of longitudinal deck displacements, rail forces, ambient temperature, concrete temperature and rail temperature over the 2016 period. Time series graphs were plotted using an R Software script that is shown in Figure 4-8.



```

RStudio
File Edit Code View Plots Session Build Debug Profile Tools Help
Go to file/function Addins
Time Series Plots.R* x
Source on Save Run
1 #library(ggplot2)
2 #library(scales)
3 #par(mar = c(2, 2, 2,2))
4 #ggplot(data = Combined_2016, mapping = aes(x = Date_Time), col = "grey") +
5 #plot "RFSa1" + |
6 #plot "RFSa2"+
7 #plot "RFSa3"+
8 #"RFSa4"+
9 # Assign x and y axis labels.
10 # Assign y axis scale, colours of the individual plots
11 # Assign colour, font size and text direction for y and x axis text
12 # Assign colour, font size and text direction for y and x axis titles
13 # Assign minor grid
14 # Specify the legend font size and position.
15
16
17

```

Figure 4-8: R Script used to plot time series graphs.



4.2.2 Data Mining WIM – WIM Data

The trains from the WIM-WIM system were grouped into the categories shown in Table 4-2 in section 4.1.2. Monthly record of trains in their respective categories was tabulated. This data was then represented in bar graphs to compare the monthly and seasonal record of trains in different categories. This data will assist in investigating the effects of the presence of the train (vertical train loads) on the longitudinal displacement of the deck, rail forces and concrete temperature.

4.3 Linear Regression Analysis Theory

Regression is a fundamental statistical tool that is used to establish whether a relationship exists between two or more variables and to what extent this relationship exists (Frost, 2020). In linear regression analysis an event of interest is considered that has numerous observations. Each observation will have two or more features depending on the type of regression. Following, the assumption each of the features depends on the others, a function that maps the features to each other is sought.

The dependent features are referred to as the dependent variables or outputs and independent features are referred to as independent variables or inputs. Dependent variables are commonly denoted with y and independent variables are commonly denoted with x . In the case where there are two or more independent variables they are commonly represented as the vector $\mathbf{x} = (x_1, x_2, \dots, x_r)$. The subscript r represents the total number of inputs.

Regression assumes a linear relationship between y and \mathbf{x} such that:

$$y = \beta_0 + \beta_1 x_1 + \dots + \beta_r x_r + \varepsilon \quad \dots 4.1$$

This assumption is used to establish if a relationship exists between y and \mathbf{x} . The coefficients $\beta_0, \beta_1, \dots, \beta_r$ are regression coefficients and yet again the subscript r represents the total number of inputs and ε is the random error. The random error is the sum of the deviations within the regression line. It explains the differences between the theoretical values and the observed values.

In addition to the main effects that are shown in Equation 4.1, in regression there are interaction effects. Interaction effects occur when the effect of an independent variable on a dependent variable relies on the value of one or even more than one other independent variable (Khot, 2020). In regression an interaction effect is represented as the product of two independent variables. This is shown in Equation 4.2 below.

$$y_1 = b_0 + b_1 x_1 + b_2 x_2 + b_3 x_1 x_2 \quad \dots 4.3$$

When the relationship between the dependent and independent variable has been established. The linear regression relationship can be used to forecast responses by building a predictive model. The linear regression calculates the estimators of the regression coefficients which are commonly referred to as predicted weights. The predicted weights are denoted by b_0, b_1, \dots, b_r such that estimated regression function is as shown in Equation 4.4 below:

$$f(\mathbf{x}) = b_0 + b_1 x_1 + \dots + b_r x_r \quad \dots 4.5$$



Linear regression is about determining the predicted weights that correspond to the smallest residual value. Residual value is the difference between the observed value and the value predicted by the model. To get the predicted weights that corresponds to the smallest residual value, regression minimizes the root mean squared error (RMSE). This approach is called the method of ordinary least squares. RMSE values are influenced by the range of dependent variable. To compare RMSE values across models the RMSE values must be normalized, using Equation 4.6, such that they produce values between 0 and 1, where values closer to 0 represent better fitting models.

$$\text{Normalized RMSE(NRMSE)} = \text{RMSE} / (\text{range of dependent variable}) \quad \dots 4.7$$

The fit of a linear regression model can also be indicated by the coefficient of determination denoted by R^2 . R^2 indicates how much of the variability in y is caused by its relationship with x . R^2 is represented by values between 0 and 1, where 1 is a perfect fit as the observed values and the predicted values fit completely with each other.

There are three main types of linear regression, single-variate linear regression, multiple linear regression and polynomial linear regression. Single variate linear regression has a single independent variable, whereas multiple linear regression has two or more dependent variables. Polynomial linear regression is more of a generalized case of linear regression which assumes a polynomial relationship between the dependent and independent variable. This study will make use of the single-variate linear regression and the multiple linear regression.

A big concern that is associated with regression models is overfitting and underfitting. Overfitting occurs when a model describes features that are because of the variance in the data rather than the underlying distribution of the data. In such cases when model is applied to known data it yields high values of R^2 and it is applied on new data sets it yields low values of R^2 . In contrast underfitting happens when the model is too simple and fails to capture the dependencies in known data and new data.

There are numerous techniques that can be used to prevent underfitting and over fitting in predictive models. One standard technique is splitting your total data into training and testing data sets. The training data set is used to develop the model. The testing data is run against model. The results from the training and testing data sets are compared. If the results are the same, it means the model works well.

In addition to an equation that describes the statistical relationship between the dependent variable and the independent variable and R^2 , statistical software also generates a p-value for each term in the equation (Stojiljkovic, 2020). The p-value for each term tests the null hypothesis. We have two hypothesis:

Null hypothesis(H_0): The independent variable and dependent variable are not related ($\beta_1 = 0$)

Alternative hypothesis(H_1): The independent variable and dependent variable are related ($\beta_1 \neq 0$)

A p-value that is less than or equals to 0.05 indicates that H_0 may be rejected. That is, the independent variable does influence the dependent variable.



4.4 Linear Regression Analysis in Python

4.4.1 Track - Bridge Interaction Investigation Using Single Variate Regression

This section describes the methodology that was followed to address the objective 2, 3 and 4 as listed below:

2. Investigate the effect of rail temperature variation on rail forces and the longitudinal displacement of the deck.
3. Examine the effect of variation in concrete temperature on the longitudinal deck displacement, rail forces and variation in rail temperature as well as the effect of longitudinal deck displacement on rail forces.
4. investigate the effects of the presence of the train (vertical train loads) on the longitudinal displacement of the deck, rail forces, rail temperature and concrete temperature.

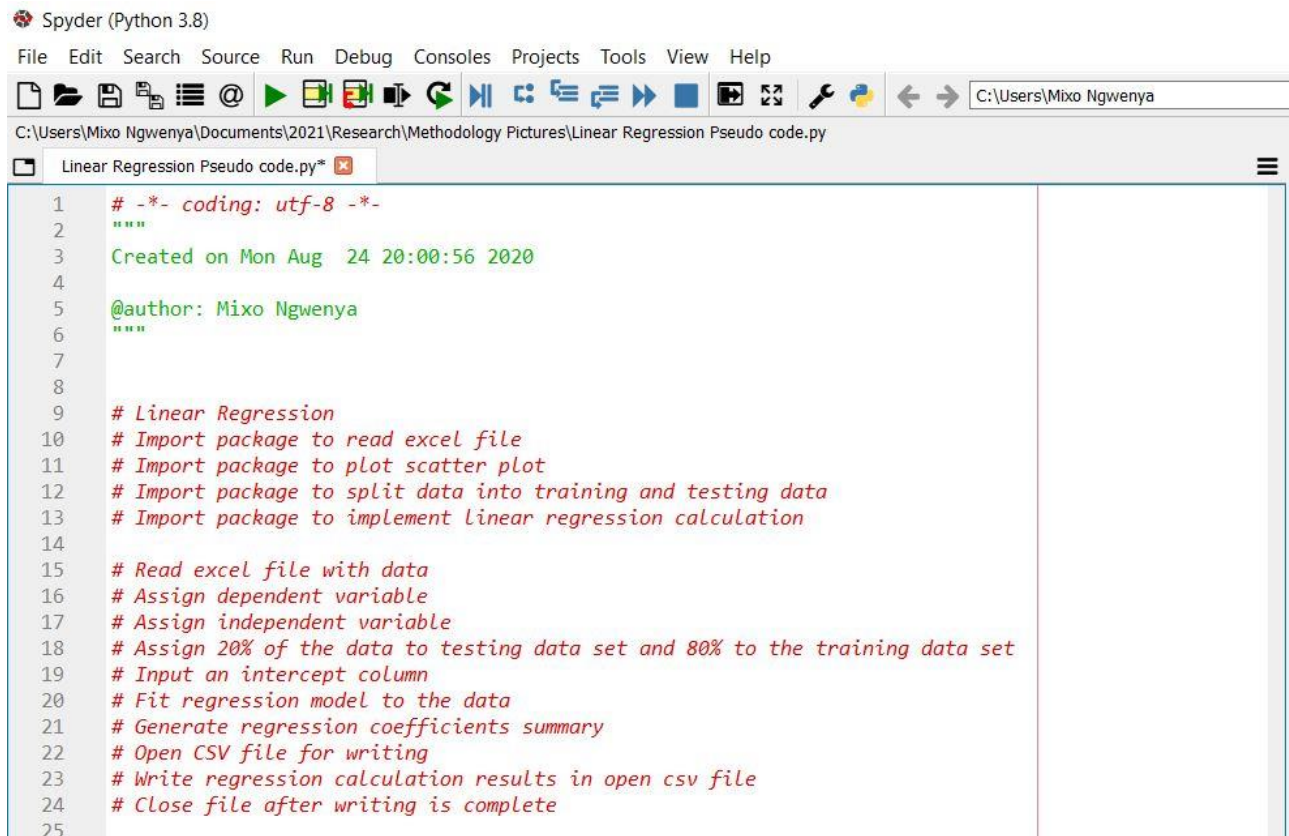
In preparation to investigate the relationships listed above the dependent and independent variables were listed in Table 4-3 below:

Table 4-3: Dependent and Independent Variables for Linear Regression.

Objective No.	Dependent Variable	Independent Variable
2	RFSiR3	DDSiR
2	RFSiR3	ATS
2	RFSiR3	CTS
2	RFSiR3	RTR
3	DDSiR	ATS
3	DDSiR	CTS
3	DDSiR	RTR
4	RFSiR3	Train Categories
4	DDSiR	Train Categories
4	CTS	Train Categories
4	RTR	Train Categories

Each row in Table 4-3 represents a relationship that was investigated using linear regression in Python. Python develops a regression model using the ordinary least squares method, denoted as `ols` in the script. Figure 4-9 shows a single-variate regression script, each line in the script is explained on the right side of the figure. Although Figure 4-9 shows a script for training data, this process was carried out for both training and testing data. To confirm the fit scatter plot of each data set was plotted its regression model.





```
1  # -*- coding: utf-8 -*-
2  """
3  Created on Mon Aug 24 20:00:56 2020
4
5  @author: Mixo Ngwenya
6  """
7
8
9  # Linear Regression
10 # Import package to read excel file
11 # Import package to plot scatter plot
12 # Import package to split data into training and testing data
13 # Import package to implement linear regression calculation
14
15 # Read excel file with data
16 # Assign dependent variable
17 # Assign independent variable
18 # Assign 20% of the data to testing data set and 80% to the training data set
19 # Input an intercept column
20 # Fit regression model to the data
21 # Generate regression coefficients summary
22 # Open CSV file for writing
23 # Write regression calculation results in open csv file
24 # Close file after writing is complete
25
```

Figure 4-9: Linear Regression Python Script.

The results from the single variate linear regression exercise will be used to develop a multiple linear regression model.

4.4.2 Multiple Linear Regression Predictive Maintenance Model

To develop a predictive multiple linear regression model that will assist in the management and maintenance heavy haul railway bridges with an expansion length greater than 90m, the results generated in single-variate linear regression analysis were used. The developed prediction model accepts ambient temperature as input and produces rail forces, longitudinal deck displacement, rail temperature and concrete temperature as an output.

According to section 2.3 track and the bridge are interconnected and thus the behaviour of the track has an effect on the behaviour bridge and inversely the behaviour of the bridge has an effect on the behaviour of the track. Thus, it can be said that the concrete temperature, rail temperature, rail forces and longitudinal deck displacements are interdependent at different extents. These relationships were used to develop a predictive multiple linear regression model. The predictive model was implemented using a four-step process as explained overleaf.



The first step involved using the results that were generated using the methods in section 4.4.1, to identify dependent variables that are linearly related to ATS. Amongst the dependent variables that are linearly related to ATS, the dependent variable with the highest R^2 was named y_1 . ATS became x_1 and was used to predict y_1 such that:

$$y_1 = b_0 + b_1x_1$$

The second step considered dependent variables that are linearly related to x_1 and amongst them identify the variable with greatest value of R^2 , which was named y_2 . In this second step y_1 became x_2 and the interaction between x_1 and x_2 was included such that:

$$y_2 = b_0 + b_1x_1 + b_2x_2 + b_3 x_1x_2$$

In the third step dependent variables that are linearly related to x_2 were considered and, just like in step two, amongst the variables with greatest value of R^2 was named y_3 and y_2 became x_2 . The regression equation in step 3 then consisted of 3 independent variables and all the possible interactions of the independent variables were considered such that:

$$y_3 = b_0 + b_1x_1 + b_2x_2 + b_3 x_1x_2 + b_4 x_3 + b_5 x_2x_3 + b_6 x_1x_3 + b_7 x_1x_2x_3$$

In the fourth and final there was one variable that had not been added to the model. This variable was named y_4 and y_3 became x_4 such that multiple linear regression was:

$$y_4 = b_0 + b_1x_1 + b_2x_2 + b_3 x_1x_2 + b_4 x_3 + b_5 x_2x_3 + b_6 x_1x_3 + b_7 x_1x_2x_3 + b_8 x_4 + b_9 x_1x_4 + b_{10} x_2x_4 + b_{11} x_1x_4 + b_{12} x_1x_2x_4 + b_{13} x_2x_3x_4 + b_{14} x_1x_3x_4 + b_{15} x_1x_2x_3x_4$$

The four steps that were followed to develop the predictive multiple linear regression model were implemented in python using pandas, sklearn and statsmodel in python. The model was trained and tested using 80 and 20 split. 80 percent of the data was used to train the m



5. Data Analysis

5.1 Data Descriptions

5.1.1 Introduction

In this section measures of central tendency, measures of dispersion and measures of distribution are used to describe the SS system data for this study. Additionally, the trains from the WIM – WIM system are categorised in this section.

5.1.2 Longitudinal Deck Displacement Statistical Summaries

Table 5-1: Longitudinal Deck Displacement Statistical Summary.

	DDSaL (mm)	DDSaR (mm)	DDSiL (mm)	DDSiR (mm)
count	369087	369087	369087	369087
mean	-26.59	-39.74	-53.91	-54.12
std	22.24	22.23	20.36	20.41
min	-72.18	-81.20	-99.97	-99.99
25%	-43.27	-57	-69.57	-69.82
50%	-25.66	-39.09	-53.48	-53.74
75%	-10.41	-23.18	-39.17	-39.28
max	44.49	28.24	12.19	11.64
range	116.67	109.44	112.16	111.63

Table 5-1 shows the statistical summaries of the longitudinal desk displacements measured at all four sides of the bridge where the LVDTs have been placed as mentioned in section 3.3.2. From the summaries above it can be observed that the mean, minimum values and maximum values on the Sishen side of the deck are approximately the same, whilst those on the Saldanha side have 7 mm difference. The ranges suggest that the left side of the Saldanha deck expands and contracts more than the right side.



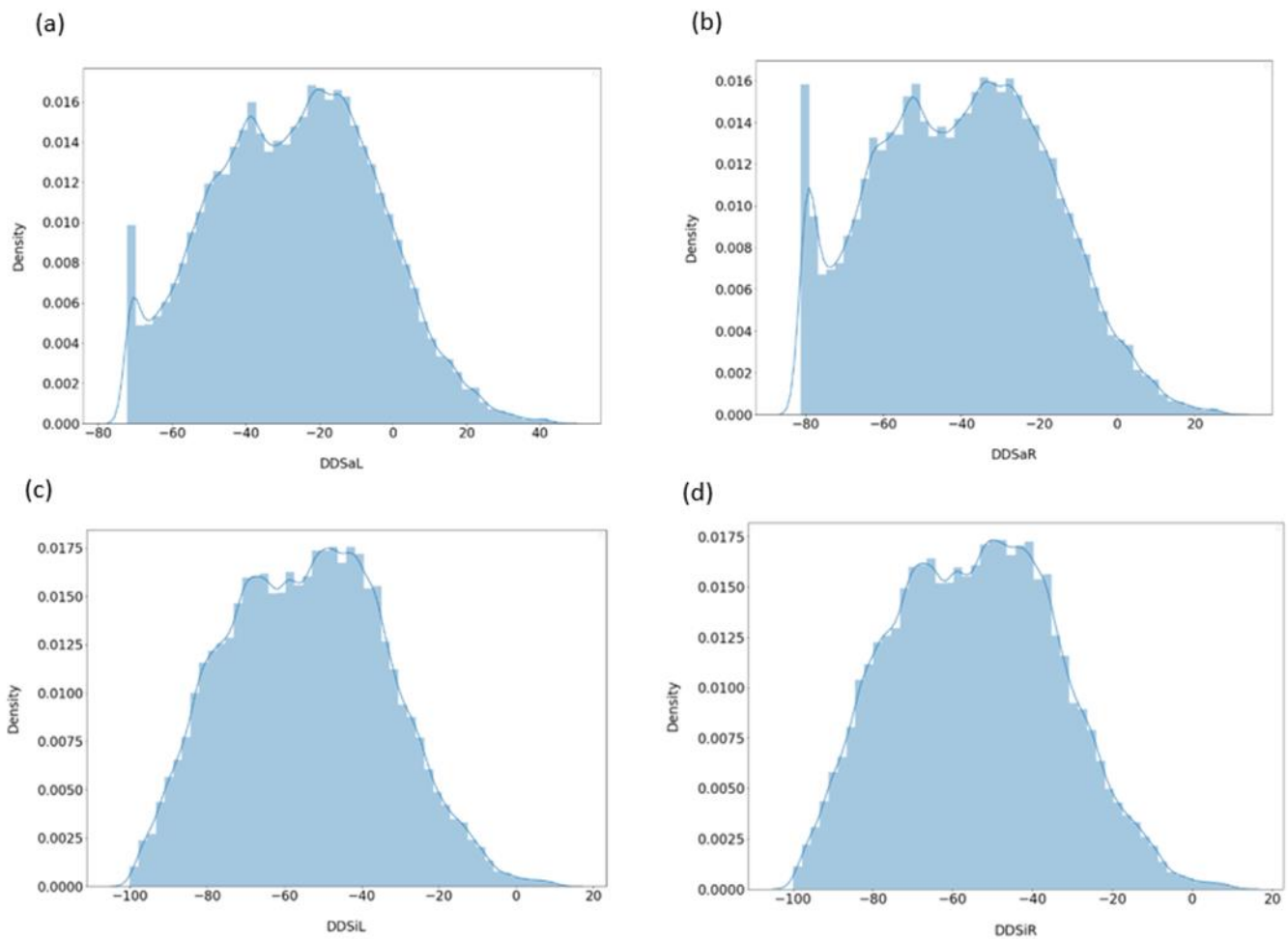


Figure 5-1:: Longitudinal Deck Displacement Probability Density Functions.

Figure 5-1 shows the probability density functions of the longitudinal displacement measured at all four locations of the bridge. Graph (a) and (b) represent probability functions for the Saldanha side of the deck and these functions are skewed to the right. The probability functions for the Sishen side of the bridge deck are both symmetric and are represented in graph (c) and (d). Whilst the probability density functions on the Sishen side of the bridge deck are similar, the functions on the Saldanha side of the bridge deck have slight differences.



5.1.3 Rail Forces Statistical Summaries

Table 5-2: Saldanha Left Rail Force Statistical Summary.

	RFSaL1 (kN)	RFSaL2 (kN)	RFSaL3 (kN)	RFSaL4 (kN)
count	369087	369087	369087	369087
mean	448.91	439.36	452.10	440.16
std	410.16	409.23	405.24	405.56
min	-1068	-1078	-1034	-1050
25%	171	162	177	165
50%	482	473	485	473
75%	745	735	745	733
max	1683	1669	1671	1661
range	2751	2747	2705	2711

Statistical summaries of the rail force measurements taken on the left side of the Saldanha side of the deck are shown in Table 5-2. From the table it is observed that the mean, minimum and maximum values although they could be said to be similar are not the same. It is to be noted that these values are measured at the same point and at the same time



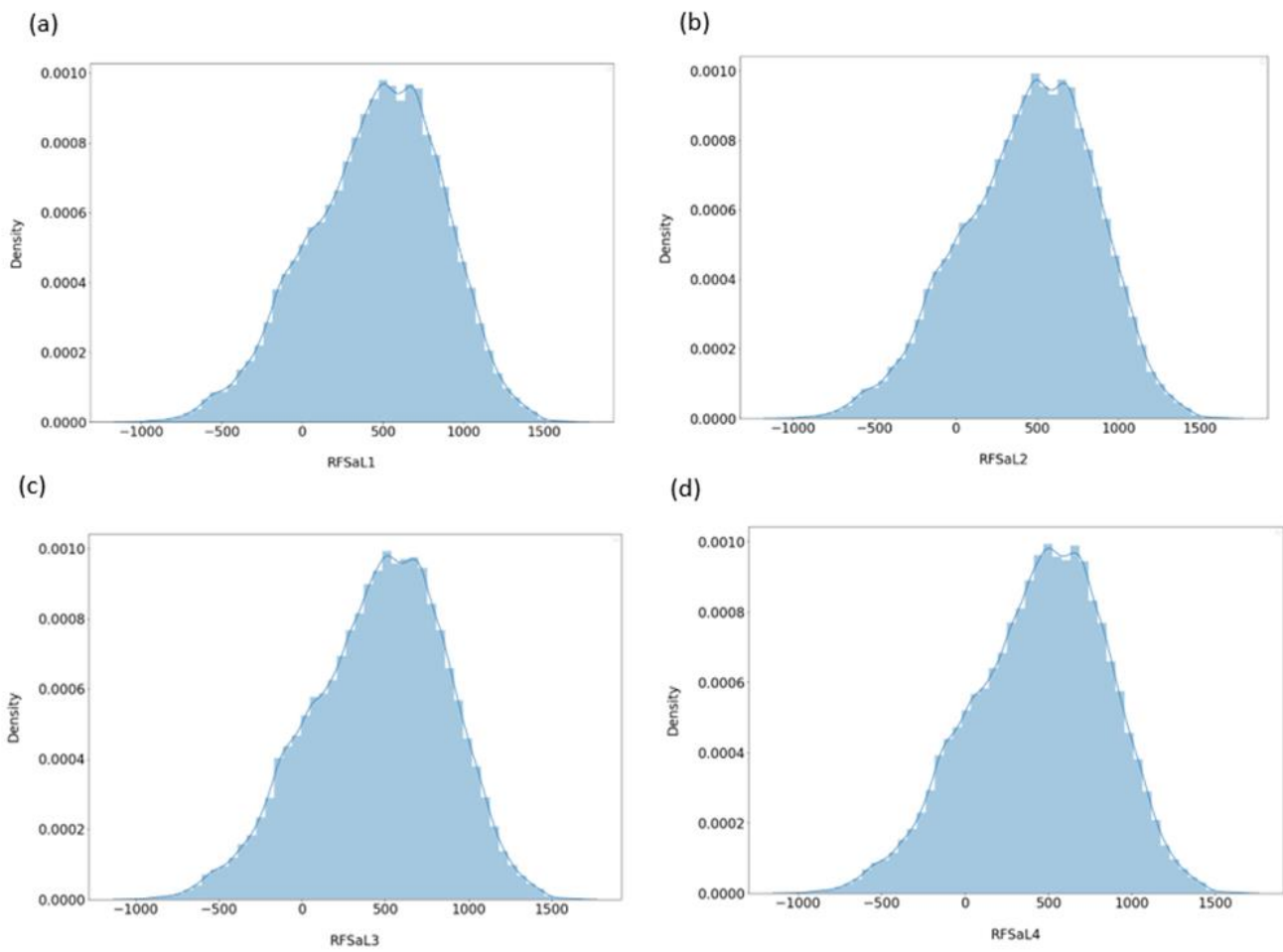


Figure 5-2: Saldanha Left Rail Force Probability Density Functions.

The probability density functions of the rail force measurements taken on the left side of the Saldanha side of the deck are shown in Figure 5-2. They are all similar and all slightly skewed to the left, towards the tension force side.



Table 5-3: Saldanha Right Rail Force Statistical Summary.

	RFSaR1 (kN)	RFSaR2 (kN)	RFSaR3 (kN)	RFSaR4 (kN)
count	369087	369087	369087	369087
mean	605.08	591.84	585.36	577.07
std	411.65	409.12	411.54	421.48
min	-956	-908	-941	-987
25%	327	310	306	291
50%	636	621	618	610
75%	903	886	882	880
max	1815	1796	1819	1843
range	2771	2704	2760	2830

Statistical summaries of the rail force measurements taken on the right side of the Saldanha side of the deck are shown in

Table 5-3. From the summaries above it can be observed that the mean, minimum values and

	RFSaR1 (kN)	RFSaR2 (kN)	RFSaR3 (kN)	RFSaR4 (kN)
count	369087	369087	369087	369087
mean	605.08	591.84	585.36	577.07
std	411.65	409.12	411.54	421.48
min	-956	-908	-941	-987
25%	327	310	306	291
50%	636	621	618	610
75%	903	886	882	880
max	1815	1796	1819	1843
range	2771	2704	2760	2830

maximum values of measurements 3 and 4 although they could be said to be similar are not the same. The same is true for measurements 1 and 2. It is to be noted that these values are measured at the same point and at the same time.



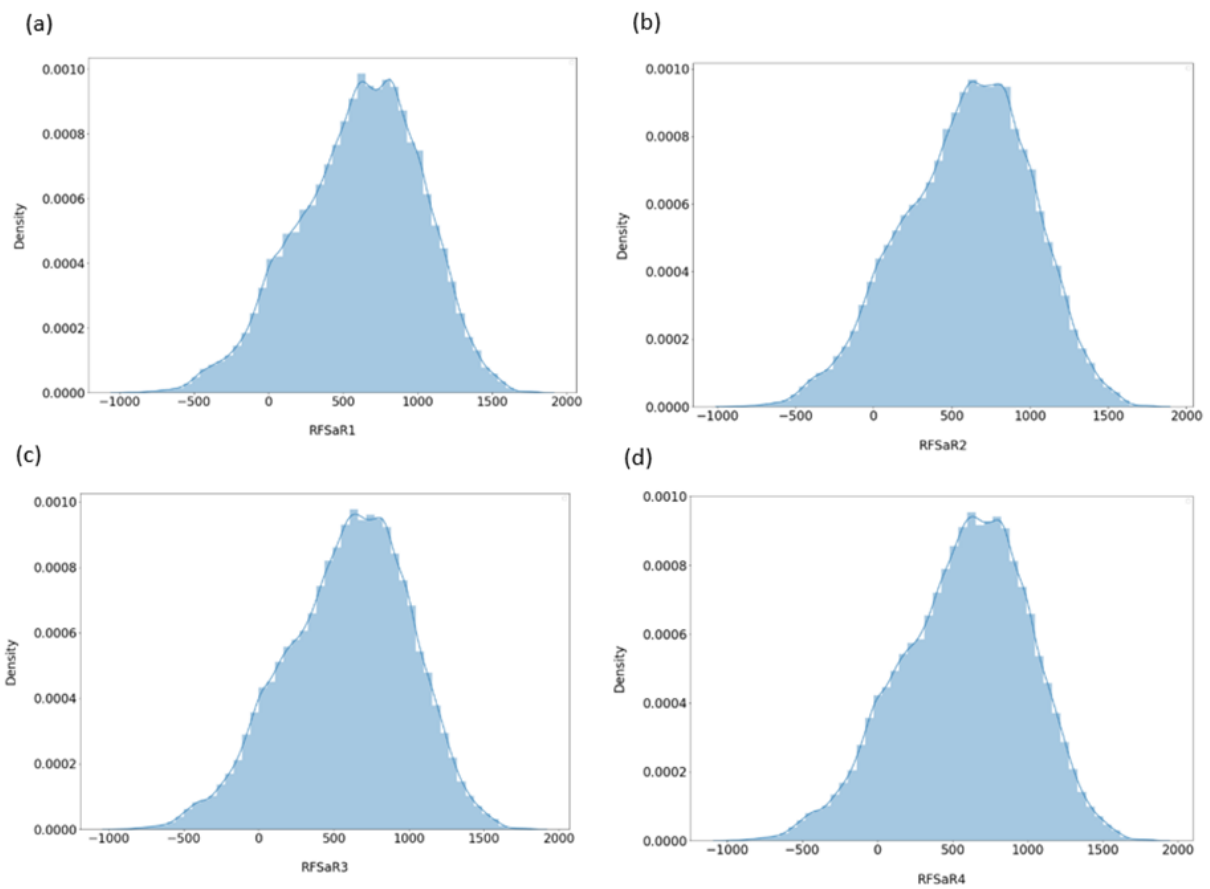


Figure 5-3: Saldanha Right Rail Force Probability Density Function.

The probability density functions of the rail force measurements taken on the left side of the Saldanha side of the deck are shown in Figure 5-3. They are all similar and all slightly skewed to the left, towards the tension force side



Table 5-4: Sishen Left Rail Force Statistical Summary.

	RFSiL1 (kN)	RFSiL2 (kN)	RFSiL3 (kN)	RFSiL4 (kN)
count	369087	369087	369087	369087
mean	480.35	403.03	409.48	443.65
std	401.07	401.49	397.42	428.73
min	-983	-1073	-1039	-1157
25%	208	131	139	153
50%	510	433	440	474
75%	769	693	697	759
max	1696	1619	1624	1734
range	2679	2692	2663	2891

Statistical summaries of the rail force measurements taken on the left side of the Sishen side of the deck are shown in Table 5-4. From the summaries above it can be observed that the mean, minimum values and maximum values of measurements 2 and 3 although they could be said to be similar are not the same. The same is true for measurements 1 and 4. It is to be noted that these values are measured at the same point and at the same time.



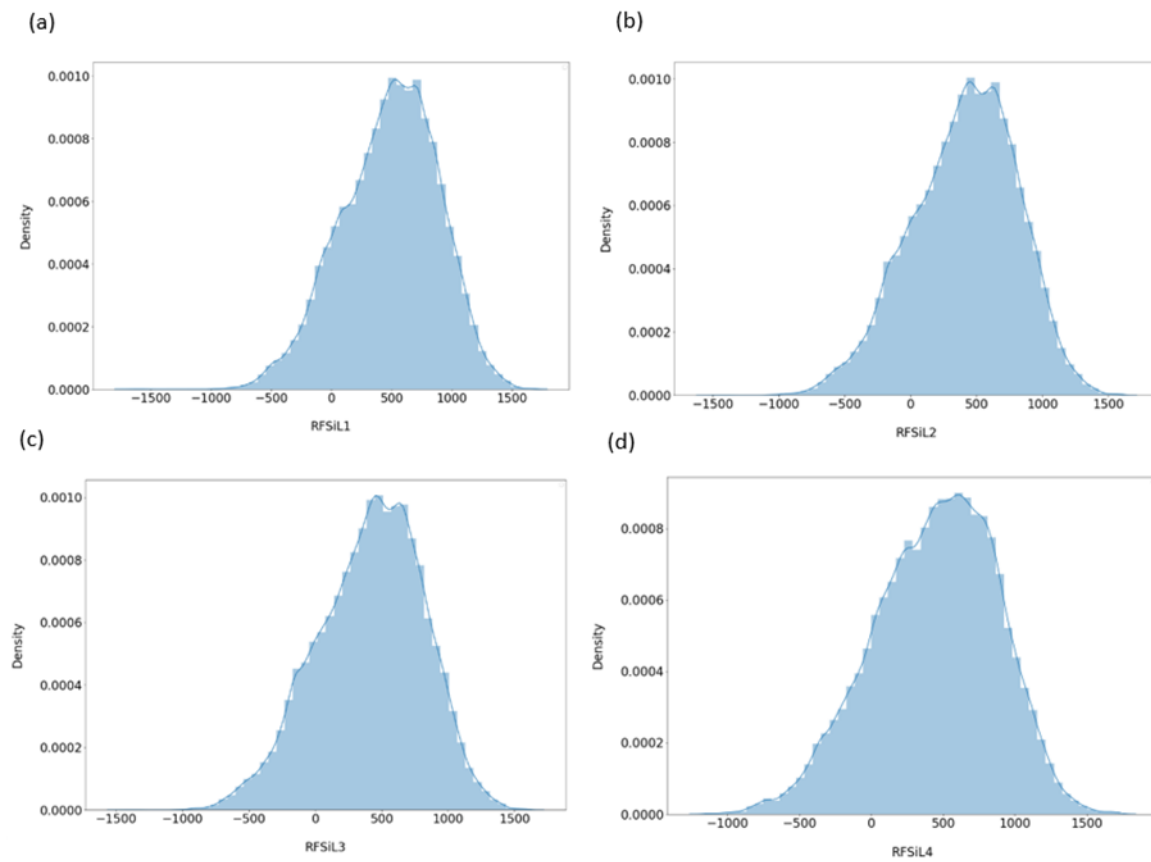


Figure 5-4: Sishen Right Rail Force Probability Density Function.

The probability density functions of the rail force measurements taken on the left side of the Saldanha side of the deck are shown in Figure 5-4. They are all similar and all slightly skewed to the left.



Table 5-5: Sishen Right Rail Force Statistical Summary.

	RFSiR1 (kN)	RFSiR2 (kN)	RFSiR3 (kN)	RFSiR4 (kN)
count	369087	369087	369087	369087
mean	554.84	537.12	563.90	528.75
std	417.78	404.64	411.41	410.21
min	-983	-942	-1288	-971
25%	271	262	284	250
50%	583	567	594	559
75%	856	829	861	825
max	1790	1772	1803	1772
range	2773	2714	3091	2743

Statistical summaries of the rail force measurements taken on the left side of the Sishen side of the deck are shown in Table 5-5. From the summaries above it can be observed that the mean, minimum values and maximum values of measurements 1, 2 and 4 although they could be said to be similar are not the same. The measurements for 4 are significantly higher than the rest. It is to be noted that these values are measured at the same point and at the same time. It will be conservative to consider the values from RFSiR3 when investigating track – bridge interactions. RFSiR3 has the greatest range compared to all other rail force measurements on both the Sishen and Saldanha side of the bridge deck.



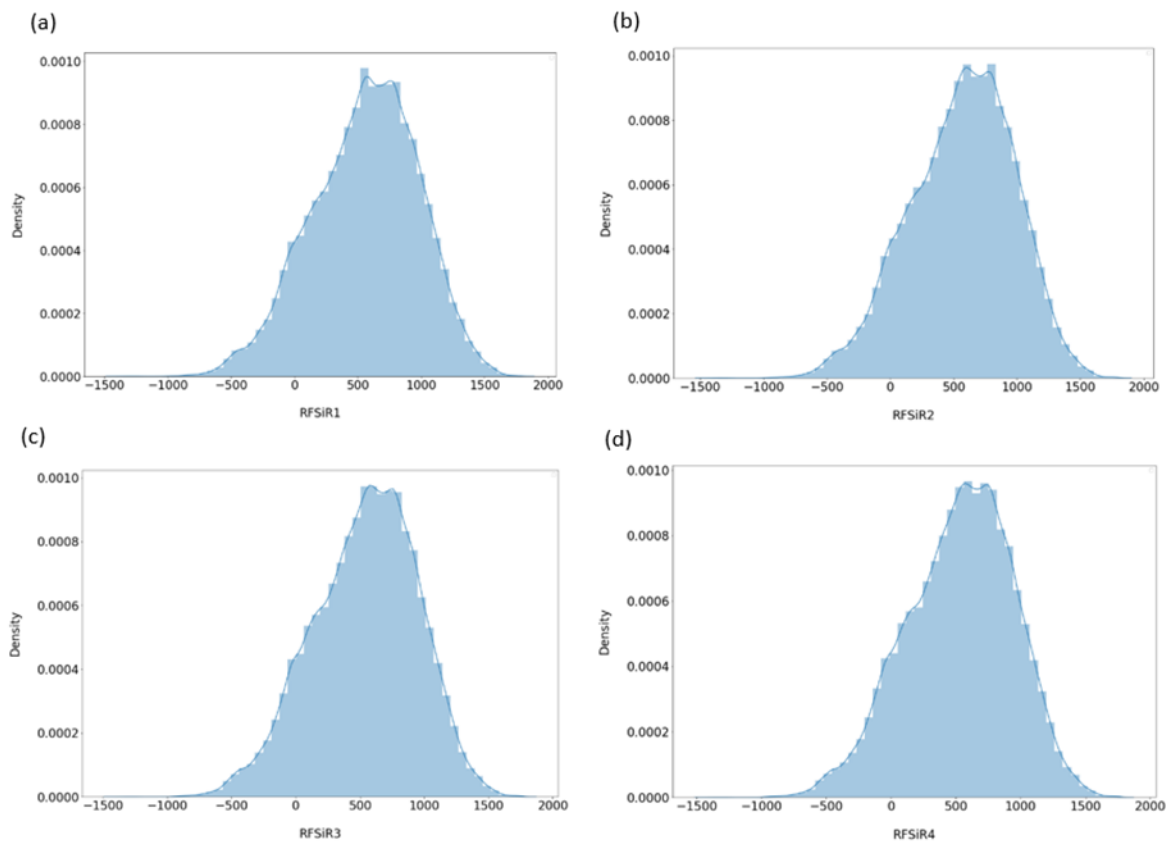


Figure 5-5: Sishen Right Rail Force Probability Density Function.

The probability density functions of the rail force measurements taken on the left side of the Saldanha side of the deck are shown in Figure 5-5. They are all similar and all slightly skewed to the left.



5.1.4 Ambient Temperature Statistical Summaries

Table 5-6: Ambient Temperature Statistical Summary.

	ATN (°C)	ATS (°C)
count	369087	369087
mean	19.32	19.60
std	6.07	6.07
min	3.55	3.76
25%	15.11	15.39
50%	18.52	18.80
75%	22.87	23.16
max	45.23	45.50
range	41.68	41.74

Table 5-6 shows the statistical summaries of the ambient temperature on the north and south side of the bridge. From the summaries above it can be observed that the mean, minimum and maximum values on the north and south side of the deck are approximately the same. This is to be expected.

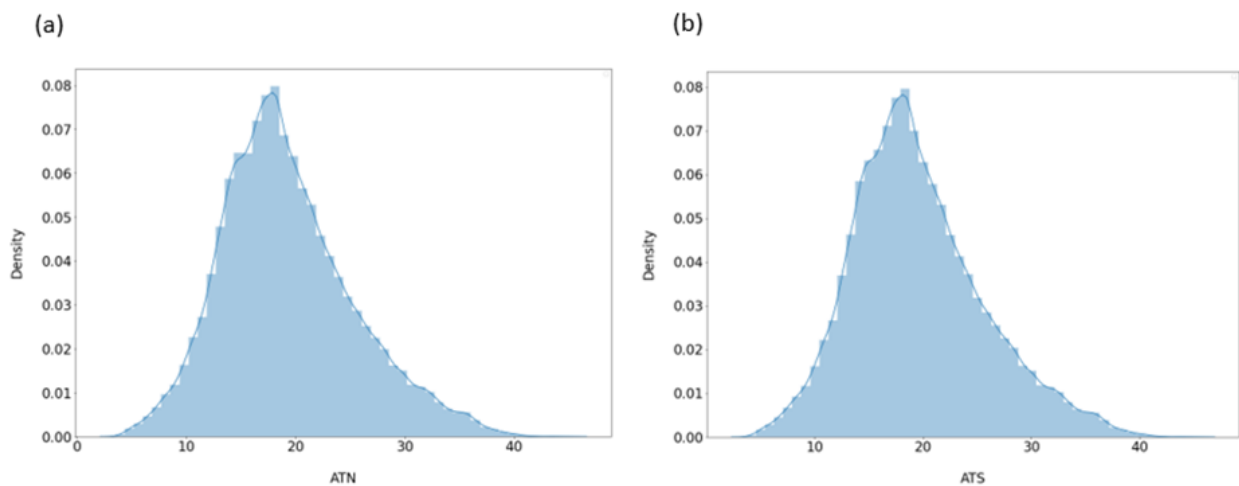


Figure 5-6: Ambient Temperature Statistical Summary.

The probability density functions of ambient temperature on the north and south side of the bridge are shown in Figure 5-7. They are all similar and all slightly skewed to the right as is expected.



5.1.5 Concrete Temperature Statistical Summaries

Table 5-7: Concrete Temperature Statistical Summary.

	CTN (°C)	CTS (°C)
count	369087	369087
mean	22.33	21.04
std	4.13	3.73
min	11.29	11.09
25%	19.16	18.19
50%	22.42	21.03
75%	25.27	23.47
max	35.69	33.57
range	24.40	22.48

Table 5-7 shows the statistical summaries of the concrete temperature on the north and south side of the bridge. From the summaries above it can be observed that the mean and minimum values on the north and south side of the deck are approximately the same. This is to be expected. However, there is a slight difference in the maximum values.

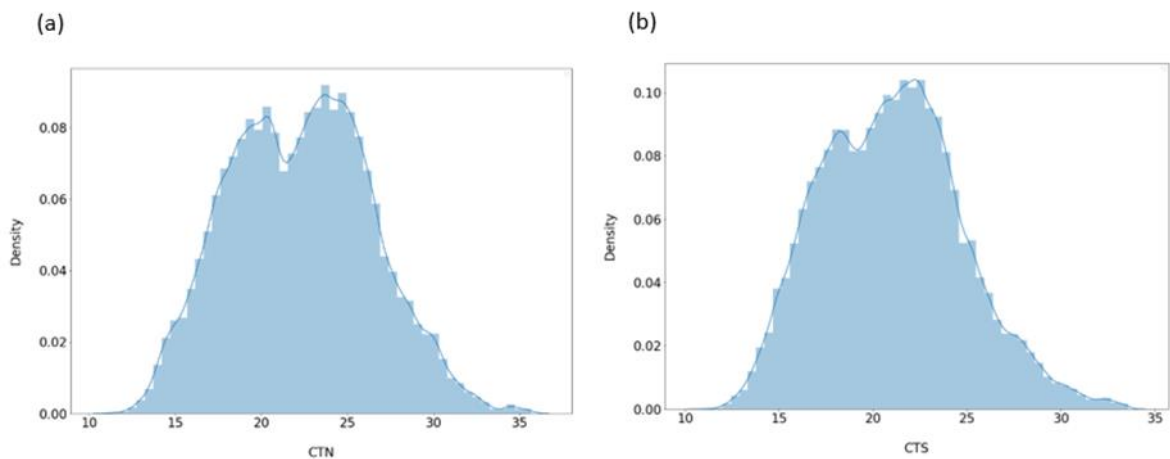


Figure 5-7: Concrete Temperature Probability Density Function.

The probability density functions of concrete temperature on the north and south side of the bridge are shown in Figure 5-7. Concrete temperature on the north side (a) is slightly bimodal, whereas concrete temperature on the south side is skewed to the right.



5.1.6 Rail Temperature Statistical Summaries

Table 5-8: Rail Temperature Statistical Summary.

	RTL (°C)	RTR (°C)
count	369087	369087
mean	23.16	22.65
std	10.72	9.85
min	0.08	2.14
25%	14.88	15.13
50%	20.56	20.22
75%	30.95	29.45
max	57.79	57.34
range	57.71	55.20

Table 5-8 shows the statistical summaries of the concrete temperature on the left and right side of the bridge. From the summaries above it can be observed that the mean and maximum values on the north and south side of the deck are approximately the same. This is to be expected. However, there is a slight difference in the minimum values.

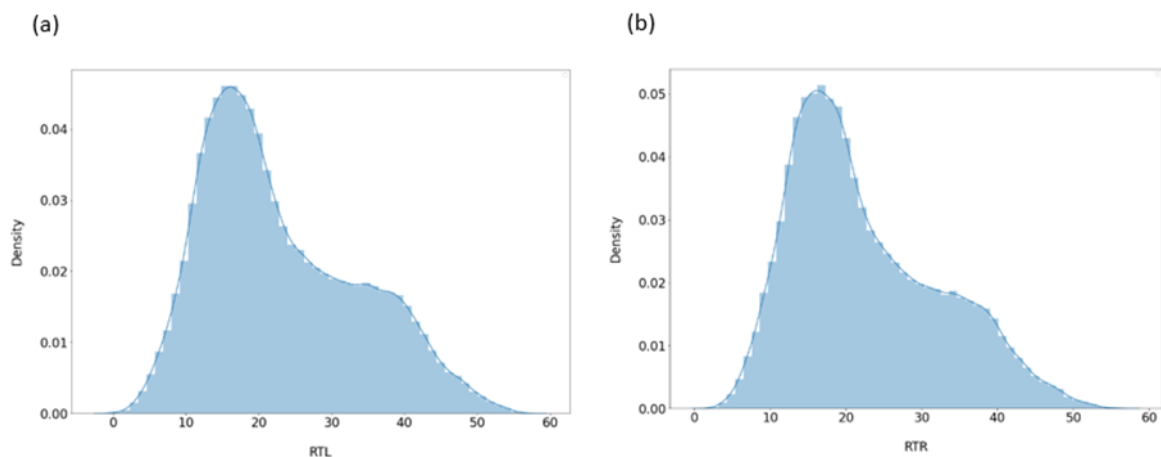


Figure 5-8: Rail Temperature Probability Density Function.

The probability density functions of rail temperature on the left and right side of the bridge are shown in Figure 3-2. Rail temperature on the left side (a) and rail temperature on the right side (b) are slightly bimodal.



5.1.7 Train Categories

Table 5-9: Categorization of loaded trains that travelled across the ORV in 2016.

Month	Category A	Category B	Category C	Category D	Category E	Category F	Total
January	3	1	3	15	0	0	22
February	21	3	15	101	1	2	143
March	31	0	19	127	1	6	184
April	27	0	18	128	4	1	178
May	32	1	22	116	3	1	175
June	32	2	16	123	5	0	178
July	31	3	17	140	2	2	195
August	22	1	20	145	1	4	193
September	23	4	14	121	4	7	173
October	21	2	10	118	0	5	156
November	29	2	22	160	0	0	213
December	29	0	21	161	0	1	212
Total	301	19	197	1455	21	29	2022

On Table 5-9 loaded trains that travelled across the ORV 2016 are grouped into the categories that were discussed in section 4.1.2 in preparation to present this information graphically. Table 5-9 shows that more loaded trains travelled across the ORV in November and December respectively than in any other month. It is important to note that most of the trains that travel across ORV are Category D trains. Category D trains are trains with 4 to 6 locomotives and 312 to 342 wagons. These are the longest trains that travel across the ORV.



Table 5-10: Categorization of unloaded trains that travelled across the ORV in 2016.

Month	Category A	Category B	Category C	Category D	Category E	Category F	Total
January	3	0	5	13	1	0	22
February	24	0	21	106	1	2	154
March	31	4	19	123	0	4	181
April	30	3	21	126	1	0	181
May	32	3	22	115	2	0	174
June	34	6	16	119	3	0	178
July	30	0	17	137	3	0	187
August	19	4	19	141	1	3	187
September	25	3	17	117	4	4	170
October	18	5	19	113	0	3	158
November	28	5	27	153	1	0	214
December	29	3	28	155	0	1	216
Total	303	36	231	1418	17	17	2022

On Table 5-10 unloaded trains that travelled across the ORV 2016 are grouped into the categories that were discussed in section 4.1.2 in preparation to present this information graphically. Table 5-10 shows that more loaded trains travelled across the ORV in November and December respectively than in any other months. It should be noted that most of the trains that travel across ORV are Category D trains. Category D trains are trains with 4 to 6 locomotives and 312 to 342 wagons. These are the longest trains that travel across the ORV.

According to Figure 5-9 and Figure 5-10 overleaf most of the loaded trains that travel across the ORV are Category D trains, with more trains travelling across the ORV in summer and winter than in spring autumn. However, more Category A and C trains travelling across the ORV in Autumn than in Winter.



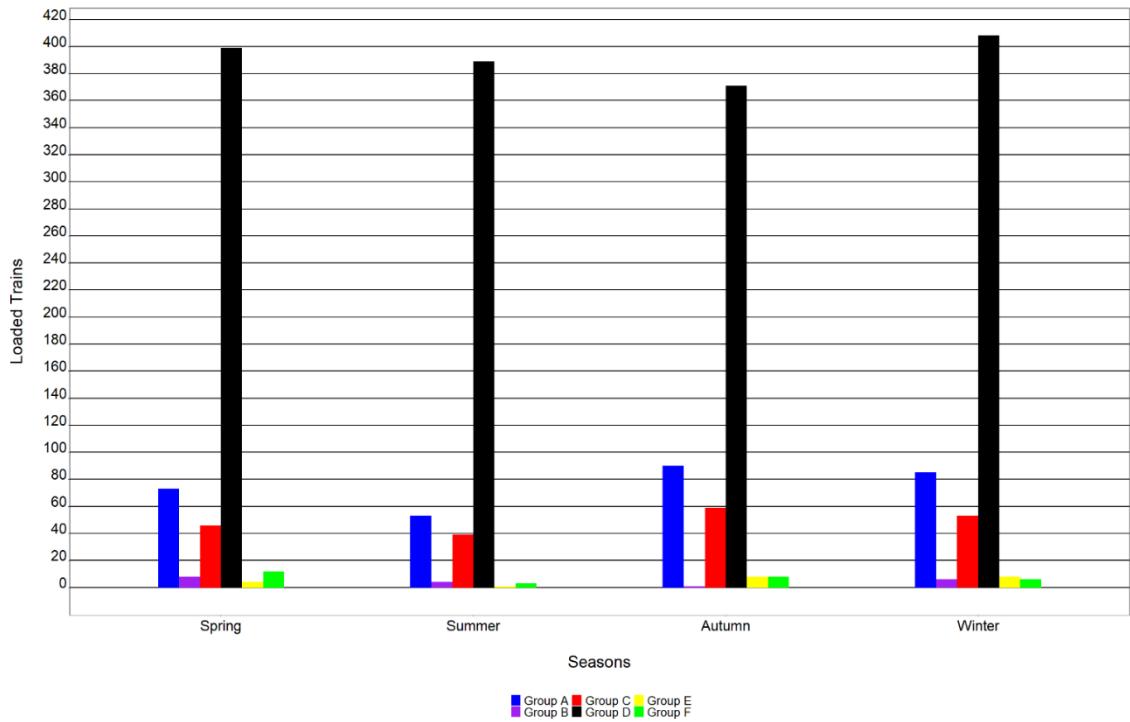


Figure 5-9: Seasonal comparison of categorized loaded trains for the 2016 period.

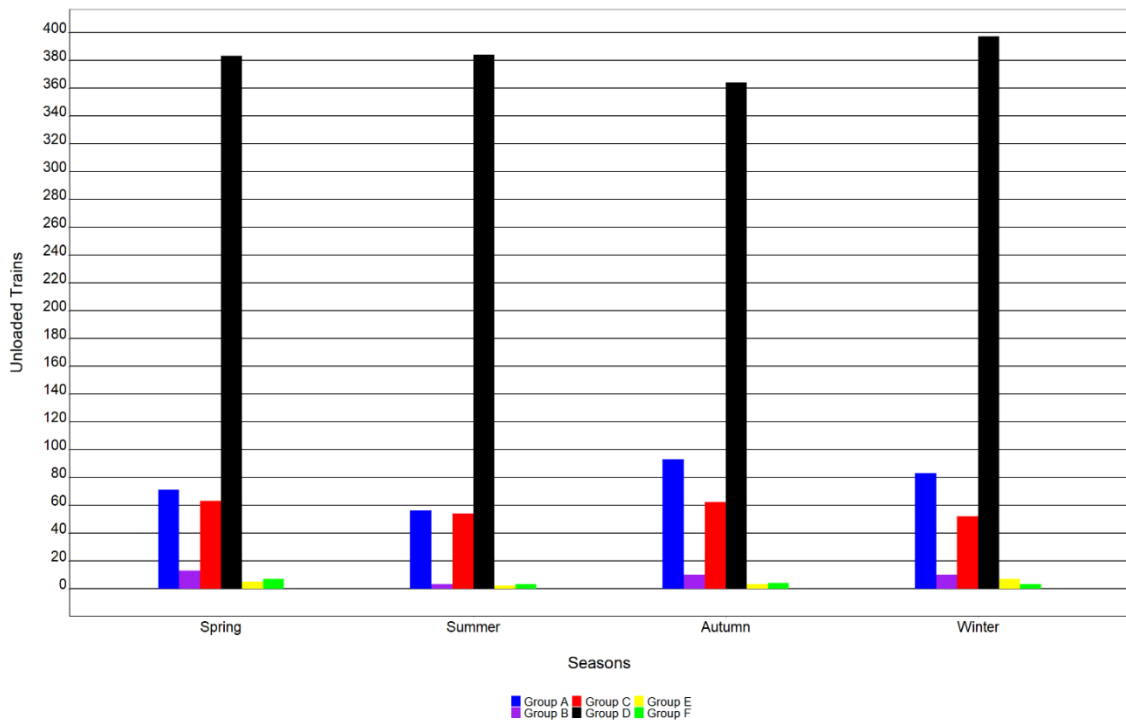


Figure 5-10: Seasonal comparison of categorized unloaded trains for the 2016 period.



5.2 Observed Patterns

This section explores the observed patterns of rail forces, longitudinal deck displacements, ambient temperature, concrete temperature and rail temperature over time.

5.2.1 Longitudinal Deck Displacement

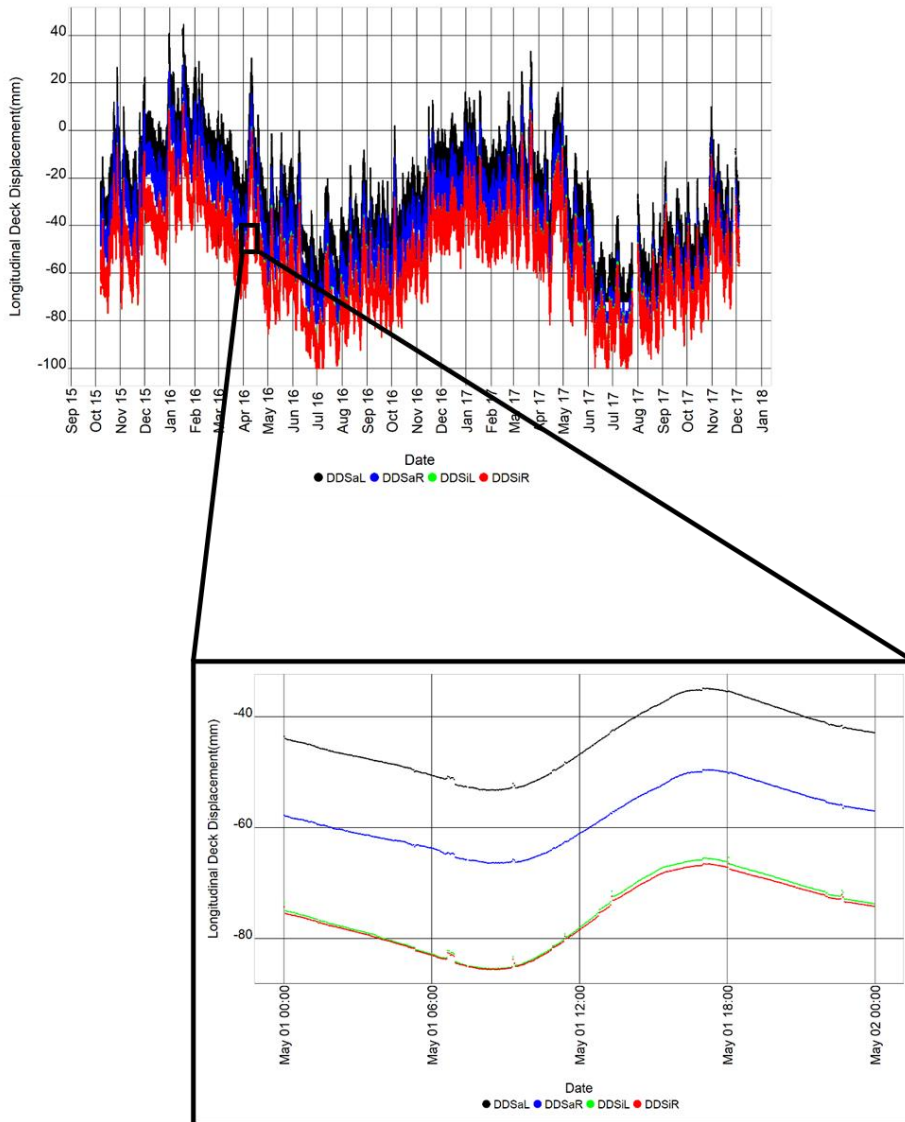


Figure 5-11: Longitudinal deck displacement time series.

An increase in the positive direction in longitudinal deck displacement represents longitudinal deck expansion and an increase in the negative direction represents contraction. According to Figure 5-11 the longitudinal deck displacement tends to expand in spring and contract in Autumn. In Summer longitudinal deck displacement is at its maximum expansion and its maximum contraction is observed in winter. The daily variation shows an increase in expansion from midnight and an increase in contraction from mid-morning to late afternoon.



5.2.2 Rail Forces Left Rail Saldanha Deck

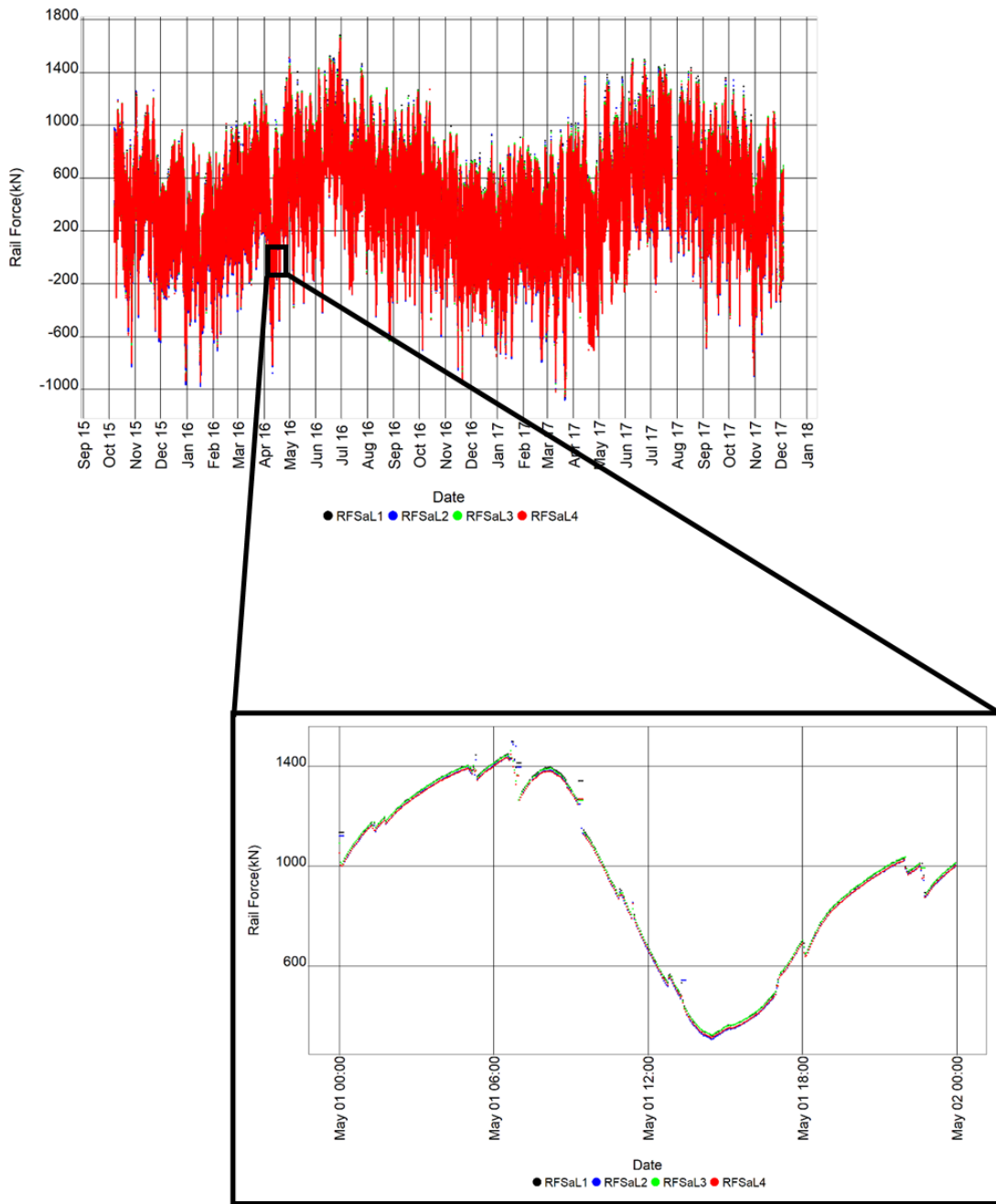


Figure 5-12: Saldanha Deck Left Rail Force time series.

According to Figure 5-12 on the left side of the Saldanha side of the deck compressive force increases in spring and tension force increases in Autumn. In Summer the compressive force is at its maximum and maximum tension force observed in winter. The daily variation shows an increase in tension from midnight and an increase in compressive force from mid-morning to late afternoon. Furthermore, sudden decreases are also observed at maximum tension force. For this study these will be referred to as rail force jumps.



5.2.3 Rail Forces Right Rail Saldanha Deck

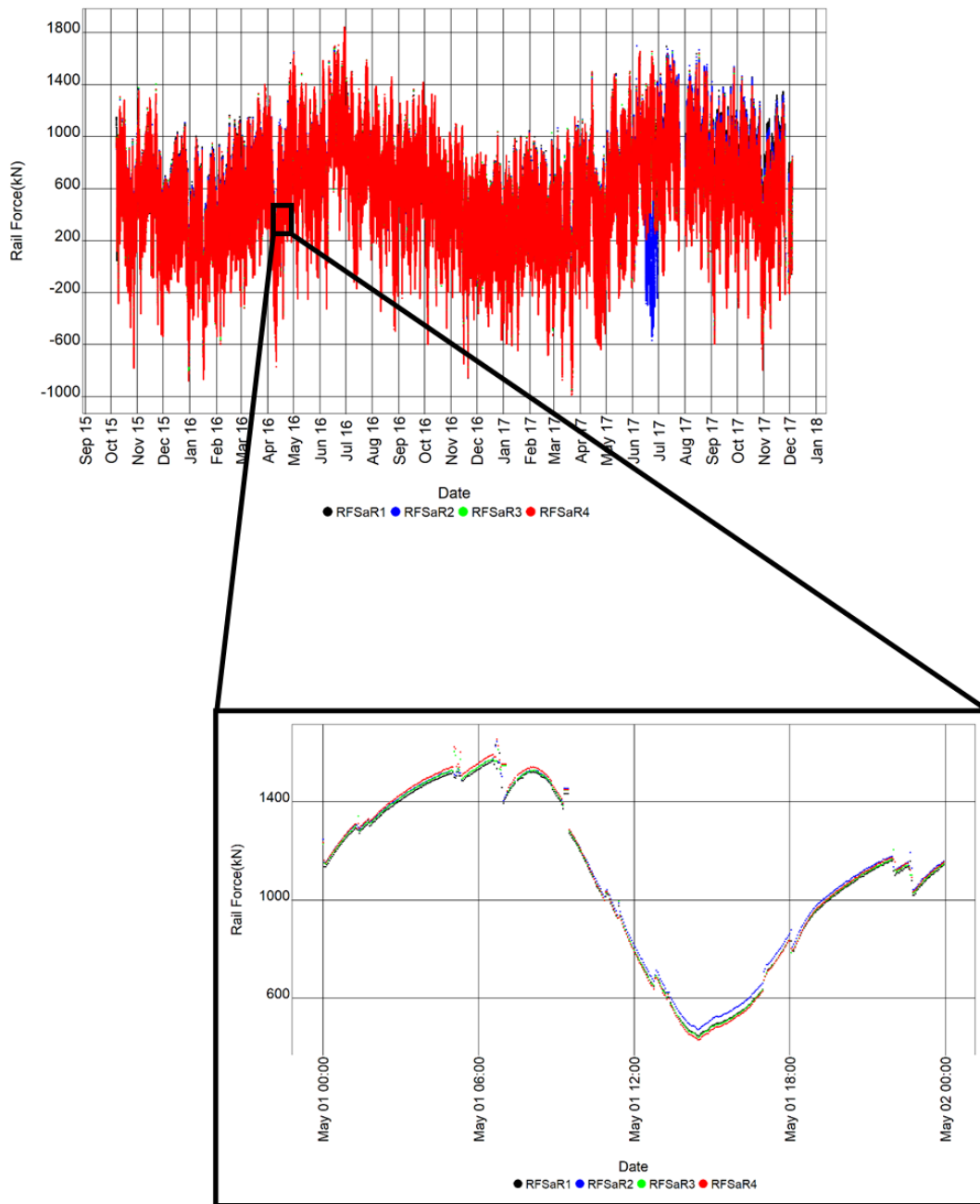


Figure 5-13: Saldanha Deck Right Rail Force time series.

As shown in Figure 5-13 on the right side of the Saldanha side of the deck compressive force increases in spring and tension force increases in Autumn. In Summer the compressive force is at its maximum and maximum tension force observed in winter. The daily variation shows an increase in tension force from midnight and an increase in compressive force from mid-morning to late afternoon. Additionally, rail force jumps are also observed at maximum tension force.



5.2.4 Rail Forces Left Rail Sishen Deck

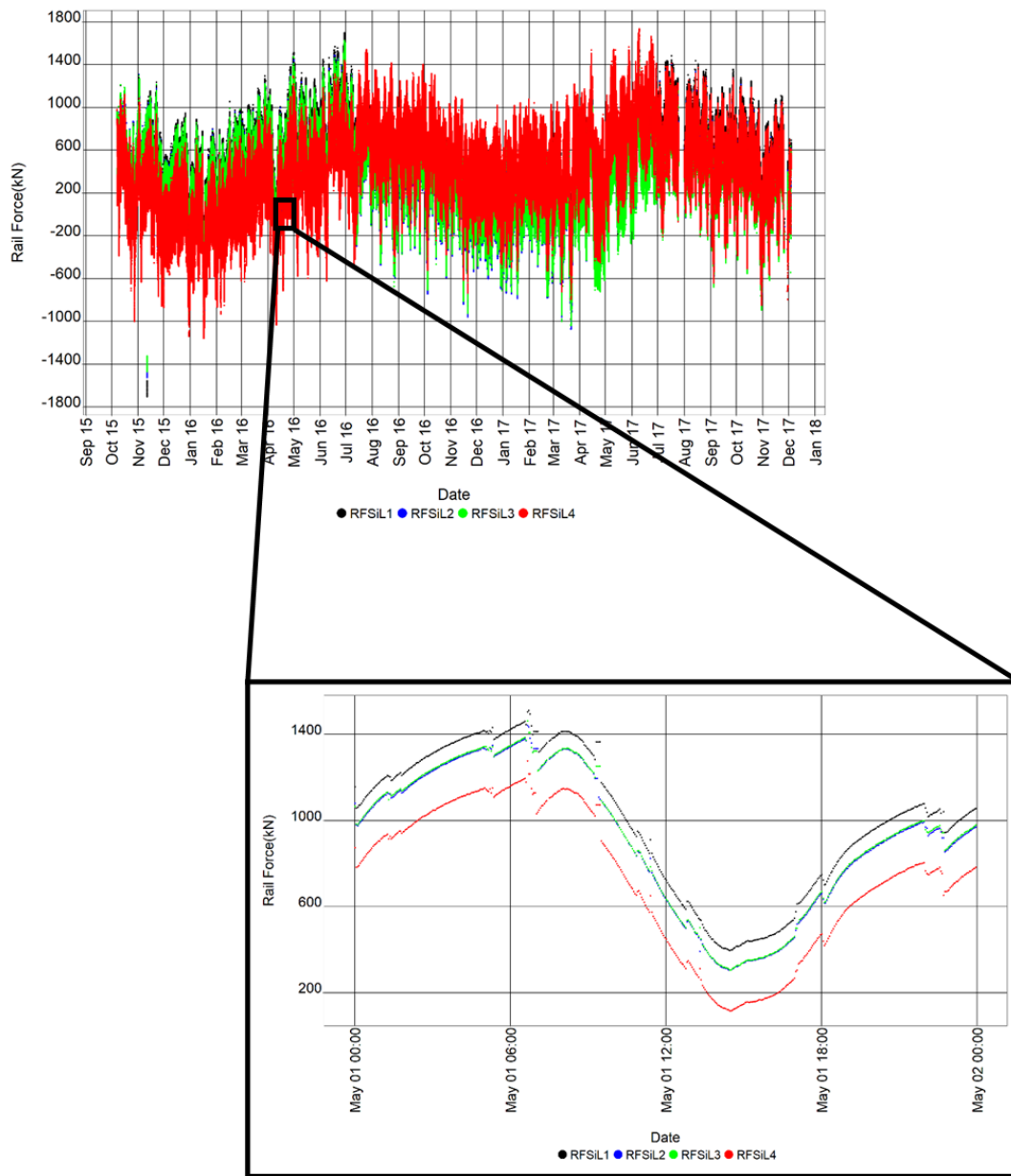


Figure 5-14: Sishen Deck Left Rail Force time series.

As demonstrated in Figure 5-14 on the left side of the Sishen side of the deck compressive force increases in spring and tension force increases in Autumn. In Summer the compressive force is at its maximum and maximum tension force observed in winter. The daily variation shows an increase in tension force from midnight and an increase in compressive force from mid-morning to late afternoon. Moreover, rail force jumps are also observed at maximum tension force. It is important to note that the daily variations highlight that the rail force measurements of the left side of the Sishen side of the deck are distinctly different.



5.2.5 Rail Forces Right Sishen Deck

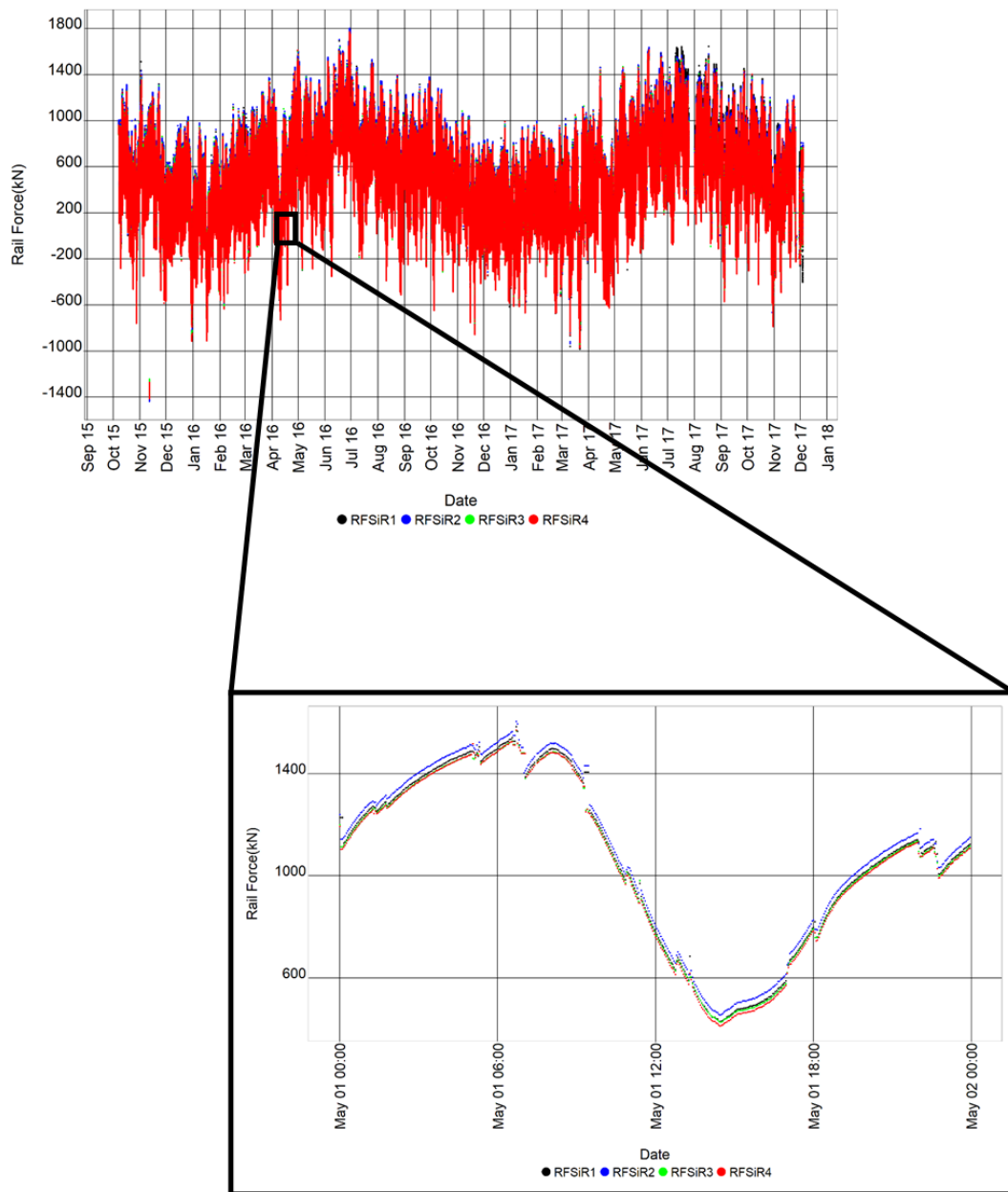


Figure 5-15: Sishen Deck Right Rail Force time series.

As shown in Figure 5-15 on the left side of the Sishen side of the deck compressive force increases in spring and tension force increases in Autumn. In Summer the compressive force is at its maximum and maximum tension force observed in winter. The daily variation shows an increase in tension force from midnight and an increase in compressive force from mid-morning to late afternoon. Additionally, rail force jumps are also observed at maximum tension force.



5.2.6 Ambient Temperature

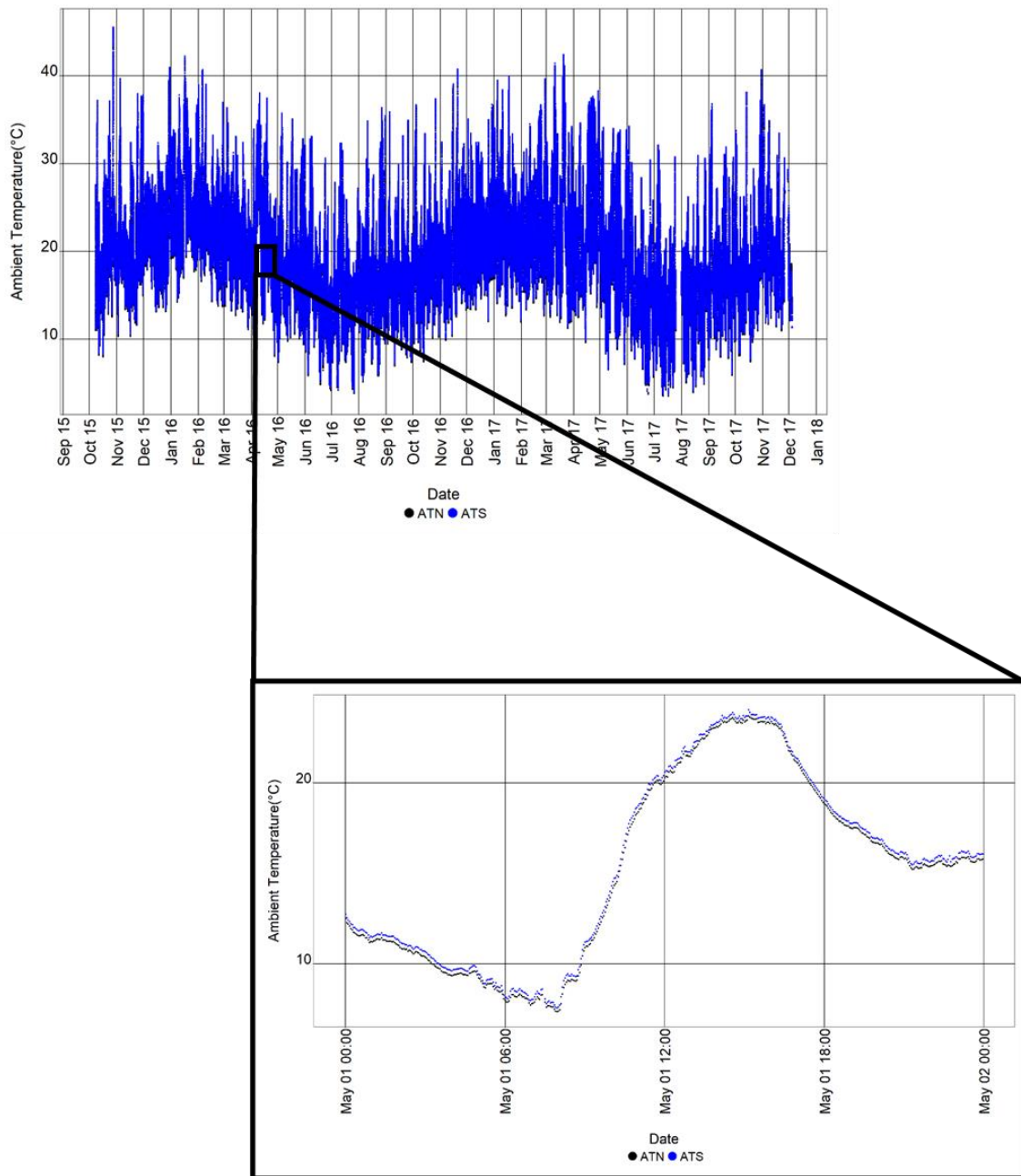


Figure 5-16: Ambient temperature time series.

According to Figure 5-16 ambient temperature increases in spring and decreases in Autumn. In Summer ambient is at its maximum and minimum ambient temperature is observed in winter.

The daily variation shows a decrease in ambient temperature from midnight and an increase from mid-morning to late afternoon.



5.2.7 Concrete Temperature

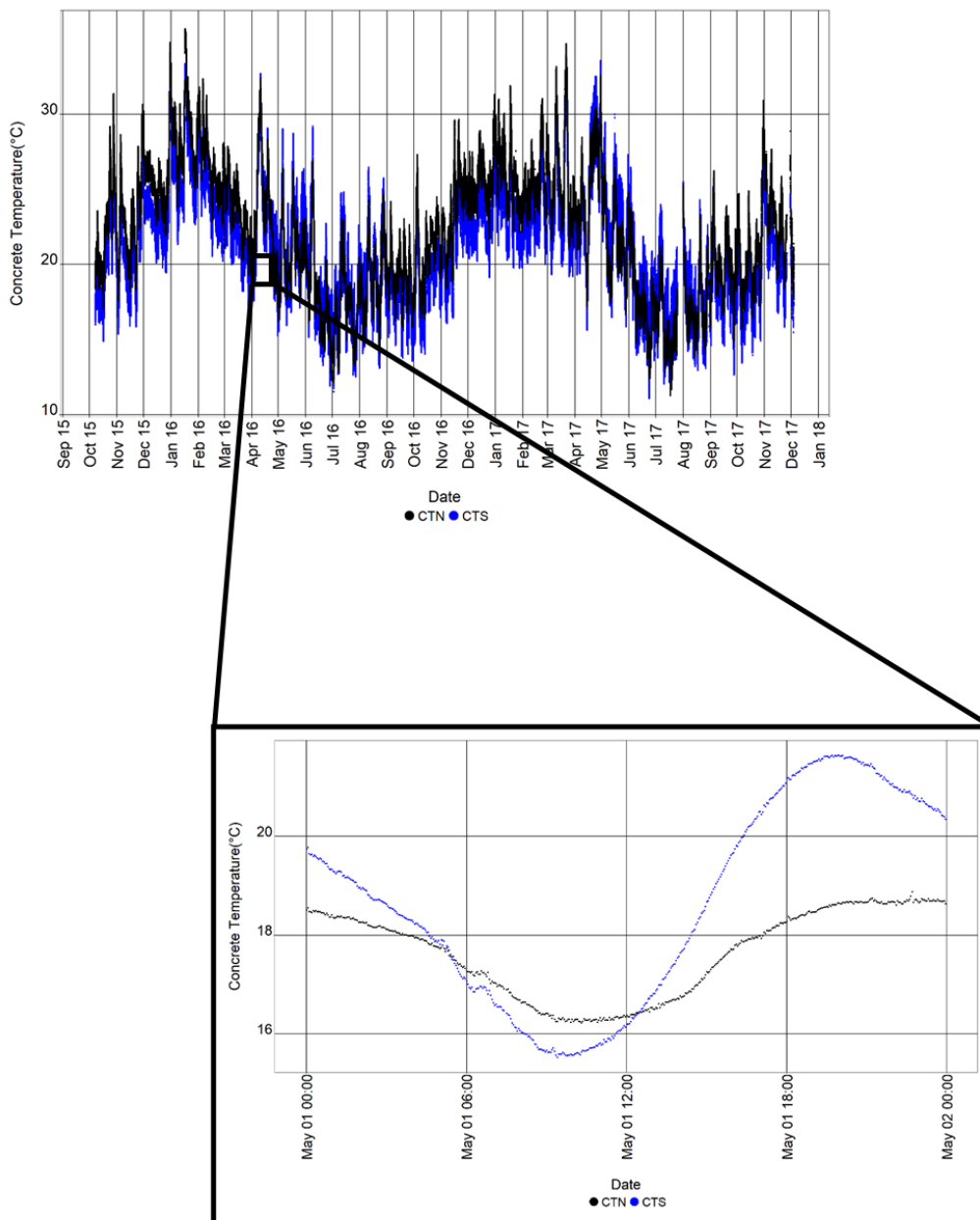


Figure 5-17: Concrete temperature time series.

Figure 5-17 shows an increase in concrete temperature in spring and decreases in Autumn. In Summer concrete temperature is at its maximum and minimum concrete temperature is observed in winter.

The daily variation shows a decrease in concrete temperature from midnight and an increase from mid-morning to late afternoon. Furthermore, a lag between the CTN and CTS values is observed.



5.2.8 Rail Temperature

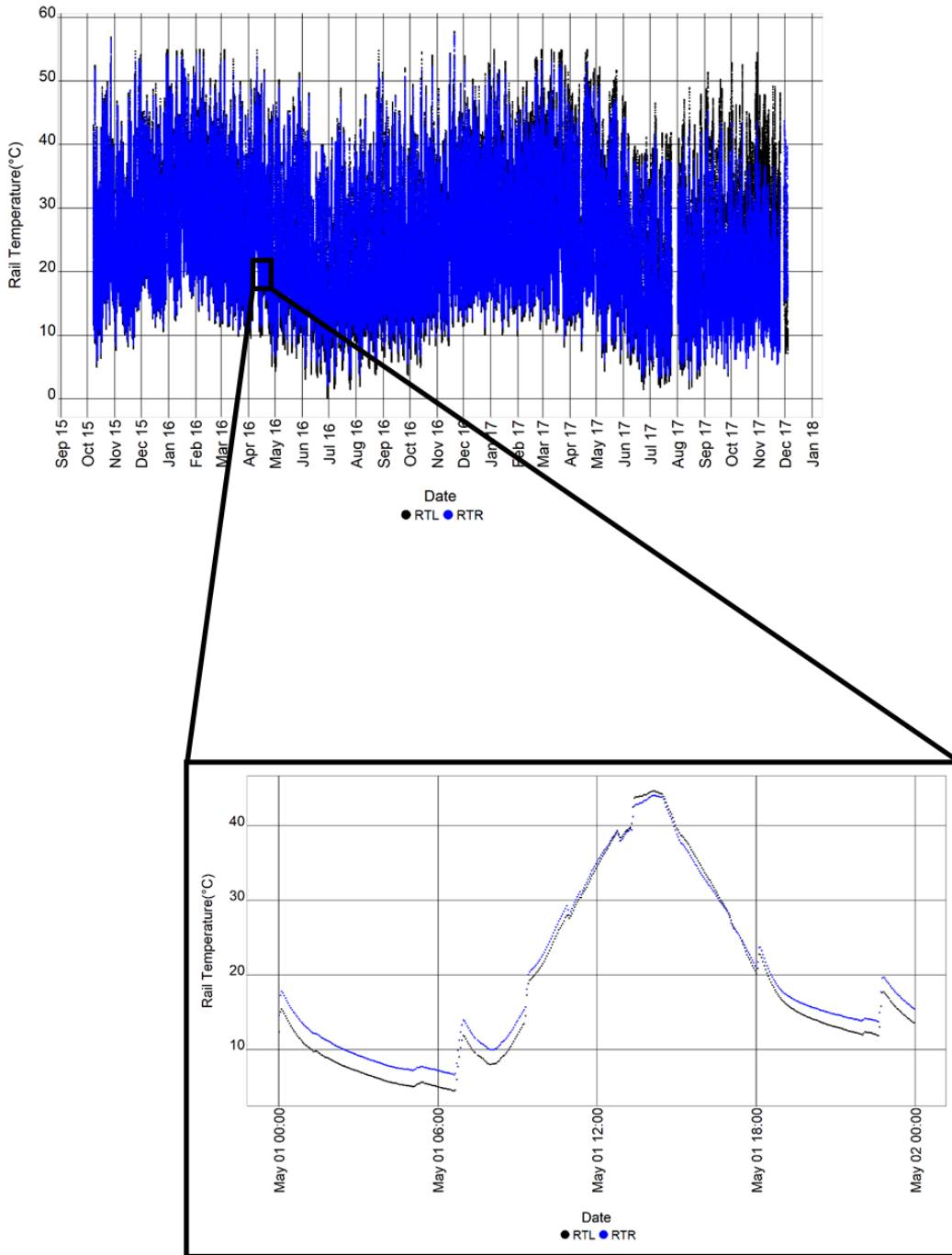


Figure 5-18: Rail temperature time series.

Figure 5-18 displays an increase in rail temperature in spring and decreases in Autumn. In Summer rail temperature is at its maximum and minimum rail temperature is observed in winter.

The daily variation shows a decrease in rail temperature from midnight and an increase from mid-morning to late afternoon. Additionally, rail temperature jumps are observed at minimum rail temperature.



5.2.9 Summary of the Section

From the observed patterns it is demonstrated that, with the increasing ambient temperature, the deck tends to expand longitudinally, the deck concrete temperature increases, rail temperature increases and the rail experiences compressive forces . When the ambient temperature decreases the deck concrete temperature decreases, the deck contracts longitudinally, rail temperature decreases and the rail experiences tension forces.

The daily observations revealed rail force and rail temperature jumps. The rail force jumps occurred at maximum tension force and rail temperature jumps occurred at minimum rail temperature.



5.3 Track Bridge Interactions/Associations

5.3.1 Introduction

This section will investigate the effect of rail temperature variation on rail forces and longitudinal displacement of the deck. Examine the effect of variation in concrete temperature on longitudinal deck displacement, rail forces and variation in rail temperature as well as the effect of longitudinal deck displacement on rail forces. It will also investigate the effects of the presence of the train on the longitudinal displacement of the deck, rail forces and concrete temperature.

5.3.2 Effect of Rail Temperature Variation

Table 5-11: Training and Testing Results of RFSiR3 vs RTR.

Dependent Variable: RFSiR3 (kN)					
Term	Coefficient	P – Value	95% CI	R ²	NRMSE
Training					
Intercept	1340.1250	0.0	(1338.280;1341.970)	0.746	0.07
RTR (°C)	-35.4479	0.0	(-35.523; -35.373)		
Testing					
Intercept	1341.6103	0.0	(1337.896; 1345.325)	0.743	0.07
RTR (°C)	-35.5231	0.0	(-35.674; -35.373)		

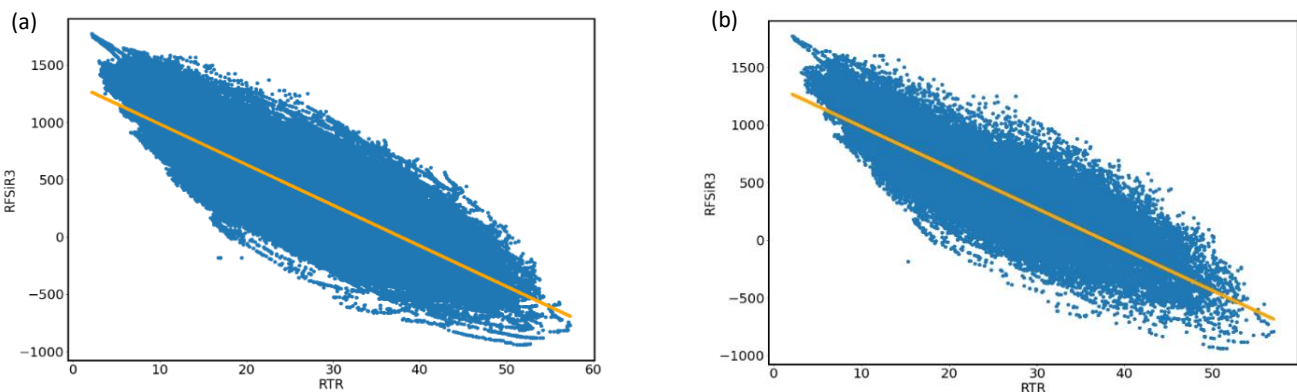


Figure 5-19: (a) Training results of RFSiR3 vs RTR. (b) Training results of RFSiR3 vs RTR.

Table 5-11 shows the results from the linear regression analysis of RFSiR3 and RTR. The p-value is 0 which is less than 0.05 and therefore the null hypothesis is rejected. RFSiR3 and RTR are related. R² is 0.7 which represents a strong correlation between RFSiR3 and RTR. The NRMSE is less than 0.1, therefore the linear regression model is a good fit for the relationship between RFSiR3 and RTR. Table 5-11 and Figure 5-24 indicate that RFSiR3 is inversely proportional to RTR.



Table 5-12: Training and Testing Results of DDSiR vs RTR.

Dependent Variable: DDSiR (mm)					
Term	Coefficient	P- Value	95% CI	R ²	NRMSE
Training					
Intercept	-78.6429	0.0	(-78.800; -78.486)	0.273	0.16
RTR (°C)	1.0825	0.0	(1.076;1.089)		
Testing					
Intercept	-78.7259	0.0	(-79.041; -78.411)	0.274	0.16
RTR (°C)	1.0872	0.0	(1.074;1.1)		

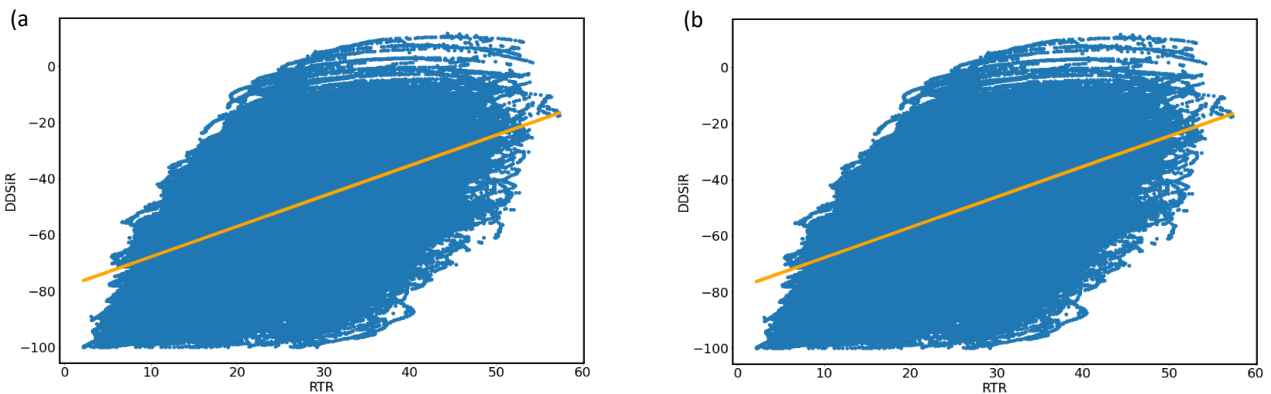


Figure 5-20: (a) Training results of DDSiR vs RTR. (b) Testing results of DDSiR vs RTR.

The results from the linear regression analysis of DDSiR and RTR are shown in Table 5-12. The p-value is 0 which is less than 0.05 and therefore the null hypothesis is rejected. DDSiR and RTR are related and R^2 is 0.27. R^2 of less than 0.3 represents a very small correlation. The NRMSE is 0.16. Even though the NRMSE value indicates that the model is a good fit and the training and testing graphs in Figure 5-20 indicate a linear relationship, it is important to consider R^2 . R^2 suggests that the relationship between DDSiR and RTR does not have a strong correlation. The shape of the scatter plot suggests that there is a phase lag between longitudinal deck displacement and the rail temperature. This is to be expected because deck is displaced longitudinally due to changes in concrete temperature and there is a phase lag between concrete temperature and rail temperature.



5.3.3 Effect of Concrete Temperature Variation

Table 5-13: Training and Testing Results of DDSiR vs CTS.

Dependent Variable: DDSiR (mm)					
Term	Coefficient	P – Value	95% CI	R ²	NRMSE
Training					
Intercept	-158.5917	0.0	(-158.767; -158.416)	0.826	0.08
CTS (°C)	4.9662	0.0	(4.958; 4.974)		
Testing					
Intercept	-158.8287	0.0	(-159.179; -158.479)	0.828	0.08
CTS (°C)	4.9782	0.0	(4.962;4.995)		

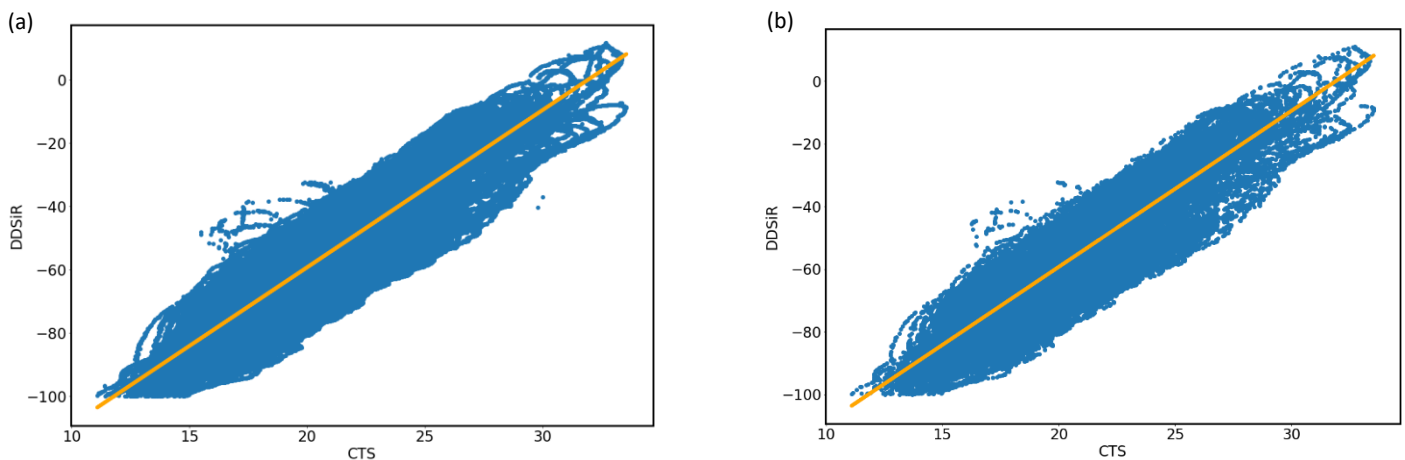


Figure 5-21: (a) Training results of DDSiR vs CTS. (b) Testing results of DDSiR vs CTS.

Table 5-13 shows the results from the linear regression analysis of DDSiR and CTS. The p-value is 0 which is less than 0.05 and therefore the null hypothesis is rejected. DDSiR and CTS are related. R² is 0.8 which represents a strong correlation between DDSiR and CTS. The NRMSE is less than 0.1, it can be inferred that the linear regression model is a good fit for the relationship between DDSiR and CTS. Table 5-13 and Figure 5-21 indicate that DDSiR is directly proportional to CTS.



Table 5-14: Training and Testing Results of RFSiR3 vs CTS.

Dependent Variable: RFSiR3 (kN)					
Term	Coefficient	P – Value	95% CI	R ²	NRMSE
Training					
Intercept	1941.6536	0.0	(1935.078; 1948.230)	0.380	0.10
CTS (°C)	-66.7691	0.0	(-67.077; -66.461)		
Testing					
Intercept	1946.6078	0.0	(1933.462; 1959.754)	0.381	0.10
CTS (°C)	-66.9914	0.0	(-67.607; -66.376)		

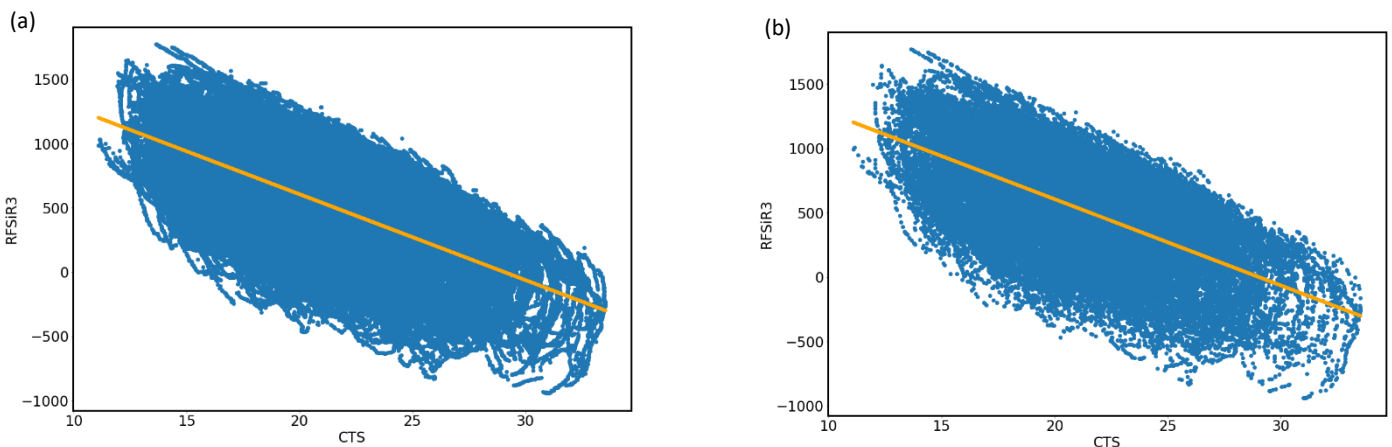


Figure 5-22: (a) Training results of RFSiR3 vs CTS. (b) Testing results of RFSiR3 vs CTS.

The results from the linear regression analysis of RFSiR3 and CTS are shown in Table 5-14. The p-value is 0 which is less than 0.05 and therefore the null hypothesis is rejected. RFSiR3 and CTS are related. R² is 0.38 which represents a low correlation between RFSiR3 vs CTS. The NRMSE is 0.1. Even if the NRMSE value indicates that that the model is a good fit and the training and testing graphs in Figure 5-22 indicate a linear relationship, it is important to consider R². R² suggests that the relationship between RFSiR3 and CTS does not have a strong correlation. This is also indicated by the scatter around the fitted model.



Table 5-15: Training and Testing Results of RTR vs CTS.

Dependent Variable: RTR (°C)					
Term	Coefficient	P – Value	95% CI	R ²	NRMSE
Training					
Intercept	3.9777	0.0	(3.786;4.169)	0.113	0.17
CTS (°C)	0.8879	0.0	(0.879;0.897)		
Testing					
Intercept	3.9768	0.0	(3.595;4.359)	0.114	0.17
CTS (°C)	0.8871	0.0	(0.869;0.905)		

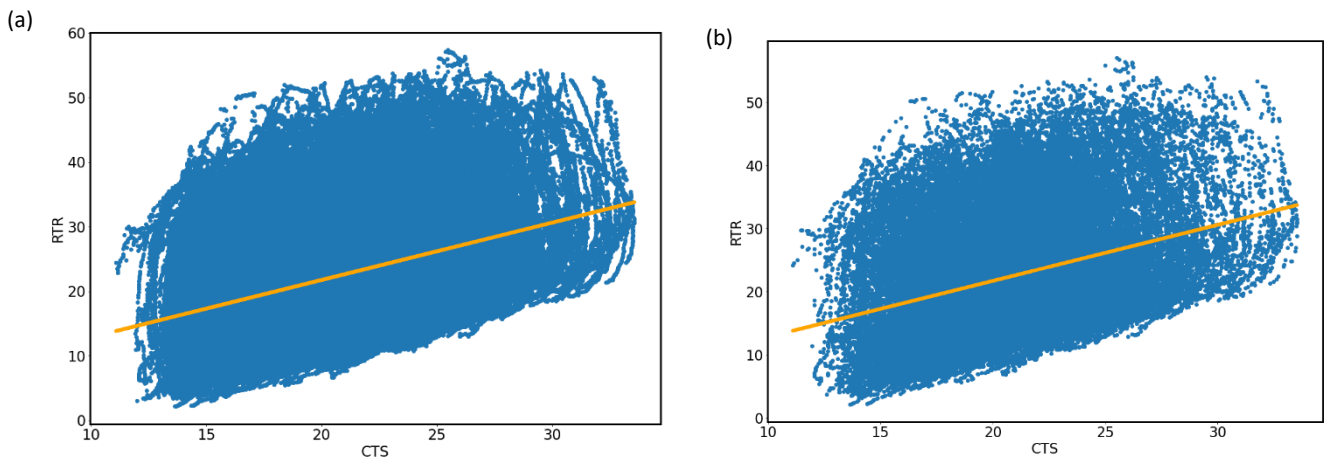


Figure 5-23: (a) Training results of RTR vs CTS. (b) Testing results of RTR vs CTS.

The results from the linear regression analysis of RTR and CTS are shown in Table 5-15. The p-value is 0 and it is less than 0.05 and therefore the null hypothesis is rejected. RTR and CTS are related. R² is 0.114 and NRMSE is 0.17. R² of less than 0.3 represents a very small correlation. Even though the NRMSE value indicates that that the model is a good fit and the training and testing models in Figure 5-23 indicate a linear relationship, it is important to consider R². R² suggests that the relationship between DDSiR and RTR has a very small correlation. This is to be expected because of the phase lag between the concrete temperature in the deck and rail temperature in the track.



5.3.4 Effect of the Longitudinal Deck Displacement

Table 5-16: Training and Testing Results of RFSiR3 vs DDSiR.

Dependent Variable: RFSiR3 (kN)					
Term	Coefficient	P – Value	95% CI	R ²	NRMSE
Training					
Intercept	-292.6302	0.0	(-295.255; -290.006)	0.598	0.08
DDSiR (mm)	-15.3305	0.0	(-15.376; -15.285)		
Testing					
Intercept	-292.2358	0.0	(-297.477; -286.994)	0.598	0.08
DDSiR (mm)	-15.3323	0.0	(-15.423; -15.242)		

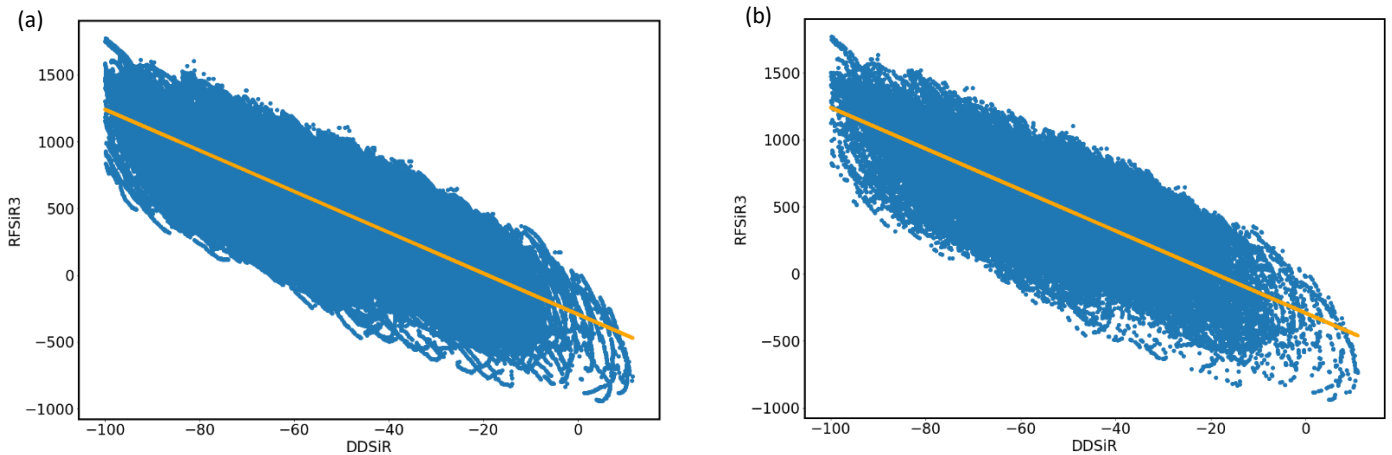


Figure 5-24: (a) Training results of RFSiR3 vs DDSiR. (b) Training results of RFSiR3 vs DDSiR.

The results from the linear regression analysis of RFSiR3 and DDSiR are shown in Table 5-16. The p-value is 0 and therefore it is less than 0.05. The null hypothesis is rejected. RFSiR3 and DDSiR are related. R² is 0.6 which represents a moderate correlation between RFSiR3 and DDSiR. The NRMSE is less than 0.1, it can be inferred that the linear regression model is a good fit for the relationship between RFSiR3 and DDSiR. Table 5-16 and Figure 5-24 indicate that RFSiR3 is directly proportional to DDSiR. This is to be expected.



5.3.5 Effect of the Presence of Train

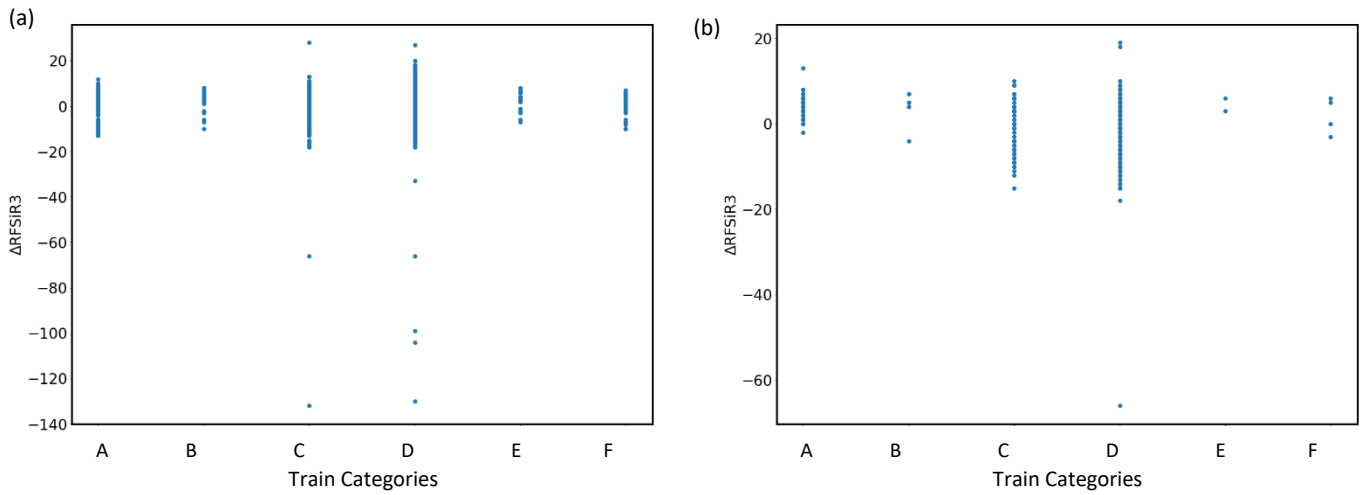


Figure 5-25: (a) $\Delta RFSiR3$ vs Loaded Train Categories (b) $\Delta RFSiR3$ vs Unloaded Train Categories.

According to Figure 5-25 does not give any evidence of correlation between changes RFSiR3 and the presence of trains.

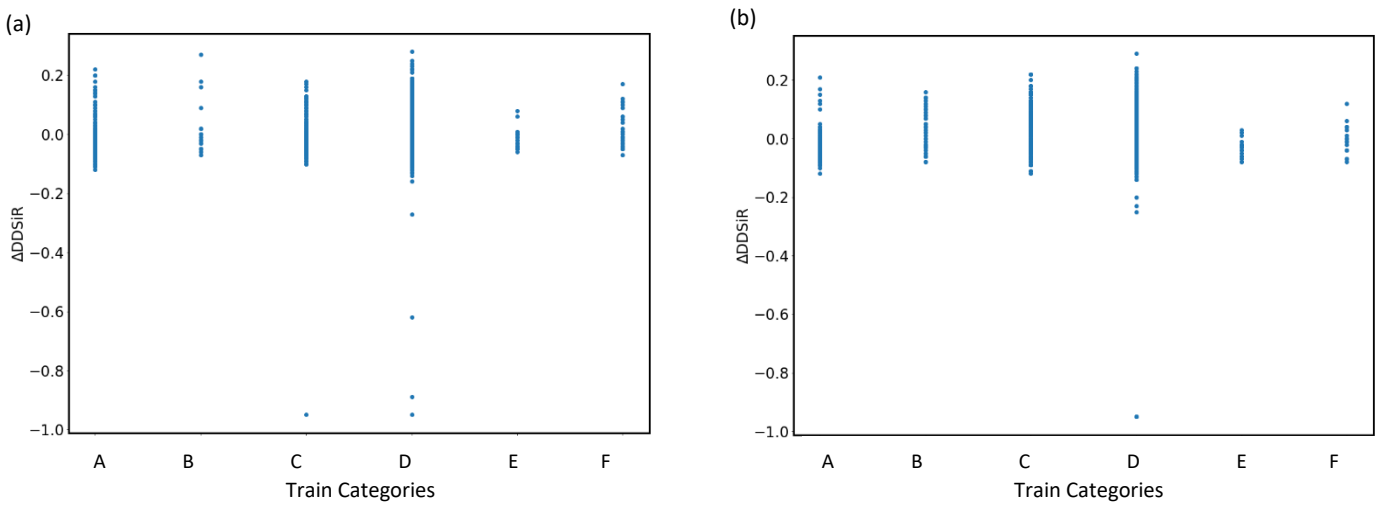


Figure 5-26: (a) $\Delta DDiSiR$ vs Loaded Train Categories (b) $DDiSiR$ vs Unloaded Train Categories.

Figure 5-26 does not give any evidence of correlation between changes in DDiSiR and the presence of trains.



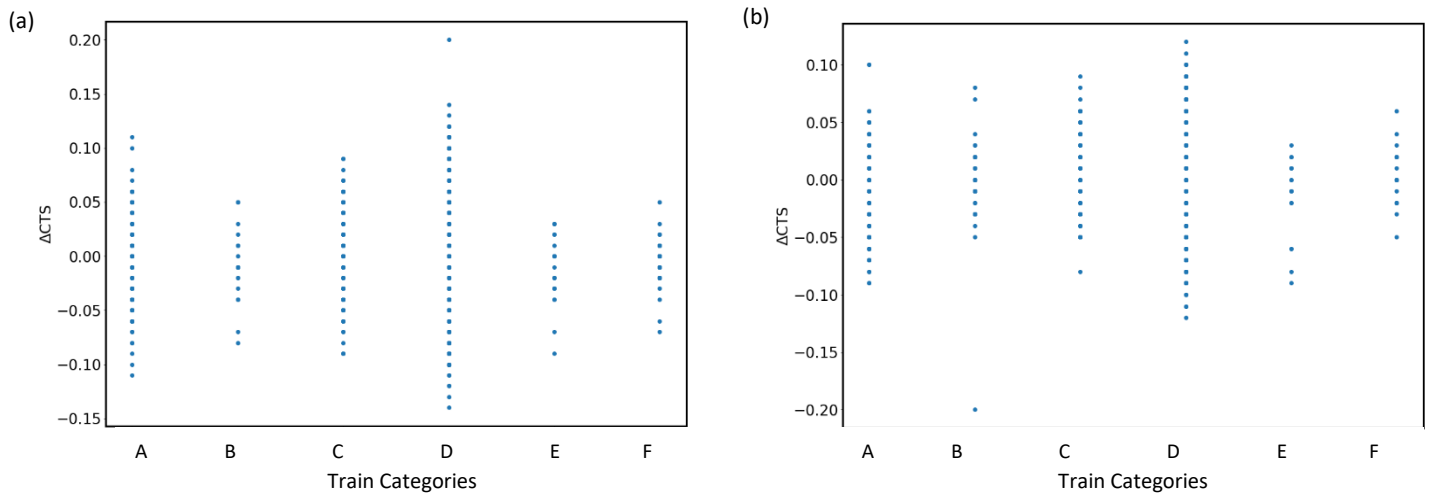


Figure 5-27: ΔCTS vs Loaded Train Categories (b) ΔCTS vs Unloaded Train Categories.

Figure 5-27 shows that there is no relation between DDSiR and the Presence of a Train.



5.3.6 Effect of Ambient Temperature Variation

Table 5-17: Training and Testing Results of RFSiR3 vs ATS.

Dependent Variable: RFSiR3 (kN)					
Term	Coefficient	P – Value	95% CI	R ²	NRMSE
Training					
Intercept	1727.2726	0.0	(1725.240; 1729.305)	0.830	0.05
ATS (°C)	-60.7112	0.0	(-60.810; -60.612)		
Testing					
Intercept	1730.02	0.0	(1725.935; 1734.110)	0.829	0.05
ATS (°C)	-60.8403	0.0	(-61.040; -60.641)		

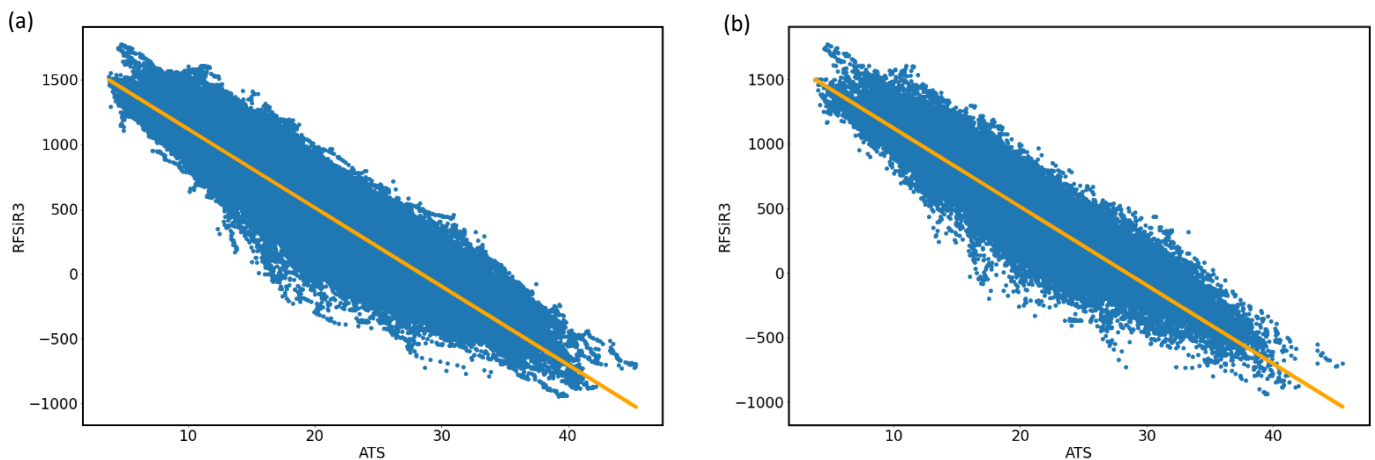


Figure 5-28: (a) Training results of RFSiR3 vs ATS. (b) Testing results of RFSiR3 vs ATS.

The results from the linear regression analysis of RFSiR3 and ATS are shown in Table 5-17. The p-value is 0, it is less than 0.05 and therefore null hypothesis is rejected. RFSiR3 and ATS are related. R² is 0.8 which represents a strong correlation between RFSiR3 and ATS. The NRMSE is less than 0.1, it can be inferred that the linear regression model is a good fit for the relationship between RFSiR3 and ATS. Table 5-17 and Figure 5-28 indicate that RFSiR3 is inversely proportional to ATS.



Table 5-18: Training and Testing Results of DDSiR vs ATS.

Dependent Variable: DDSiR					
Term	Coefficient	P – Value	95% CI	R ²	NRMSE
Training					
Intercept	101.4053	0.0	(-101.579; -101.232)	0.515	0.13
ATS	2.4120	0.0	(2.404; 2.420)		
Testing					
Intercept	101.64	0.0	(-101.987; -101.293)	0.517	0.13
ATS	2.4246	0.0	(2.408; 2.441)		

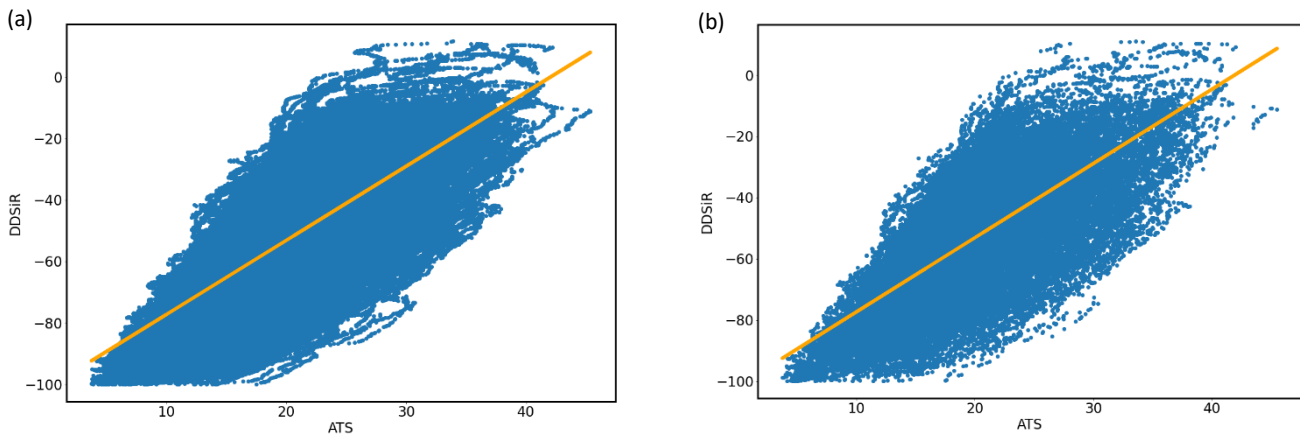


Figure 5-29: (a) Training results of DDSiR vs ATS. (b) Testing results of DDSiR vs ATS.

The results from the linear regression analysis of DDSiR and ATS are shown in Table 5-18. The p-value is 0, it is less than 0.05 and therefore null hypothesis is rejected. RFSiR3 and ATS are related. R² is 0.5 which represents a low correlation between DDSiR and ATS. The NRMSE is less than 0.1, it can be inferred that the linear regression model is a good fit for the relationship between DDSiR and ATS. Table 5-18 and Figure 5-29 indicate that DDSiR is directly proportional to ATS.



5.3.7 Summary of the Section

Track- Bridge Interactions in high-speed rail have been researched quite extensively, whilst to the author's knowledge there has been no documented report on track-bridge interactions in heavy haul railway bridges. For this study research on high-speed rail has been used as benchmark to achieve the following:

- Investigate the effect of rail temperature variation on rail forces and the longitudinal displacement of the deck.
- Examine the effect of variation in concrete temperature on the longitudinal deck displacement, rail forces and variation in rail temperature as well as the effect of longitudinal deck displacement on rail forces.
- Investigate the effects of the presence of the train (vertical train loads) on the longitudinal displacement of the deck, rail forces and concrete temperature.

According to the results in this study rail temperature in railway bridges is inversely proportion to the rail forces in the rail. As the rail heats up it expands resulting in compressive forces in the rail. This is because the section of the rail that is on the bridge is the central zone of the railway line. As stated in section 2.2.42.2.4.2, contraction and expansion are not permitted in the central zone of CWRs. It can thus be said that as the central zone of the railway track resists the expansion force, compressive forces are transferred to the rail.

Although the longitudinal deck displacement and rail temperature model suggests that the longitudinal deck displacement and rail temperature are directly proportional, which is consistent with the observation in high-speed rail, there is very small correlation between these two variables. The longitudinal deck displacement is influenced by the variation in concrete temperature and so the lack of correlation could be attributed to the phase lag between the concrete temperature and the rail temperature. However, the phase lag was not analysed extensively in this study and therefore it cannot be inferred conclusively from this study that as the rail expands it influences the deck to displace longitudinally. More measurements and tests need to be conducted to establish the relationship between longitudinal deck displacement and rail temperature.

Literature on high-speed proposes that as concrete temperature in railway bridges increases, the deck expands and is displaced longitudinally as well as when concrete temperature in railway bridges decreases the deck contracts, and it expands longitudinally. The results in this study are consistent with the proposals that were put forward in literature. Longitudinal deck displacement is directly proportional to concrete temperature variation.

There is a small correlation between concrete temperature in the deck and forces in the rail as well as between concrete temperature in railway bridges and temperature in the rail. Research on high-speed rail has put forth that when CWR is placed on a bridge connected by ballast the two systems are interconnected and therefore an increase/decrease in concrete temperature of the bridge deck will



result in additional forces in the track. However, from the results in this study it is not possible to confidently confirm or deny that this is true. More research needs to be carried out.

Longitudinal deck displacement of the bridge deck and rail forces in the rail are inversely proportional. The bridge deck expands longitudinally it transmits compressive forces into the rails and as it contracts it transmits tension forces into the rails. This is consistent with the literature reviewed in this study.

According to the results in this study there is no correlation between the effect of the presence of the train on the longitudinal displacement of the deck, rail forces and concrete temperature respectively.



5.4 Predictive Multiple Linear Regression Model Discussion

This chapter will describe the results of a predictive multiple linear regression model that will assist in the management and maintenance heavy haul railway bridges with an expansion length greater than 90m. Additionally it will present the user interface for this model.

The Predictive Multiple Linear Regression Model was developed using the results from section 5.3 using a four-step process. In developing this model, it essential to ensure that for each step the correlation is equal to or greater than 0.7. A correlation of 0.7 represents a strong relation.

The model was trained and tested using a 80/ 20 split. 80% of the data was used to train the model and 20% to test it.

The first step in the model uses the results from the linear regression analysis of RFSiR3 and ATS as shown in Table 5-19. The p-value is 0, it is less than 0.05 and therefore the null hypothesis is rejected and RFSiR3 and ATS are related. R^2 is 0.8 which represents a strong correlation between RFSiR3 and ATS. Therefore, RFSiR may be predicted using forecast ATS.

Table 5-19: Model Step 1 - Predicting fail force from forecast temperature.

Dependent Variable: RFSiR				
Term	Coefficient	P – Value	95% CI	R ²
Training				
Intercept	1727.2726	0.0	(1725.240;1729.305)	0.830
ATS	-60.7112	0.0	(-60.810; -60.612)	
Testing				
Intercept	1730.02	0.0	(1725.935; 1734.110)	0.829
ATS	-60.8403	0.0	(-61.040; -60.641)	



The second step of the model is the multiple linear relationship between RFSiR3 and ATS versus RTR. The results from this multiple linear regression analysis are shown in

Table 5-20. The p-value is 0, it is less than 0.05 and therefore null hypothesis is rejected. RFSiR3, ATS and RTR are related. R^2 is 0.8 which represents a strong correlation between RFSiR3, ATS and RTR. Therefore, RTR may be predicted using RFSiR and ATS.

Table 5-20: Model Step 2 - Predicting rail temperature from variables in step 1.

Dependent Variable: RTR				
Term	Coefficient	P – Value	95% CI	R²
Training				
Intercept	10.5650	0.0	(10.386;10.744)	0.793
ATS	0.8697	0.0	(0.863;0.876)	
RFSiR3	-0.0080	0.0	(-0.008;-0.008)	
Testing				
Intercept	10.6342	0.0	(10.275;10.993)	0.790
ATS	0.8655	0.0	(0.852;0.879)	
RFSiR3	-0.0079	0.0	(-0.008;-0.008)	



The third step of the model is the multiple linear relationship between RFSiR3, ATS and RTR versus DDSiR. The results from this multiple linear regression analysis are shown in Table 5-21. The greatest p-value is 0.624, it is greater than 0.05 and therefore null hypothesis cannot be rejected. It cannot be said that RFSiR3, ATS, RTR and DDSiR are related. Although it cannot be said that variables on Table 5-21 are related, these variables have an R^2 of 0.72 which represents a strong correlation between RFSiR3, ATS, RTR and DDSiR. Therefore, DDSiR may be predicted using RFSiR, ATS and RTR.

Table 5-21: Model Step 3 - Predicting longitudinal deck displacement from variables in step 2.

Dependent Variable: DDSiR				
Term	Coefficient	P – Value	95% CI	R²
Training				
Intercept	-54.3030	0.0	(-55.554; -53.050)	0.72
ATS	2.5072	0.0	(2.454; 2.560)	
RFSiR3	-0.0421	0.0	(-0.043; -0.041)	
RTR	-0.0520	0.019	(-0.095; -0.008)	
Testing				
Intercept	-55.5632	0.0	(0.025; 0.975)	0.72
ATS	2.5452	0.0	(-58.077; -53.049)	
RFSiR3	-0.0411	0.0	(2.440; 2.651)	
RTR	-0.0219	0.624	(0.001; 0.001)	



The fourth and final step of the model is the multiple linear relationship between RFSiR3, ATS and RTR, DDSiR versus CTS. The results from this multiple linear regression analysis are shown in Table 5-22. The p-value is 0, it is less than 0.05 and therefore null hypothesis is rejected. It can be said that RFSiR3, ATS, RTR, DDSiR and CTS are related. These variables have an R^2 of 0.861 which represents a strong correlation between RFSiR3, ATS, RTR, DDSiR and CTS. Therefore, CTS may be predicted using RFSiR, ATS, RTR and DDSiR.

Table 5-22: Model Step 4 - Predicting concrete temperature from variables in step 3.

Dependent Variable: CTS				
Term	Coefficient	P – Value	95% CI	R²
Training				
Intercept	31.2698	0.0	(30.764; 31.776)	0.861
ATS	0.2588	0.0	(0.239; 0.279)	
RFSiR3	-0.0057	0.0	(-0.006; -0.005)	
RTR	-0.0760	0.0	(-0.093; -0.059)	
DDSiR	0.0487	0.0	(0.040; 0.057)	
Testing				
Intercept	31.7590	0.0	(30.753; 32.765)	0.861
ATS	0.2282	0.0	(0.188; 0.268)	
RFSiR3	-0.0058	0.0	(-0.007; -0.005)	
RTR	-0.0912	0.0	(-0.006; -0.004)	
DDSiR	0.0611	0.0	(1.03e-05; 3e-05)	

The Interface of the predictive model is represented in Figure 5-30 overleaf. This interface prompts the user to enter the ambient temperature for it to predict, the rail force (RFSiR), rail temperature(RTR), concrete temperature(CTS) and longitudinal deck displacement(DDSiR). The predicted results are shown in Figure 5-31.



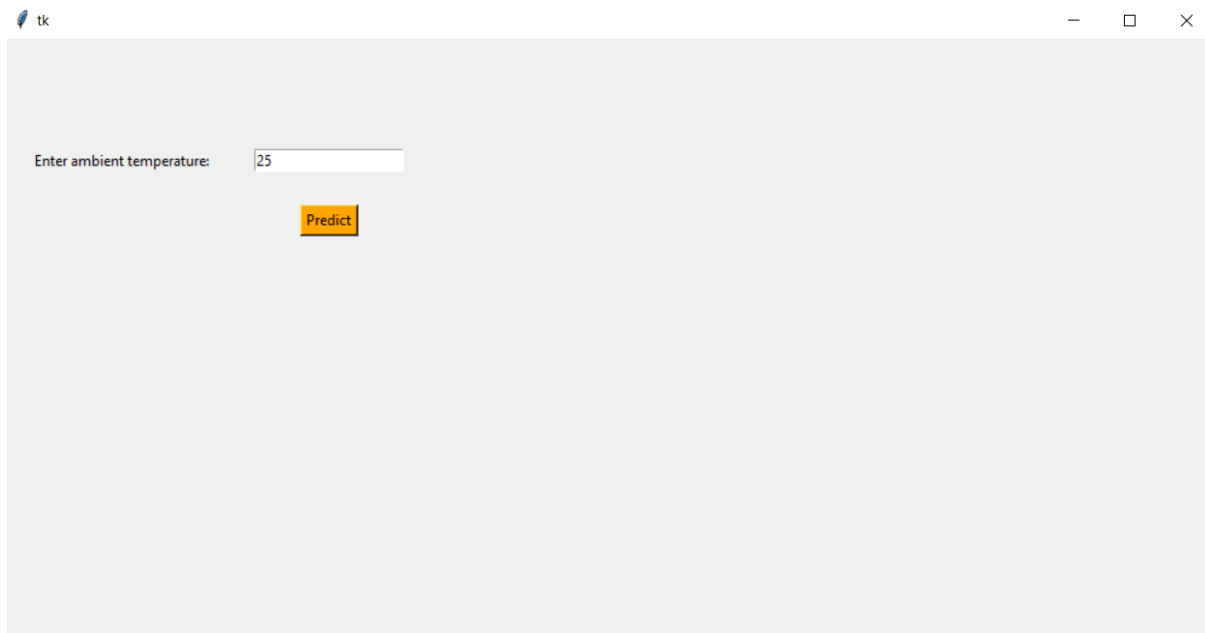


Figure 5-30: Predictive Multiple Linear Regression Model Interface.

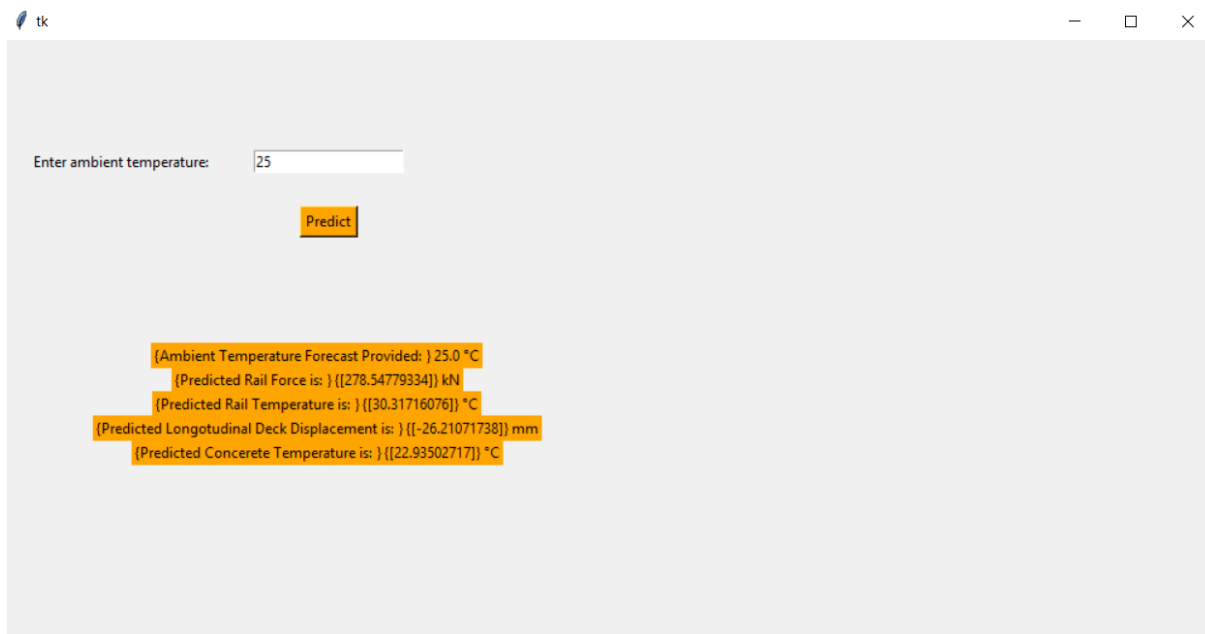


Figure 5-31: Predictive Multiple Linear Regression Model Interface Results.



6. Conclusions

In recent years there has been a general trend to increase axle loads and operating speeds of trains to keep up with export demands and growing mining trends. This trend has introduced concerns regarding the structural integrity of railway bridges, particularly old railway bridges which might be subjected to high loads than had previously been allowed for. One major concern in the structural integrity of railway bridges is the manifestation of rail bridge interaction forces.

Whilst there have been numerous studies on track-bridge interactions in high-speed rail, there has been no documented report that addresses the design and management of track bridge interaction in heavy haul railway bridges with an expansion length greater than 90m.

Resultantly, using ORV as a case study this study explored the observed patterns of rail forces, longitudinal deck displacements, ambient temperature, concrete temperature and rail temperature over time using time series graphs. It used linear regression to investigate the effect of rail temperature variation on rail forces and the longitudinal displacement of the deck as well as to examine the effect of variation in concrete temperature on the longitudinal deck displacement, rail forces and variation in rail temperature. It examined the effect of longitudinal deck displacement on rail forces and investigated the effects of the presence of the train on the longitudinal displacement of the deck, rail forces and concrete temperature also using linear regression. Finally, this study developed a predictive multiple linear regression model that will accept ambient temperature as an input and produces rail force, rail temperature, concrete temperature and longitudinal deck displacement measurements as outputs.

From this study it was observed that when the ambient temperature increases, the deck tends to expand longitudinally, the deck concrete temperature tends to increase. The rail temperature increases and the rail experiences compressive forces. In contrast when the ambient temperature decreases the deck concrete temperature decreases, the deck contracts longitudinally, rail temperature decreases and the rail experiences tension forces.

In this study the following was demonstrated:

- Rail temperature variation in railway bridges is inversely proportion to the rail forces in the rail.
- Longitudinal deck displacement is directly proportional to concrete temperature variation.
- longitudinal deck displacement of the bridge deck and rail forces in the rail are inversely proportional.

This is consistent with the literature on the manifestation of track-bridge interactions in high-speed rail, which advances that in the central zone of CWRs displacement is prohibited and resultantly as the rail cools down and warms up forces develop in the rail. And because the railway track is connected to the bridge deck the rail attempt to displace the bridge deck in the same direction as the forces in the rail forcing the deck to expand or contract in the opposite direction. This gives rise to



the inversely proportional relationship of the rail temperature and longitudinal deck displacement and the inversely proportional relationship of the rail force and the longitudinal deck displacement.

The effect of the presence of the train on the longitudinal displacement of the deck, rail forces and rail temperature, could not be established conclusively.

It is recommended that more research is carried out on the above - mentioned relationships.

In conclusion, this developed predictive model allows stations to plan and maximize train travel on favourable days. This predictive model will serve as a benchmark for further of heavy haul railway bridge management guidelines.



7. Recommendations

The following recommendations are made for further research in this study area:

- Due to the lack of data, the effect of track-bridge interactions on the heavy haul railway bridge substructure was not investigated. It is therefore recommended that the effect of track bridge interaction on the substructure of the bridge is investigated. Either through analysis of field measurements or finite element analysis.
- Acceleration and braking forces are not measured on the ORV and this hinders investigation of track-bridge interaction due to braking and acceleration of heavy haul trains. It is therefore recommended that field measurements of braking and acceleration forces exerted by heavy haul trains are recorded and analysed.
- The relationship between the longitudinal deck displacement and rail temperature, concrete temperature in railway bridges and forces in the rail and the effect of the presence of the train on the longitudinal displacement of the deck, rail forces, rail temperature as well as concrete temperature, could not be established conclusively in this study. It is recommended that interactions of these variables is researched further.



8. Bibliography

1. Ali AsifK, A. *et al.* (2016) ‘INTERNATIONALJOURNALOFRESEARCH SCIENCE& MANAGEMENT STRENGTH PROBLEMS ASSOCIATED WITH TRACK BRIDGE INTERACTION IN PRESENCE OF CONTINUOUSLY WELDED RAIL’, C) *International Journal of Research Science*, 3(8). Available at: <http://www.ijrsm.com>.
2. AREMA, A. A. R. E. a. M.-o.-W., 2003. Railway Structures. In: A. A. R. E. a. M. AREMA, ed. *AREMA Manual for Railway Engineering*. Lanham: American Railway Engineering and Maintenance-of-Way Association, pp. 320-368.
3. Babu, S. G., 2017. *NPTEL*. [Online] Available at: <http://nptel.ac.in/courses/105108075/module6/lecture20.pdf> [Accessed 20 August 2017].
4. Bester, J., 2015. The Olifants River Bridge - The Inherent Problem. *SAICE, Railway and Harbour Divison* , May, pp. 1-7.
5. Bruestle, K. and Manager, S. P. (no date) ‘Continuous Welded Rail’, *Grandad Sez: Grandad’s Railway Engineering Section*. Available at: <http://www.grandadsez.co.uk/railways/continuous-rail.html>.
6. Bruton, M., 2011. SA’s Sheffel Bogie Keeps on Rolling. *Cape Argus* , 7 April .
7. Busatta, F. and Moyo, P. (2015) ‘Vibration Monitoring of a Large Scale Heavy Haul Railway Viaduct’, *MATEC Web of Conferences*, 24(April). doi: 10.1051/mateconf/20152404007.
8. Chandler, N., 2015. South Africa's World Record Breaking Train. *The Heritage Portal*, 20 October.
9. Ciaran, R., 2018. Train Derailments Cost Kumba R2bn in the First Half. *Moneyweb*, 25 July.
10. Cutillas, S., 2009. *Track-bridge interaction problems in bridge design*. Madrid, Taylor & Francis Group.
11. De Backer, H. *et al.* (2019) ‘Application limits for continuously welded rails on temporary bridge decks’, *Sustainability (Switzerland)*, 11(4), pp. 482–497. doi: 10.1177/0954409716631581.
12. De Backer, H., Mys, J. & Schotte, K., 2017. *Continuously Welded Rails on Temporary Bridge Decks*. Vancouver, Canada, 39th IABSE SYmposium - Engineering the Future , p. 1.
13. Diop, S. *et al.*, 2011. *A Review of Problem Soils in South Africa*, Cape Town: Council for Geoscience.
14. Dutoit, D., 2009. *New evolutions for high speed rail line bridge design criteria and corresponding design procedures..* Paris , Taylor & Francis Group.



15. Elkhoury, N. *et al.* (2018) 'Degradation Prediction of Rail Tracks: A Review of the Existing Literature', *The Open Transportation Journal*, 12(1), pp. 88–104. doi: 10.2174/1874447801812010088.
16. Esveld, C., 2001. *Modern Railway Track*. 2nd ed. Delft : Delft University of Technology .
17. Faris, M. *et al.* (2018) 'Distributed Optimization for Railway Track Maintenance Operations Planning', *IEEE Conference on Intelligent Transportation Systems, Proceedings, ITSC*, 2018-Novem(December), pp. 1194–1201. doi: 10.1109/ITSC.2018.8569335.
18. Freyer, R., 2004 . *TECHNICAL AUDIT: FORCE MONITORING ON THE OLIFANTS RIVER BRIDGE - OREX*. s.l., Spoornet, A division of Transnet Limited.
19. Frost, J., 2020. *Introduction to Statistics: An Intuitive Guide for Analyzing Data and Unlocking Discoveries*. 2nd ed. United States: James D Frost.
20. Goicela-Ruigómez, J., 2009. *Service limit states for railway bridges in new Design Codes IAPF and Eurocodes*. Madrid , Taylor & Francis Group.
21. Hagaman, B. (1991) 'Lateral Track Stability 1991', *Transportation Research Record*, 1289(Rail).
22. Indian Geotechnical Society, I., 2015. *50th Indian Geotechnical Conference*. Pune, Indian Geotechnical Society.
23. Illsley, K. (2020) 'Rail Stress due to Track-Bridge Interaction with various track and traffic conditions', 138(January), pp. 1–4.
24. Indraratna, B., Salim, W. & Rajjijatkamjorn, C., 2011. *Advanced Rail Geotechnology - Ballasted Track*. 1st ed. London: CRC Press.
25. IS-15284, 2003. *Design and Construction for Ground Improvement Guidelines*. 1 ed. New Delhi: Pranhat Offset Press.
26. Jamal, H., 2017. *about Civil.com*. [Online]
Available at: <https://www.aboutcivil.org/railway-ballast-material>
[Accessed 28 August 2021].
27. Kadam, G., 2021. *Rail Joints*. Mumbai : VMP'MPCOE.
28. Kaewunruen, S. and Remennikov, A. (2008) 'Dynamic properties of railway track and its components: a state-of-the-art review', *New Research on Acoustics*, pp. 197–220. Available at: <http://ro.uow.edu.au/cgi/viewcontent.cgi?article=1512&context=engpapers>.
29. Khot, S., 2020. Understanding Interaction Effects. *Towards Data Science* , 4 March .
30. Kim, E. *et al.* (2019) 'Post-construction alignment revision in direct-fixation railroad tracks', *Sustainability (Switzerland)*, 11(21). doi: 10.3390/su11216166.
31. Kostet, D., 2018. *Railway bridges with floating slab track systems* , Luleå: Luleå University of Technology Department of Civil, Environmental and Natural Resources Engineering.



32. Kumar, R. and Upadhyay, A. (2013) 'Effect of temperature gradient on track-bridge interaction', *Interaction and multiscale mechanics*, 5(1), pp. 1–12. doi: 10.12989/imm.2012.5.1.001.
33. Kuys, W., 2011. *Heavy Haul Operations in South Africa*. Calgary, Transnet Freight Rail.
34. Lee, K.-C. *et al.* (2015) 'Rail-Structure Interaction Analysis of Sliding Slab Track on Bridge', (March), p. V001T01A010. doi: 10.1115/jrc2015-5661.
35. Liedtke, S., 2019. Transnet Launches World's Largest Production Train. *Creamer Media's Engineering News* , 19 October .
36. Lim, N. H., Park, N. H. and Kang, Y. J. (2003) 'Stability of continuous welded rail track', *Computers and Structures*, 81(22–23), pp. 2219–2236. doi: 10.1016/S0045-7949(03)00287-6.
37. Lombard, P., 1982. *Sishen-Saldanha: First Six Proc. 2nd Int Heavy Haul Railway Conf.* Colorado , s.n.
38. Madhav, M. R. & Muira, N., 1998. Study of Reinforcement Granular Pad-Inclusion-Soft-Clay Systems. *Research of Lowland Technology* , Issue 7, pp. 88-98.
39. Maree, H., 1987. Forces in Railway Track Structure on the Olifants River Bridge. *RAM*, 3(1), pp. 1-7.
40. McCammon, D. & Richards, D., 2006. *Module 15: Railway Structures*. s.l.:Rudolph Stevens .
41. Mundrey, J., 2010. *Railway Track Engineering*. Fourth Edition ed. New Delhi : Mc-Graw .
42. Narendra, A. M., 2011. *Railway Track - Bridge Structure Interaction for Continuous/Long Welded Rails (CWR/LWR)*, Roorkee: Indian Institute of Technology Roorkee .
43. National Academies of Sciences, E. a. M., 2012. *The Track Design Handbook for Light Rail Transit*. 2nd ed. Washington DC: The National.
44. Pauwels, J., 2015. *Application Limits for Continuously Welded Rail on Temporary Bridge Decks* , Ghent : Universiteit Gent.
45. Popović, Z. *et al.* (2018) 'Interaction Phenomenon Between Train, Track and Bridge', in *Advances in Intelligent Systems and Computing*. Springer Verlag, pp. 3–11. doi: 10.1007/978-3-319-70987-1_1.
46. Ramondence, P., Martin, D. & Schmitt, P., 2009. *Track - bridge interaction - the SNCF experience*. Paris , Taylor & Francis Group.
47. Stojiljkovic, M., 2020. Linear Regression in Python. *Real Python* , February .
48. Sung, D.-Y. & Han, S.-C., 2018. Fatigue life evaluation of continuous welded rails on concrete slab track in Korea high-speed railway. *Advances in Structural Engineering* , 15 March, pp. 1990-2004.
49. s. s., R. *et al.* (2018) 'A finite element model of vehicle-bridge interaction considering



- braking and acceleration', *Engineering Structures*, 303(1–2), pp. 46–57. doi: 10.1016/j.jsv.2006.11.034.
50. Schanack, F. *et al.* (2014) 'Displacement Relative Method for Track-Structure Interaction', *The Scientific World Journal*, 2014, pp. 1–7. doi: 10.1155/2014/397515.
51. Stansfield, A. (2019) 'The role of energy absorbing materials in heavy haul rail for minimising track degradation', 137(January).
52. Hajializadeh, D. and Žnidarič, A. (2020) 'Development and Testing of a Railway Bridge'.
53. Tsanakakis, K., 2013. *The Railway Track and its Long Term Behaviour*. Berlin : Springer.
54. UIC, U. I. d. C. d. f., 2001. *UIC Code 774 - 3R Track/Bridge Interaction Recommendations for Calculations*, Paris: Union Internationale des Chemins de fer.
55. University of Eastern Mediterranean, U., 2017. *Department of Civil Engineering*. [Online] Available at: http://civil.emu.edu.tr/old_website/data/civl454/CH1-%20Int%20to%20gr%20modf.pdf [Accessed 6 November 2017].
56. Von Gericke, R., 1986. *Measures Taken by the South Africa Transport Services to Reduce Transportation Costs of Coal on the Ermelo Richards Bay Line Proc. 3rd Int Heavy Haul Railway Conf.*. Vancouver , s.n.
57. Waters, J. & Selig, T., 1994. *Track Geotechnology and Substructure Management*. 1st ed. Derby: Thomas Telford Books.
58. Wei, X. and Wang, P. (2011) 'Calculation and Study of Longitudinal Forces of Continuous Welded Rail Track on Deck Arch Bridge', in. American Society of Civil Engineers (ASCE), pp. 2092–2097. doi: 10.1061/41184(419)345.
59. Xu, J. *et al.*, 2107. Geometry Evolution of Rail Weld Irregularity and the Effect on Wheel-Rail Dynamic Interaction in Heavy Haul Railways. *Engineering Failure Analysis* , pp. 31-34.
60. Yun, K. M. *et al.* (2019) 'Quantification of ballasted track-bridge interaction behavior due to the temperature variation through field measurements', *NDT and E International*, 103(February 2018), pp. 84–97. doi: 10.1016/j.ndteint.2019.01.009.
61. Zhang, R., Wu, H. & Karsten, A., 2015. *Slab track performance under heavy haul revenue condition and its remediation method*. Edinburgh, 13Th International Railway Engineering Conference.

